Growth of nonmotile stress responsive bacterial colonies inside environmental constraints

Dissertation

zur Erlangung des Doktors der Naturwissenschaften
der Naturwissenschaftlich-Technischen Fakultät
der Universität des Saarlandes

von

Samaneh Rahbar

Saarbrücken, 2025

Tag des Kolloquiums:	28.10.2025
Dekan:	Prof. Dr.-Ing. Dirk Bähre
Berichterstatter:	Prof. Dr. Ludger Santen Prof. Dr. Dr. h.c. Heiko Rieger
Akad. Mitglied:	Dr. Noora Aho
Vorsitz:	Prof. Dr. Christian Wagner

Abstract

Bacterial colonies are foundational to a broad spectrum of biological processes, exhibiting intricate growth dynamics profoundly influenced by mechanical interactions between cells and their surroundings. A comprehensive understanding of these interactions is crucial for advancing our knowledge of bacterial behavior, particularly within confined or stressed environments. This dissertation analyzes how mechanical forces, originating from cell-cell and cell-substrate interactions, govern the self-organization and structural evolution of bacterial colonies subjected to specific geometric constraints. I examine the collective influence of bacterial properties, surface characteristics, and mechanosensitivity on colony alignment, growth, and structural adaptations under confinement. Employing molecular dynamics simulations, I explore the temporal impact of these factors, in conjunction with confinement geometry, on bacterial behavior. Furthermore, this research investigates the role of external mechanical stress, including isotropic pressure, in inducing morphological transitions and modulating bacterial growth dynamics. This study yields novel insights into the interplay between bacterial mechanics, confinement, and external stress, elucidating how these factors dictate bacterial adaptation and behavior within restricted environments. By integrating theoretical modeling with computational simulations, this thesis contributes to a deeper mechanistic understanding of microbial dynamics, providing new perspectives on how mechanical interactions regulate bacterial organization and expansion across diverse environmental contexts.

Zusammenfassung

Bakterielle Kolonien sind grundlegend für ein breites Spektrum biologischer Prozesse und weisen komplexe Wachstumsdynamiken auf, die stark von mechanischen Wechselwirkungen zwischen Zellen und ihrer Umgebung beeinflusst werden. Ein umfassendes Verständnis dieser Wechselwirkungen ist entscheidend, um unser Wissen über das Verhalten von Bakterien, insbesondere in engen oder gestressten Umgebungen, zu erweitern. Diese Dissertation analysiert, wie mechanische Kräfte, die aus Zell-Zell- und Zell-Substrat-Wechselwirkungen entstehen, die Selbstorganisation und die strukturelle Entwicklung von Bakterienkolonien unter spezifischen geometrischen Einschränkungen steuern. Ich untersuche den kollektiven Einfluss von Bakterieneigenschaften, Oberflächenmerkmalen und Mechanosensitivität auf die Ausrichtung, das Wachstum und die strukturellen Anpassungen der Kolonie unter Einschränkung. Durch den Einsatz von Molekulardynamik-Simulationen erforsche ich den zeitlichen Einfluss dieser Faktoren, in Verbindung mit der Geometrie der Einschränkung, auf das Verhalten der Bakterien. Darüber hinaus untersucht diese Arbeit die Rolle von externem mechanischen Stress, einschließlich isotropem Druck, bei der Auslösung morphologischer Übergänge und der Modulation der bakteriellen Wachstumsdynamik. Diese Studie liefert neue Einblicke in das Zusammenspiel zwischen bakterieller Mechanik, Einschränkung und externem Stress und beleuchtet, wie diese Faktoren die bakterielle Anpassung und das Verhalten in begrenzten Umgebungen bestimmen. Durch die Integration von theoretischer Modellierung mit computergestützten Simulationen trägt diese Dissertation zu einem tieferen mechanistischen Verständnis der mikrobiellen Dynamik bei und bietet neue Perspektiven darauf, wie mechanische Wechselwirkungen die bakterielle Organisation und Expansion in verschiedenen Umweltkontexten regulieren.

Publications

Effect of mechanical interactions on bacterial self-organization and growth rate inside an isotropic and anisotropic confinement

arXiv, 2024
Samaneh Rahbar, Ludger Santen, and Reza Shaebani

Some of the results are derived from ongoing research, which has been shared as a preprint on arXiv but has not yet undergone peer review.

Growth of nonmotile stress responsive bacteria in 3D colonies under confining pressure

Biophysical Journal, 2025, 124, 807 - 817
Samaneh Rahbar, Farshid Mohammad-Rafiee, Ludger Santen, and Reza Shaebani

Contents

1 Introduction

Understanding the growth dynamics and self-organization of non-motile bacterial colonies is a fundamental challenge in microbial ecology and biophysics, with implications spanning, medicine, and environmental science. Bacteria are not merely passive entities; their growth and organization are profoundly influenced by mechanical and environmental constraints. These research explores the intricate interplay between mechanical stresses, confinement, and bacterial growth, providing insights into the physical principles governing microbial life.

The study of rod-shaped bacteria confined within square and circular geometries underscores the critical role of mechanical interactions in shaping colony organization. My simulations reveal that the degree of nematic ordering—a measure of orientational alignment among bacteria—varies with bacterial aspect ratio and confinement geometry. Larger aspect ratios promote greater ordering, while specific confinements alter the colony's structural dynamics. Moreover, compressive forces generated during cell division significantly influence the mechanical environment, with implications for both growth constraints and colony self-organization. These findings advance our understanding of bacterial behavior in confined spaces, providing a framework for exploring how physical constraints impact microbial ecology and potential biotechnological applications.

Expanding on this theme, we examined the growth of stress-responsive bacterial colonies under isotropic confining pressure in nutrient-rich environments. Using a novel simulation method, we demonstrated that external pressure acts as a soft constraint, enabling colony expansion despite mechanical stress. Unlike rigid confinements, which halt growth, isotropic pressure permits nearly linear long-term population and size growth. Mechanosensitivity—a measure of how bacteria robustly or weakly respond to mechanical stress—modestly impacts growth rates and colony size but becomes significant under certain parameter regimes. By developing an analytical estimate of bacterial doubling time and a population dynamics model consistent with simulations, my work provides a quantitative understanding of bacterial adaptation to mechanical stresses. These findings align with experimental observations of Escherichia coli colonies un-

der pressure, offering a robust theoretical framework for interpreting stress-response mechanisms.

Together, these studies illuminate the role of mechanical interactions and environmental constraints in bacterial growth and self-organization. They bridge the gap between experimental observations and theoretical models, advancing our understanding of bacterial adaptation to varying mechanical and environmental conditions. This thesis builds upon these insights, seeking to unravel the physical principles governing microbial life and their broader implications for ecology, biotechnology, and beyond.

2 Physical Background

The mechanical interactions at the microscopic scale play a pivotal role in shaping the behavior and organization of bacterial colonies. This chapter explores the intricate dynamics of contact mechanics and the stresses that arise within these densely packed systems, focusing on the stress tensor and its relationship with internal pressure. These mechanical forces, combined with surface adhesion, govern the collective movement and structural stability of bacterial populations.

In this context, the interplay between mechanical and biological factors leads to a variety of phenomena, including the isotropic-nematic transition, where colonies undergo a shift from disordered to ordered states. This transition often gives rise to buckling instabilities and variations in local packing density, which are critical in understanding the morphology and spatial distribution within the colony. Furthermore, these mechanical processes are tightly coupled with population dynamics, influencing growth patterns, nutrient distribution, and the colony's overall development.

By examining these factors in detail, this chapter aims to shed light on the fundamental principles that govern the growth and organization of bacterial colonies. The insights gained here have implications for understanding not only bacterial communities but also other systems where mechanics and collective dynamics intersect.

2.1 Contact Mechanics

Contact mechanics is the study of the interactions between solid bodies when they come into contact, specifically the deformation of materials and the forces involved. In many systems, the behavior of contacting bodies is governed by elastic deformation, particularly when the contact is non-damaging. Contact mechanics helps predict the distribution of stress, strain, and the resulting forces between surfaces in contact. This theory is critical in a variety of fields, including materials science, tribology, and increasingly, biological systems. Its applications extend to bacterial adhesion, biofilm deformations, and bacterial surface interactions.

The theoretical foundation of contact mechanics, especially in biological systems, often draws from Hertzian contact theory, which models the deformation of elastic bodies under contact. Although initially developed for engineering applications, its principles are highly applicable to biological systems, particularly for small-scale deformations such as bacterial cell adhesion. To derive the key relationships, the following assumptions of the classical Hertzian contact model are considered:

- Both contacting bodies are isotropic and homogeneous.
- Deformations are small and within the elastic limit.
- The surfaces are smooth, leading to frictionless contact.
- The contact area is much smaller than the characteristic dimensions of the bodies.

These assumptions ensure that the contact problem can be treated using linear elasticity theory.
To derive the Hertzian contact force, consider the contact between two spheres with radii R_1 and R_2 under an applied normal load F. When the spheres are pressed together, a circular contact area forms, with radius a. The effective radius of curvature R of the system is given by

$$\frac{1}{R} = \frac{1}{R_1} + \frac{1}{R_2} \tag{2.1.0.1}$$

This relationship arises from the geometry of the two spheres and ensures that the curvature at the contact point is appropriately represented.
Similarly, if the bodies are described by Young's moduli E_1 and E_2 and Poisson's ratios ν_1 and ν_2, the effective modulus of elasticity E^* is defined as

$$\frac{1}{E^*} = \frac{1-\nu_1^2}{E_1} + \frac{1-\nu_2^2}{E_2} \tag{2.1.0.2}$$

The effective modulus describes the combined stiffness of the contacting bodies. Under a normal load F, the spheres deform, creating a contact area with radius a. Using elasticity theory, the contact radius is related to the applied load by

$$a = \left(\frac{3FR}{4E^*}\right)^{\frac{1}{3}} \tag{2.1.0.3}$$

This equation is derived by balancing the strain energy stored within the material with the work done by the external force, following the principles of linear elasticity.

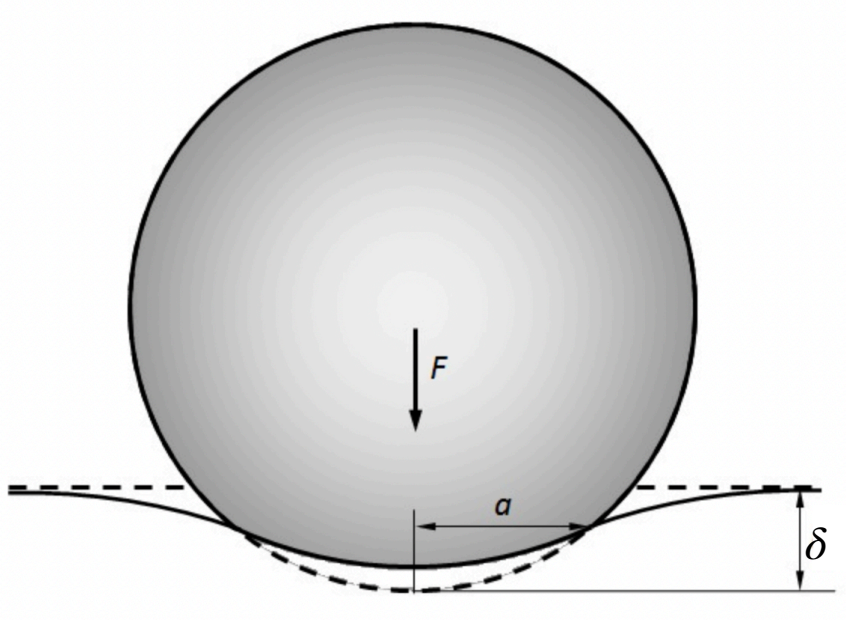

Figure 2.1: Contact of an elastic sphere with an elastic space which F is the applied force, a the radius of contact, d the total deformation. Reprinted from `https://upload.wikimedia.org/wikipedia/commons/8/82/Contact_sphere-plane.jpg`.

The pressure distribution over the contact area is assumed to be parabolic, with a maximum pressure p_0 at the center of the contact region, diminishing towards the edges. The pressure distribution $p(r)$ as a function of the radial distance r from the center is given by

$$p(r) = p_0 \left(1 - (\frac{r}{a})^2\right)^{\frac{1}{2}} \tag{2.1.0.4}$$

The parabolic distribution ensures that the contact stresses are consistent with the applied load and the elastic properties of the materials.

As it has shown in Fig. 2.1 the total deformation δ of the two bodies in contact can be related to the contact radius a and the effective radius R by

$$\delta = \frac{a^2}{R} \tag{2.1.0.5}$$

The normal load F is then related to the deformation by

$$F = \frac{3}{4} E^* \sqrt{R} \delta^{\frac{3}{2}} \tag{2.1.0.6}$$

This non-linear relationship reflects the increasing stiffness of the contact as the deformation grows, which is a hallmark of Hertzian contact theory.

The interplay of contact forces and contact vectors governs local mechanical interactions within bacterial colonies, shaping their alignment, deformation, and stress distribution. While contact mechanics provides insight into pairwise interactions, the cumulative effect of these forces across the colony requires a macroscopic framework for analysis. This is achieved through the stress tensor, which encapsulates the overall mechanical state and allows quantification of key properties such as internal pressure.

For instance, in bacterial colonies, contact mechanics governs phenomena like the adhesion of cells to surfaces, the stress distribution in biofilms, and the collective alignment of cells due to mechanical interactions. These forces, when analyzed at a macroscopic scale, reveal patterns of growth and deformation influenced by environmental conditions and mechanical constraints.

Understanding the transition from local interactions to global stress provides a foundation for exploring the mechanical behavior of bacterial systems under varying environmental conditions [1, 2, 3].

2.2 Stress Tensor and Internal Pressure in Bacterial Colonies

The stress tensor is a critical concept for quantifying the mechanical state of a bacterial colony. It encapsulates the internal forces that cells exert on each other through contact interactions, providing a detailed picture of how mechanical stresses develop within the colony. In densely packed bacterial systems, individual cells experience forces due to physical interactions with their neighbors [4, 5].

The contact forces f_{ij} can be derived from contact mechanics models, such as Hertzian theory for elastic bodies, where the normal force is related to the overlap between two bacteria. Tangential forces may be considered if friction is taken into account. These forces are typically short-range interactions that depend on the distance between neighboring cells.

The virial theorem is routinely used to compute stress tensor $\sigma_{\nu,\mu}$ over the entire volume [4, 6],

$$\sigma_{\nu,\mu} = \frac{1}{V}\left(\frac{1}{2}\sum_{i=1}^{N}\sum_{j=1}^{N_c^i} r_{c_{ij},\nu} f_{c_{ij},\mu}\right) \tag{2.2.0.1}$$

where V is the volume (or area in 2D) over which the stress is average. The sum runs over all interacting bacterial pairs i, j within the region of interest. This expression captures the contributions of individual bacterial interactions to the overall stress state in the system [7].

The stress tensor σ is calculated as the sum of the contact forces f_{ij} multiplied by the displacement vectors r_{ij}, where r_{ij} represents the contact vector between bacteria i and j. This tensor formulation captures both the magnitude and the direction of forces transmitted through the bacterial network.

The scalar internal pressure P is a measure of the isotropic component of the stress tensor, representing the tendency of the system to expand uniformly due to internal forces [8]. It can be computed as the negative trace of the stress tensor [7]

$$P = \frac{1}{D} Tr(\sigma), \tag{2.2.0.2}$$

where $Tr(\sigma) = \sum_k \sigma_{kk}$ is the trace of the stress tensor (sum of diagonal components), d is the dimensionality of the system (D = 2 for two dimensions, D = 3 for three dimensions). This formulation ensures that P represents the average mechanical pressure arising from contact interactions in the colony [9].

The internal pressure P corresponds to the isotropic component of the stress tensor. In systems with isotropic stress, where the stress is equally distributed in all directions, the trace of the stress tensor is a scalar quantity that represents this uniform pressure. The negative sign in Eq. (2.2.0.2) accounts for the compressive nature of internal pressure, which resists expansion. The internal pressure is directly linked to the packing density of bacteria and their interactions. High internal pressure suggests a dense, packed colony with substantial mechanical interactions between bacteria, whereas low pressure reflects less dense or more loosely packed configurations.

Internal pressure in bacterial colonies is not only crucial for understanding the mechanical state of the colony but also for explaining emergent behaviors such as shape formation, alignment, and division. For example, in confined environments or under external compression, bacteria may exhibit changes in morphology, transitioning from spherical to elongated shapes as they adjust to the mechanical constraints. Additionally, the pressure can influence the coordination of cell division, potentially leading to collective growth patterns or the formation of dense biofilms. Experimental measurements of colony growth under controlled mechanical conditions have shown that pressure can play a key role in triggering phase transitions, such as the formation of nematic-like ordering in dense bacterial colonies or the onset of jamming behavior at high packing fractions.

2.3 Frictional Forces in Bacterial Motion

The frictional forces experienced by bacteria on a substrate arise from the complex interplay of molecular interactions and mechanical properties at the interface. Adhesive molecules such as proteins, polysaccharides, and lipoproteins mediate strong bonds with the substrate, facilitating attachment. However, these same interactions contribute to frictional forces that resist bacterial motion. Unlike adhesion, which describes the static attachment of bacteria to a surface, friction arises when bacteria attempt to move relative to the substrate [10].
The frictional force, F_f , depends on the contact area, the density of adhesive molecules, and the molecular interactions at the interface. The effective frictional force can be expressed as:

$$F_f = \zeta_{eff} L_{contact} v, \tag{2.3.0.1}$$

where ζ is the frictional coefficient per unit of length that accounts for molecular adhesion, surface roughness, and local deformation. The effective contact length, $L_{contact}$, is influenced by the roughness of the bacterial wall, which increases the area of interaction between the bacterium and the substrate. where v is the velocity of the bacterium relative to the substrate. This enhanced contact amplifies adhesive interactions by engaging a greater number of adhesive molecules [10, 11]. As a result, adhesion forces manifest as an effective frictional force F_f , that resists bacterial motion or deformation.
Understanding these frictional forces is critical for predicting bacterial motion, biofilm stability, and responses to mechanical stresses. By focusing on friction, we gain insight into how bacteria overcome resistive forces to colonize surfaces, migrate, and adapt to physical constraints [12].

2.4 Mechanical Interactions Driving Order and Disorder in Bacterial Systems

In non-motile bacterial systems, understanding the transition between isotropic and nematic phases, alongside the associated buckling instabilities and local packing effects, provides insights into the collective behaviors and organization of microbial communities. These transitions significantly influence how bacterial cells interact, move, and form complex structures in both natural and synthetic environments. Lacking of self-propulsion machinery for non-motile bacteria, they are able to take advantage of the short range forces resulting from their contact to reorient the neighbouring bacteria

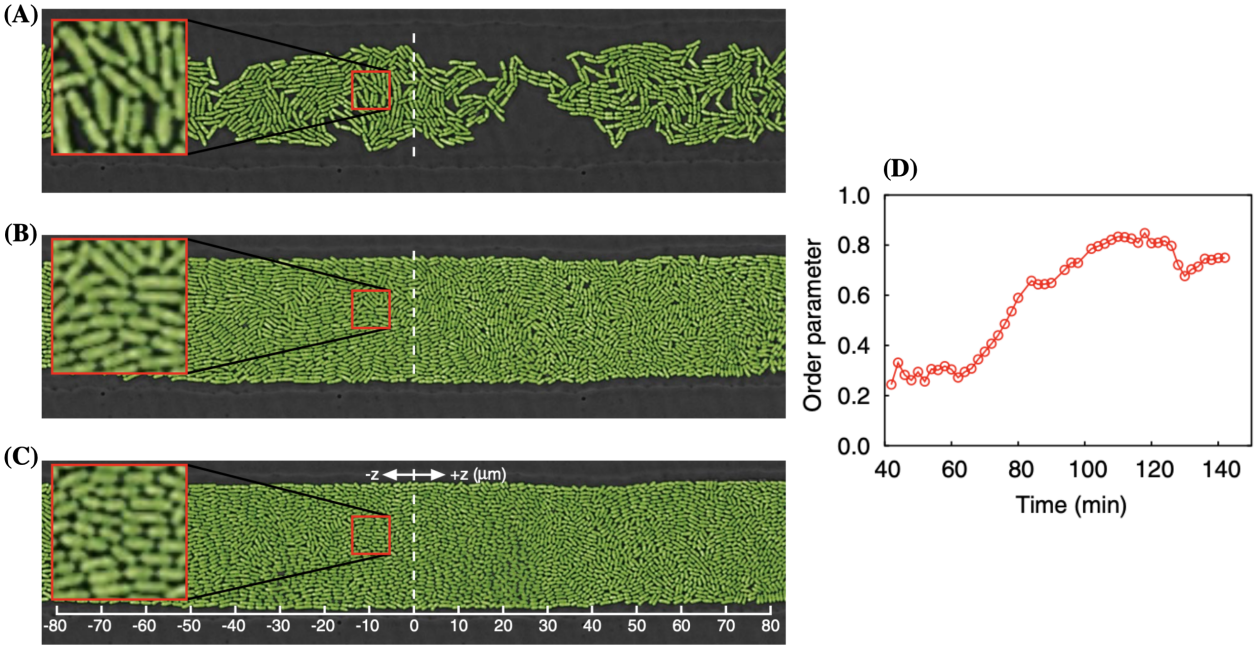

Figure 2.2: Experimental results for bacterial growth and ordering from an evenly distributed low-density seeding of cells. (A–C) Three snapshots of *E. coli* monolayer growth and ordering in a quasi-2D open microfluidic cavity taken at 60, 90, and 138 min from the beginning of the experiment. (D) represents the time evolution of the order parameter, S. Figure and the caption reprinted from Volfson et. al. [15].

and the force generated by growth to achieve expansion and lead to persistent disorder inside the colony. In the following we mention that how the mechanical forces can lead to order and disordered structure inside a colony of non-motile bacteria .

2.4.1 Onsager Theory and Isotropic-Nematic Transition

In densely packed bacterial systems, interactions between neighboring cells lead to short-range ordering, where local alignments emerge due to physical contact and spatial constraints. These interactions, primarily mediated through direct mechanical forces, encourage cells to align their orientations, resulting in a gradual transition from a disordered arrangement to more organized structures. This process forms the basis of isotropic-nematic transitions, where bacterial colonies evolve from an isotropic state, characterized by random orientations, to a nematic phase, defined by long-range orientational order.

The isotropic-nematic transition in bacterial colonies can be quantitatively described using Onsager theory. Originally developed to model the phase behavior of rod-like particles in a solution, Onsager theory provides a framework for understanding how particle shape, density, and interactions dictate the onset of ordering[13, 14]. In bacte-

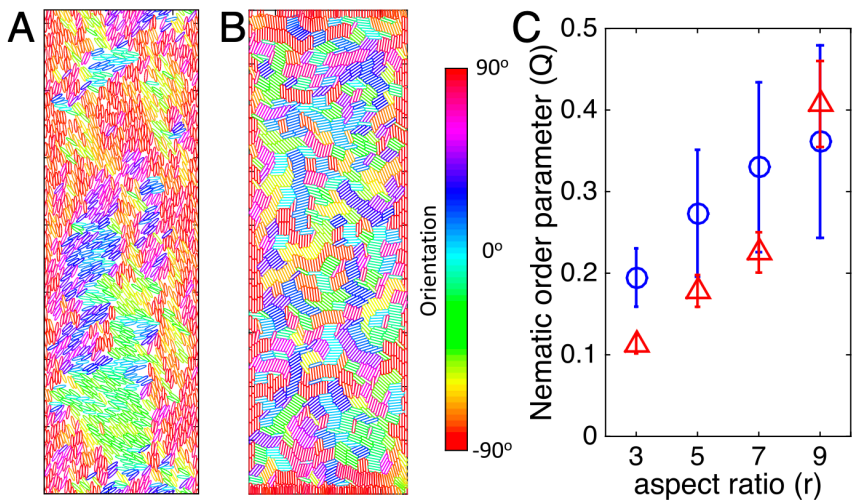

Figure 2.3: (A and B) Snapshots of the simulation at step 2,000 for (A) ellipses or (B) spherocylinders. Color code for the orientation of particles is displayed. (C) Nematic order parameter Q in a channel. Values of nematic order param- eter are shown as circles for elliptic particles or as triangles for spherocylin- ders. In these simulations, channels are set as 60 cells across the horizontal axis. Periodic boundary conditions are applied along the vertical axis. Two hard walls are implemented on the left and right boundaries. Figure and the caption is reprinted from Li et. al [20].

rial systems, elongated cell shapes and high packing densities enhance the likelihood of alignment due to excluded volume effects—where steric hindrance between cells favors orientations that minimize overlap [15, 11].

At lower densities, the random motion and orientation of bacteria dominate, maintaining an isotropic state Fig. 2.2(A). However, as density increases, the combined effects of steric interactions and mechanical contact forces between neighboring cells promote alignment Fig. 2.2(B-C) [16, 17]. This alignment grows stronger as the packing density approaches a critical threshold, at which point the colony undergoes a transition to a nematic phase. The nematic phase is characterized by local regions of aligned cells [18], as these regions are shown in Fig. 2.3 (A-B) with different color for both ellipses and spherocylinder particles, with their long axes oriented parallel to a preferred direction, while maintaining translational disorder [19].

This transition is further influenced by the growth and division of bacterial cells, which introduce additional mechanical stresses and alignment forces. Spatial confinement, such as that imposed by boundaries or neighboring colonies, amplifies these effects, driving the colony toward a more ordered state. The interplay between particle shape, short-range interactions, and spatial constraints highlights the complexity of isotropic-

nematic transitions in bacterial systems and their dependence on both physical and environmental factors [14].
Understanding these transitions provides insights into the collective behavior of bacterial colonies, including their growth dynamics, mechanical properties, and the emergence of large-scale order under constrained conditions.
The degree of ordering in such systems can be quantitatively described using the scalar order parameter, S, which measures the alignment of bacteria relative to each others,

$$S = \langle 2\cos_{ij}^2\theta - 1\rangle_{ij} \tag{2.4.1.1}$$

Where θ is the relative angle between two contact bacteria, and the notation $\langle\cdot\rangle_{ij}$ indicates an average over all pairs of bacteria i and j. This ensures that the order parameter reflects the collective orientation of the entire system. when the contact bacteria are perfectly aligned $S = 1$ and for the disordered state $S \approx 0$ [15, 21].
As it has shown in Fig. 2.2(D) and Fig. 2.3(C) both the length scale (aspect ratio) of cells and their population number play crucial roles in this transition. Longer bacteria exhibit stronger nematic ordering due to their increased tendency to align along a common axis, while higher cell densities increase the likelihood of contact-mediated interactions that promote nematic alignment. Additionally, the reorientation of neighboring bacteria through short-range forces contributes to localized alignment, which can propagate across the colony [22].

2.4.2 Buckling Instabilities in Bacterial Systems

Buckling instabilities in bacterial systems emerge when internal stresses, driven primarily by cellular growth, surpass the mechanical stability of the system. Under these conditions, aligned and straight bacterial chains become unstable, undergoing buckling either within the x-y plane or along the z-axis [23, 24]. Such instabilities manifest as localized perturbations in cellular alignment and can significantly disrupt nematic ordering within the colony. These distortions are typically driven by active forces arising from growth dynamics or by imbalances between contact forces and frictional forces, as well as interactions among cells and with the surrounding environment [26, 27, 28, 29, 30].
Figure 2.4 illustrates four possible modes of buckling in a bacterial chain. These include:

- In-plane symmetric mode (SM): A V-shaped deformation involving two cells rotating symmetrically (Fig. 2.4a).
- In-plane antisymmetric mode (AM): A deformation in which only one cell rotates (Fig. 2.4b).

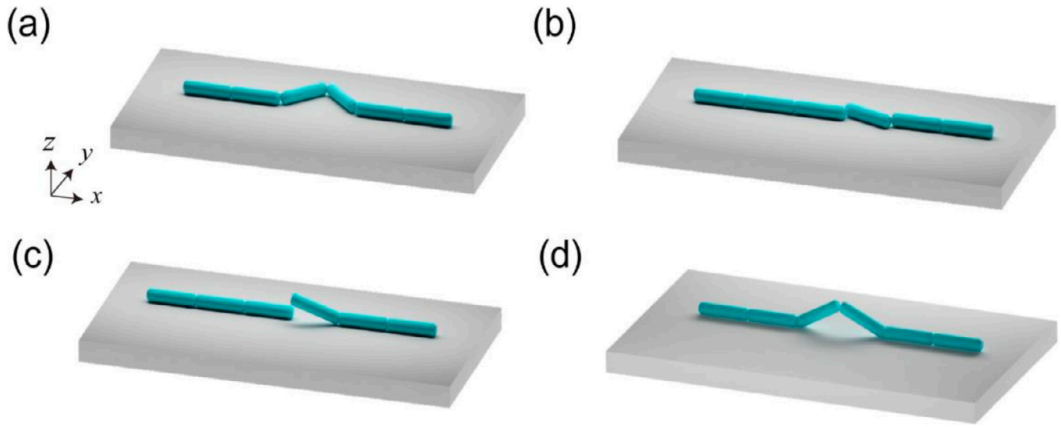

Figure 2.4: Schematic of four possible buckling modes in a bacterial chain. (a) In-plane V-shaped symmetric mode (SM) with two cells rotating symmetrically. (b) In-plane antisymmetric mode (AM) with only one cell rotating. (c) Out-of-plane AM mode where only one cell is extruded from the substrate. (d) Out-of-plane SM mode where two cells symmetrically ride up from the substrate. Figure and the caption reprinted from Liu et. al. [25].

- Out-of-plane antisymmetric mode (AM): One cell extrudes from the substrate, leading to vertical misalignment (Fig. 2.4c).
- Out-of-plane symmetric mode (SM): Two cells symmetrically rise from the substrate (Fig. 2.4d).

Such buckling modes are strongly influenced by local packing constraints, cellular interactions, and external boundary conditions.
The role of confinement in amplifying buckling instabilities is particularly significant. Boundaries, such as biofilm edges or rigid surfaces, constrain bacterial growth and promote stress accumulation, intensifying cell-cell interactions and distorting alignment. These effects give rise to heterogeneous configurations and complex spatial patterns that are often observed experimentally. Fig. 2.5 shows an example of such instabilities in a bacterial colony confined within a microfluidic trap. The local order parameter (indicated in red) highlights regions of disrupted alignment, with increasing instability over time (Fig. 2.5a, 2.5b).
Quantitatively, the critical chain length L_{cr} (length scale for chain of aligned bacteria), at which buckling occurs, depends on parameters such as adhesive drag ζ, as friction increases buckling instabilities by resisting lateral displacements, causing stress to accumulate within the bacterial chain. This resistance amplifies the internal forces required for reorganization, lowering the critical length for buckling and making the structure more prone to instability under growth-induced or external stresses.. Exper-

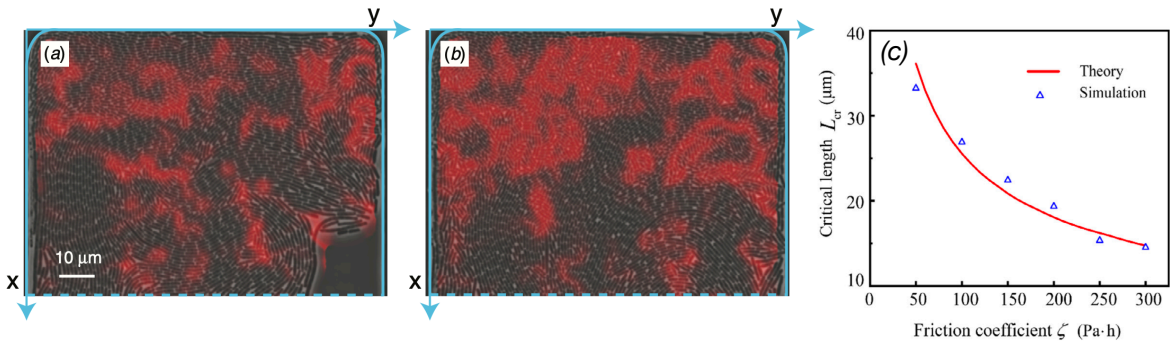

Figure 2.5: (a-b)Two snapshots with superimposed local order parameter from the experimental run in a $100 \times 90 \mu m^2$ side trap in which buckling instability was observed: (a) $t = 0$ min, (b) $t = 254$ min. Solid blue lines show the solid walls of the trap and the dashed blue lines show the open side. Red indicates low values of the local order parameter. Reprinted from Boyer et. al. (2011) [31]. (c) The critical chain length *Lcr* as a function of ζ. Triangle: particle simulations; Line: theoretical prediction. Figure and the caption reprinted from Li et. al (2020) [25].

imental and theoretical studies reveal that L_{cr} decreases with increasing ζ, as shown in Fig. 2.5c, which compares simulation results (triangles) with theoretical predictions (line) [31, 25].

Buckling instabilities offer valuable insights into the mechanical behavior of bacterial colonies, including their ability to reorganize, adapt, and persist under mechanical constraints. Understanding these phenomena has implications for biofilm formation, growth regulation, and the design of synthetic systems inspired by bacterial mechanics [12].

2.4.3 Local Packing Effects in Bacterial Ordering

The forces generated within a bacterial colony by cellular growth increase orientational entropy, disrupting the initial configuration. However, effective potential interactions and steric repulsion arising from contact forces compel neighboring cells to reorient and align laterally [32]. This lateral packing positions cells side by side in a more compact arrangement, optimizing space utilization and reducing the energy associated with continued compressive stress. In bacterial systems, variations in local packing significantly impact how cells interact and align on both microscopic and macroscopic scales. These variations play a critical role in the onset of nematic ordering, with denser regions exhibiting stronger nematic tendencies compared to sparsely packed areas [11, 14, 31].

2.4.4 Interplay of Buckling Instabilities and Local Packing in Bacterial Ordering

The interplay between buckling instabilities and local packing is a critical determinant of bacterial ordering. Variations in packing density, combined with boundary constraints, can induce transitions between ordered and disordered states. These transitions create regions of instability where nematic order fluctuates, leading to complex spatial and temporal behaviors [11, 14, 31].

Studies on bacterial systems reveal that both the degree of local packing and the onset of buckling instabilities influence intricate phenomena, such as the formation of microdomains or defects in bacterial alignment [33, 34]. These effects are modulated by the characteristic length scales of the system and the number of cells involved, underscoring the importance of microscopic and macroscopic interactions in shaping bacterial organization [11, 15, 21].

A deeper understanding of the isotropic-nematic transition, buckling instabilities, and local packing provides significant insights into the mechanisms governing microbial community behavior. The collective dynamics of bacterial colonies are shaped by particle length, packing density, and environmental constraints, which in turn influence processes like biofilm formation, motility, and responses to external forces. Such insights are pivotal for unraveling the principles behind bacterial adaptation and structural organization in diverse environments.

2.5 Population Dynamics and Bacterial Growth

Modeling bacterial population dynamics is essential for understanding growth behavior under diverse environmental and mechanical constraints. Bacteria display distinct growth regimes influenced by factors such as nutrient availability, interspecies competition, spatial limitations, and mechanical stresses. Mathematical models are widely employed to study these dynamics, offering quantitative insights into the relationship between individual cell behavior and collective population trends.

2.5.1 Exponential Growth

In nutrient-rich environments with minimal limitations, bacterial populations generally follow an exponential growth pattern. This growth can be expressed mathematically as:

$$\frac{dN(t)}{dt} = \mu N(t), \tag{2.5.1.1}$$

where $N(t)$ represents the population size at time t, and μ denotes the per-capita growth rate. The solution to this differential equation predicts exponential population growth:

$$N(t) = N(0)\exp^{\mu t} = N(0)2^{\frac{t}{T}}, \tag{2.5.1.2}$$

where $T = (\ln 2)/\mu$ is the doubling time, defined by $N(t+T) = 2N(t)$. For *E. coli* in nutrient-rich media, the doubling time T is approximately 20 minutes [35].

2.5.2 Logistic Growth

While the exponential growth model (Eq. 2.5.1.1) effectively describes early-phase bacterial growth, it becomes inaccurate when populations encounter resource limitations or spatial constraints. In such cases, growth slows and saturates as the population approaches a carrying capacity K. This behavior is captured by the logistic growth model [35, 36]:

$$\frac{dN}{dt} = \mu N\left(1 - \frac{N}{K}\right), \tag{2.5.2.1}$$

where K is the maximum population size the environment can support. The term $\left(1 - \frac{N}{K}\right)$ reduces the effective growth rate as N approaches K, reflecting the impact of nutrient depletion or accumulation of toxic byproducts. Solving Eq. 2.5.2.1 yields:

$$N(t) = \frac{N(0)\exp^{\mu t}}{1 + \frac{N(0)}{K}\left(\exp^{\mu t} - 1\right)}, \tag{2.5.2.2}$$

showing that population growth slows and eventually saturates at K.

2.5.3 Nutrient-Limited Growth

In environments where nutrient availability becomes the limiting factor, bacterial growth depends on the substrate concentration, $S(t)$. The relationship between bacterial growth and substrate availability is commonly modeled as [37, 38]:

$$\frac{dN(t)}{dt} = \mu(S)N(t), \tag{2.5.3.1}$$

where $\mu(S)$ represents the growth rate as a function of the substrate concentration. Using the Monod equation, the growth rate is given by:

$$\mu(S) = \mu_{\max} \frac{S(t)}{K_s + S(t)}, \tag{2.5.3.2}$$

where $\mu_{\max}$ is the maximum growth rate, K_s is the half-saturation constant (substrate concentration at which $\mu = \mu_{\max}/2$), and $S(t)$ is the substrate concentration at time t. As bacteria grow, they consume available nutrients, reducing $S(t)$ over time. For low S, $\mu(S)$ is approximately linear, while for high S, it approaches $\mu_{\max}$, reflecting the finite capacity of individual cells. The relationship between substrate consumption and population growth is expressed as:

$$\frac{dS}{dt} = -\frac{1}{Y}\mu(S)N, \tag{2.5.3.3}$$

where Y is the yield coefficient [1], describing the biomass produced per unit of substrate consumed. By substituting the Monod equation into the growth equation, we obtain:

$$\frac{dN}{dt} = \mu_{\max} \frac{S(t)}{K_s + S(t)} N. \tag{2.5.3.4}$$

Numerical solutions of Eqs. 2.5.3.4 and 2.5.3.3 predict that population size saturates as nutrients are depleted [35, 37].

The study of bacterial population dynamics highlights the intricate interplay between environmental conditions, nutrient availability, and growth constraints. Mathematical models, such as exponential, logistic, and nutrient-limited growth frameworks, provide powerful tools for predicting population behavior under varying scenarios. By capturing the transition from unconstrained exponential growth to saturation due to resource depletion or spatial limitations, these models offer insights into both the ecological and mechanical factors that shape microbial communities. Understanding these dynamics is essential not only for fundamental biology but also for applications in biotechnology, medicine, and environmental science, where managing bacterial populations plays a critical role.

[1] The yield coefficient represents the amount of biomass produced per unit of substrate consumed, capturing the efficiency of nutrient conversion into growth.

3 Biological Background

In this chapter, I introduce terminology and general background information from biology necessary to evaluate the content of this thesis. This includes an overview of the bacteria studied, focusing on their transition from a planktonic state to structured communities, such as biofilms and non-motile bacterial colonies. Particular attention is given to distinguishing these states and understanding how environmental factors influence their formation. I then begin with a short introduction to the rod-shaped bacterial growth dynamics and division, outlining the fundamental processes governing bacterial proliferation. Particular attention is then given to how these growth dynamics are influenced by mechanical forces and stresses, highlighting their impact on the spatial organization, division orientation, and overall behavior of bacterial colonies. This framework sets the stage for understanding the interplay between biological and mechanical factors in the systems studied in this work.

3.1 From Planktonic Bacteria to Non-Motile Colonies

Bacteria exhibit remarkable adaptability, thriving across diverse environments by dynamically altering their physiological and structural states. A central aspect of this adaptability is their transition from a planktonic, free-swimming state to more structured communities, such as biofilms or bacterial colonies. Understanding the pathways leading to these distinct states sheds light on the environmental and biological factors that drive bacterial collective behaviors.

3.1.1 The Planktonic State: A dynamic existence

In the planktonic state, bacteria exist as individual cells, swimming actively or passively drifting in liquid environments. This state is highly dynamic, characterized by bacterial motility and chemotaxis, which allow cells to navigate toward nutrient-rich zones or away from harmful stimuli [39].
As it has show in Fig. 3.1 motile bacteria are often observed moving along nutrient gradients, gravitating toward regions of higher nutrient availability. However, the

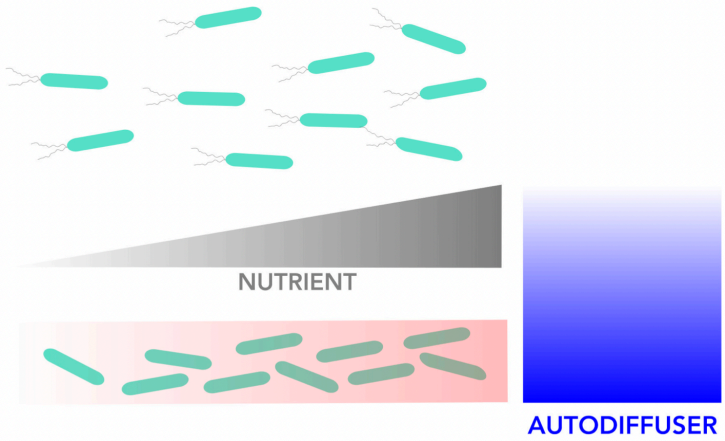

Figure 3.1: Bacteria can exist in two different states: a motile state in which they can disperse freely around their environment (top), and an immobile state in which they live together in static as a biofilm (bottom). The red gradient in the biofilm box indicates to which extent bacterial density is increasing in the biofilm from left to right alongside rising nutrient concentrations (grey gradient). The motile bacteria move towards increasing nutrient concentration to the right. The concentration of autodiffusers (molecules produced by bacteria which trigger biofilm formation; blue gradient), is highest close to the biofilm and decreases further away. Figure and the caption reprinted from Pradeep et al. [41].

planktonic lifestyle is often transient. Environmental stresses such as nutrient scarcity, changes in shear flow, or surface encounters prompt bacteria to transition to more stable and cooperative modes of existence. During this transition, bacteria begin to secrete extracellular polymeric substances (EPS), forming the structural foundation of a biofilm [40]. Overall, the switch to immobile biofilm formation is controlled by bacterial dispersion, which is dependent on nutrient levels, and occurs when the concentration of bacterial molecules known as autoinducers exceeds a certain threshold. These autoinducer signals serve as a proxy for the presence of other bacterial cells in the environment, triggering intracellular pathways that regulate gene expression and determine the lifestyle bacteria will adopt. Once the biofilm is established, its maintenance depends on the continued production of autoinducer molecules by immobilized bacteria [41].

The process of biofilm formation begins when planktonic bacteria come into contact with a surface, triggering the initial attachment phase [40]. This attachment, influenced by environmental factors such as nutrient availability and surface properties, sets the stage for the formation of a biofilm [42, 43].

As it has shown in Fig. 3.2 bacteria attach, they begin producing extracellular polymeric substances (EPS) [44], which support the development of a complex biofilm

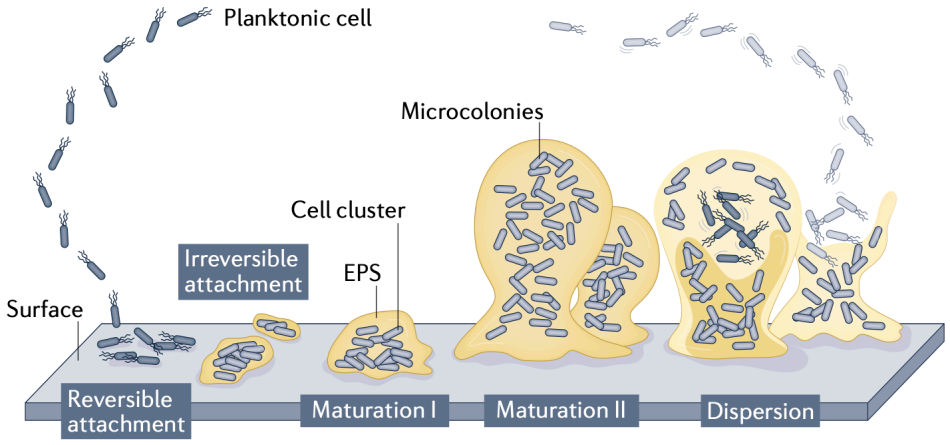

Figure 3.2: The original model of biofilm formation is based on key publications investigating Pseudomonas aeruginosa. The model proposed that the formation of biofilms is a cyclic process that occurs in a five-stage specific and progressive manner. The process is initiated following surface contact by single planktonic cells. Several developmental steps are discernible, including reversible attachment, irreversible attachment, biofilm maturation (maturation I and maturation II) and, finally, dispersion [47, 48]. During reversible attachment, bacteria attach to the substra- tum via the cell pole or via the flagellum, followed by longitudinal attachment. Transition to irreversible attachment coincides with a reduction in flagella reversal rates, a reduction in flagella gene expression and the production of biofilm matrix components. This stage is also characterized by attached cells demonstrating drug tolerance [49]. Biofilm maturation stages are characterized by the appearance of cell clusters that are several cells thick and are embedded in the biofilm matrix (maturation I stage), which subsequently fully mature into microcolonies (maturation II stage)[47, 48]. Dispersion has been reported to coincide with the decrease in and degradation of matrix components, with dispersed cells being motile and demonstrating increased drug susceptibility relative to biofilm cells. Figure and the caption reprinted from Sauer et. al. [46].

structure [45]. This biofilm is characterized by clusters of bacteria embedded in a matrix, offering increased resistance to environmental stressors and antimicrobial agents. The biofilm formation follows a specific, progressive cycle that includes reversible and irreversible attachment, maturation in two stages, and ultimately dispersion[50, 51]. The reversible attachment stage involves bacteria adhering loosely to surfaces via their flagella, whereas irreversible attachment is marked by a reduction in flagella function and the production of matrix components, which enhances drug tolerance. The maturation stages see the biofilm grow more complex, with cells forming thick clusters embedded in the matrix, eventually maturing into microcolonies. Dispersion occurs when the matrix breaks down, releasing motile cells that are more susceptible to drugs compared to their biofilm counterparts, completing the cycle [46].

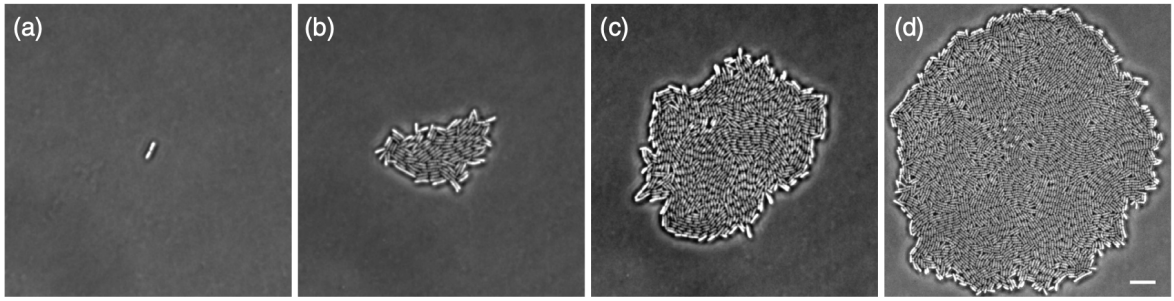

Figure 3.3: Growth of a bacterial colony. (a)–(d) Phase-contrast micrographs at different time points capture the growth of a single cell of a nonmotile strain of *Escherichia coli* (strain NCM 3722 delta-motA) into a two-dimensional colony under free boundary conditions. The scale bar corresponds to $10\mu m$. The cell doubling time was 43.5 ± 2.2 minutes. After 12 generations (d), the colony began to escape into the third dimension, forming a second bacterial layer. Figure and caption reprinted from You et al. [11].

3.1.2 Formation of Non-motile Bacterial Colonies

Bacterial communities can form either colonies or biofilms, depending on environmental conditions. Some species primarily form colonies, and in certain cases, colonies emerge even in early growth stages without transitioning into biofilms [15, 52].
In nutrient-rich environments, bacteria often prioritize rapid division over extracellular polymeric substance (EPS) production, leading to loosely packed colonies. Weak surface adhesion and the absence of biofilm-inducing signals, such as quorum-sensing molecules or surface shear, further promote colony formation. Mechanical constraints, such as confinement in host tissues, can also favor colonies by enhancing direct cell-cell interactions over stable surface attachment [53, 54, 55]. The growth dynamics of such colonies can be observed in Fig. 3.3, which illustrates the expansion of a non-motile *Escherichia coli* colony over time.

3.2 Mechanisms of Growth and Division in Bacteria

Bacterial growth dynamics are essential for understanding the behavior and development of bacterial colonies. Rod-shaped bacteria, in particular, exhibit unique patterns of growth and division, which are influenced by both environmental factors and internal cellular processes, in which we focus on this thesis.

3.2.1 Bacterial Phase Diagram

Bacteria, as unicellular organisms, exhibit diverse growth patterns influenced by their shape, nutrient availability, and environmental conditions. Regardless of morphology,

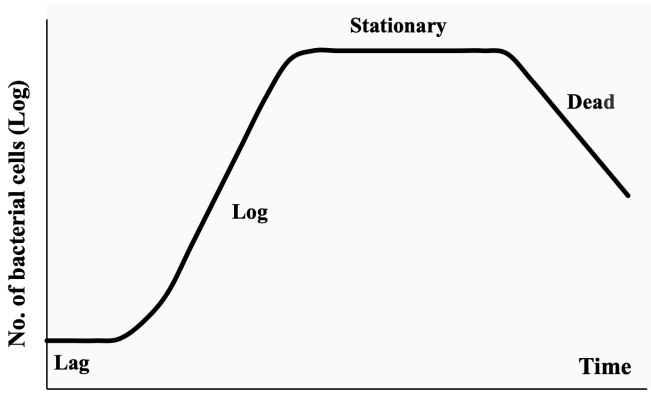

Figure 3.4: When bacteria are introduced into the fresh medium in a closed system, like a test tube, the population of cells always exhibits growth dynamics as follows. Lag phase: bacteria initially adjust to the new environment, so they appear not able to replicate but the cells might grow in volume; Log (exponential) phase: cells start dividing regularly by the process of binary fission. The culture reaches the maximum growth rate, which could be estimated by generation time or doubling time, i.e., the time per generation; Stationary phase: the number of cells undergoing division seems to be equal to that being dead due to the exhaustion of nutrients. Dead phase: bacteria lose the ability to divide and the number of dead cells exceeds that of live cells. Fig. and the caption reprinted from Wang et. al [56].

bacterial growth generally involves two key processes: elongation and division. These processes are regulated by internal cellular machinery and external factors, such as the availability of nutrients like glucose, amino acids, and minerals, which provide the essential building blocks for energy production, macromolecule synthesis, and cell wall formation.

Bacterial growth typically follows a characteristic pattern represented by a growth phase diagram Fig 3.4. In the lag phase, bacteria adapt to their environment, metabolizing nutrients without immediate division. The log phase marks the most active period of growth and division. As resources deplete or environmental stresses intensify, growth slows, leading to the stationary phase, where the rate of division balances with the rate of cell death. Finally, the death phase ensues as nutrient scarcity or waste accumulation causes the population to decline exponentially [35, 56].

3.2.2 Bacterial Division

Among the diverse bacterial shapes, rod-shaped bacteria, such as Escherichia coli, Bacillus subtilis, exhibit unique patterns of growth and division tailored to their cylindrical structure. Unlike spherical bacteria, which grow isotropically; however, in rod-shaped bacteria, division typically occurs at mid-cell through the formation of a septum

[1], a constricted region where new cell wall and membrane materials are synthesized to separate daughter cells.

As it has shown in Fig. 4.5(a) rod-shaped *Escherichia coli* cell is preparing for division, the bacterial cell contains two nucleoids, symmetrically positioned within its cytoplasm. These nucleoids, which house the bacterial DNA, have already undergone replication and segregation, ensuring that each daughter cell will inherit a complete genetic copy. The central region of the cell, free from nucleoid presence, is where the division machinery assembles. This positioning is no coincidence; the absence of nucleoids at the mid-cell ensures that the division process will not damage the DNA.

One of the crucial mechanisms guiding this process is the MinCDE system. In the figure 4.5, we see the MinC [2] gradient illustrated with arrows. This gradient, with high concentrations of the division inhibitor MinC near the poles and low concentrations at the mid-cell, prevents improper assembly of the division machinery at the cell poles. Instead, the gradient directs the formation of the FtsZ protein [3] ring—the Z-ring (green circle)—at the center of the cell [57].

The Z-ring is prominently depicted in the figure, encircling the cell at mid-cell. This ring serves as a scaffold for additional proteins that will form the divisome, a complex of enzymes and structural proteins responsible for synthesizing new cell wall and membrane material. The nucleoid occlusion mechanism complements the MinC gradient, further ensuring that the Z-ring forms only in regions devoid of DNA.

As the division process progresses, the Z-ring begins to constrict, guiding the synthesis of a septum that will ultimately separate the parent cell into two daughter cells. These daughter cells will inherit one nucleoid each and maintain the cylindrical shape characteristic of rod-shaped bacteria [58].

In contrast, Bacillus subtilis, another rod-shaped bacterium, employs a slightly different strategy during division. The process involves the formation of a cross wall of peptidoglycan, which initially divides the cytoplasm of the parent cell into two compartments. For vegetative growth, this cross wall is remodeled and cleaved to allow complete separation of the daughter cells. However, under specific conditions, such as nutrient limitation, Bacillus subtilis may form an asymmetrical septum, setting the stage for spore formation. This adaptability underscores the versatility of Bacillus sub-

[1] Septum is a partition formed by the inward growth of the cell membrane and cell wall that divides the mother cell into two daughter cells.

[2] MinC is a bacterial protein that, in cooperation with MinD and MinE, regulates the positioning of the division septum during cell division in rod-shaped bacteria, preventing septum formation at the poles.

[3] FtsZ is a bacterial protein that assembles into a ring at the site of cell division, known as the Z-ring, and coordinates the formation of the septum, facilitating cell division in bacteria.

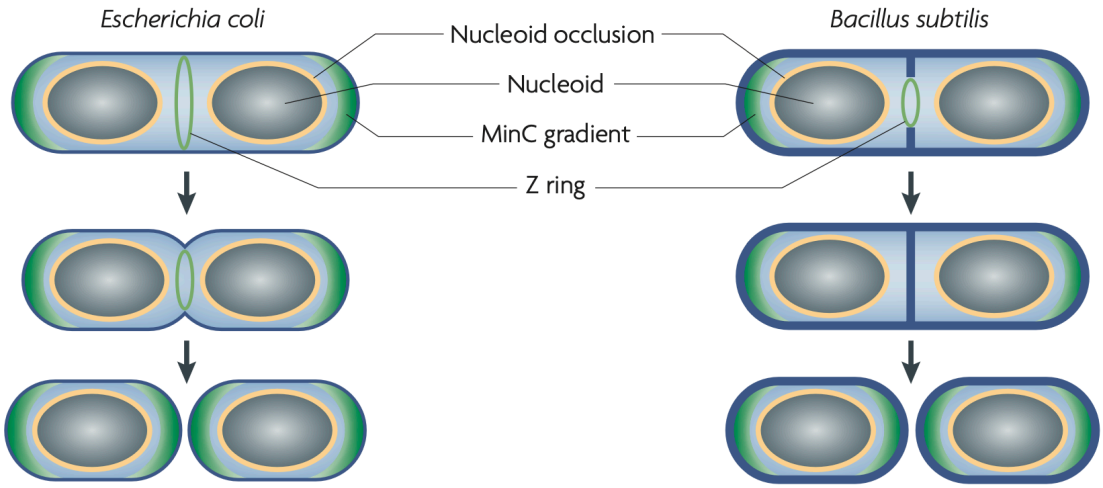

Figure 3.5: Two different modes of division. After chromosome replication and segregation into nucleoids the Z ring assembles at mid-cell. The ring then constricts to bring about division. Cell wall Cooperative assembly Nature Reviews | Microbiology synthesis follows the ring inwards. In *Escherichia coli*, synthesis of the division septum is accompanied by constriction of the outer membrane. In Bacillus subtilis, a cross wall of peptidoglycan initially divides the cell before it is degraded and remodelled to form the new, hemi-spherical cell poles. b | The spatial regulation of Z ring assembly. Nucleoid occlusion (NO), which is mediated by Noc (in B. subtilis) or SlmA (in E. coli), inhibits Z ring assembly close to the nucleoid. The Min system acts to prevent Z ring assembly at the cell poles (for simplicity, the Min dynamics in *E. coli* have been omitted). From left to right: in 'newborn' cells, both systems initially inhibit Z ring assembly throughout the cell; following cell elongation and chromosome replication, NO maintains inhibition in the cylindrical part of the cell; and finally, the progression of chromosome segregation reveals an inhibitor-free region at mid-cell, allowing the Z ring to assemble. Figure and the caption reprinted from Adam et. al. [58].

tilis in responding to environmental cues. These distinctions between *Escherichia coli* and *Bacillus subtilis* are rooted not only in their division strategies but also in their broader classification as gram-negative [4] and gram-positive [5] bacteria, respectively. The structural and functional differences associated with these classifications, such as variations in cell wall composition, will be explored in detail in the following section.

Additionally, the orientation of division is influenced by factors such as cellular shape, environmental cues, and mechanical constraints. In confined spaces or under specific growth conditions, the orientation and timing of division can be affected, leading to altered colony structures or patterns.

The biological context of bacterial growth extends beyond simple cell division. Factors such as nutrient availability, metabolic state, and mechanical forces significantly impact bacterial colony development. For rod-shaped bacteria, growth is not uniform across the entire cell but rather localized to specific regions. Mechanical stress or environmental interactions can disrupt the balance between elongation and division, resulting in morphological changes or the formation of distinct colony patterns. Additionally, changes in external conditions such as nutrient limitation or confined environments can influence bacterial organization, leading to non-motile colonies where cell-cell interactions dominate over surface adherence.

This framework highlights how bacterial colonies grow and adapt, integrating both biological regulation and environmental influences to shape their behavior and spatial organization.

3.3 Bacterial Mechanosensitivity

Bacteria, whether in a planktonic state—free-swimming or floating in liquid—or in a sessile biofilm state, are consistently subjected to mechanical forces from their environment. These forces can originate externally, such as from fluid flow or mechanical compression, or arise from cell-cell interactions within bacterial communities. The long evolutionary history of bacteria suggests that they have developed sophisticated mechanisms to adapt and respond to varying mechanical stresses, indicating an ability to actively sense and process mechanical cues [59] [60, 61, 62].

[4] Gram-negative bacteria are characterized by a thin peptidoglycan layer and an outer membrane containing lipopolysaccharides (LPS), which contribute to their resistance to certain antibiotics and environmental factors.

[5] Gram-positive bacteria are characterized by a thick peptidoglycan layer and the absence of an outer membrane. Their cell wall contains teichoic acids, which contribute to structural stability, adhesion, and interactions with the environment

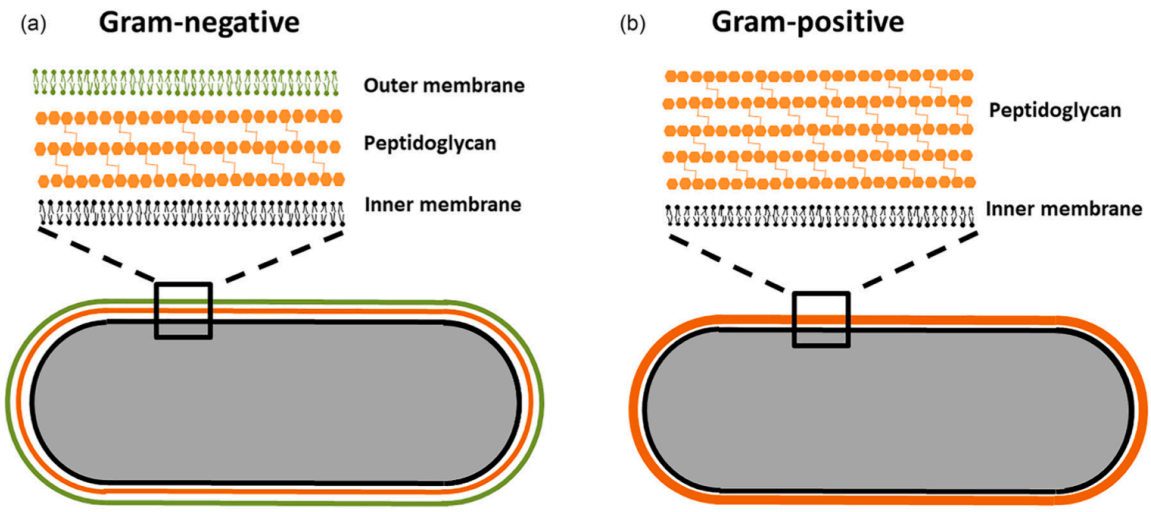

Figure 3.6: (a) Gram-negative bacteria have an inner membrane, peptidoglycan, and an outer membrane. (b) Gram-positive bacteria have an inner membrane and peptidoglycan. Figure and the caption are reprinted from Harper et. al. [70].

Mechanosensitivity in bacteria is facilitated through a variety of structures and components capable of sensing mechanical forces over different length scales [63, 64]. As illustrated in Fig. 3.6(a), in gram-negative bacteria, an additional layer of complexity exists due to the presence of two distinct membranes—the outer and inner membranes—along with the periplasmic space in between [65].

This contrasts with gram-positive bacteria, which lack an outer membrane and instead possess a thicker peptidoglycan layer that provides both structural integrity and resistance to mechanical deformation, as shown in Fig. 3.6(b). These fundamental differences between gram-negative and gram-positive bacterial envelopes [6] suggest that the mechanisms of mechanosensitivity may vary significantly between these groups, warranting comparative investigation.

Membrane proteins, typically a few nanometers, which are placed in the membrane, have been implicated in mechanosensing [66, 67]. These proteins could serve as localized sensors, responding to mechanical forces that occur on nanometer scales. However, it is unclear whether these membrane proteins function solely as localized sensors or require deformation of the entire cell envelope to activate mechanosensing. The structural differences between gram-negative and gram-positive bacteria, particularly in their cell envelopes, raise intriguing questions about how each group perceives and processes mechanical forces [68, 69]. For example, does the thicker peptidoglycan layer in gram-positive bacteria confer unique mechanosensitive properties, or does the dual-membrane

[6] Together the cell membrane(s) and cell wall are referred to as the bacterial envelope

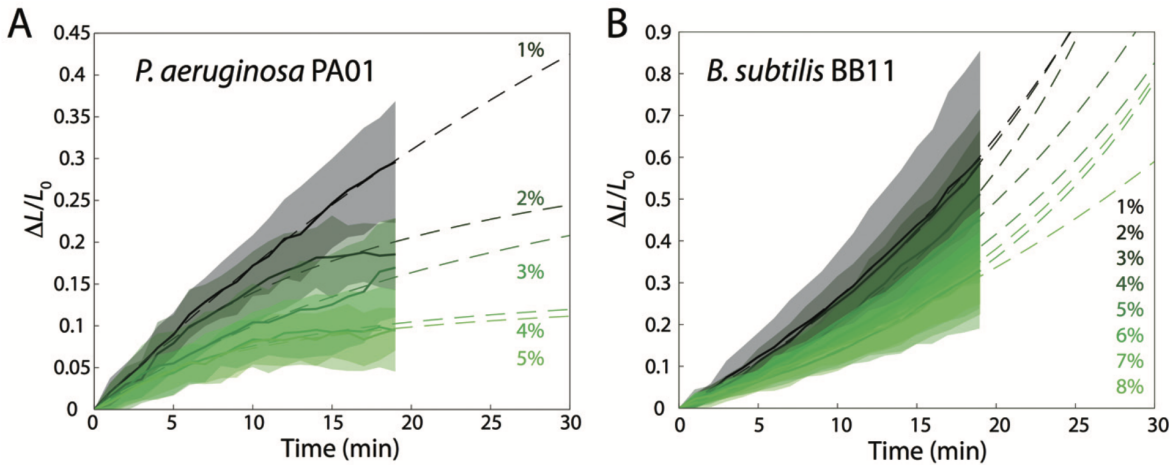

Figure 3.7: (A) *P. aeruginosa* PAO1 and (B) *B. subtilis* BB11 cells exhibit growth inhibition when embedded in agarose gels of increasing stiffness. Solid lines represent average growth curves, while dashed lines depict early growth trends during the first 20 minutes. Shaded regions indicate one standard deviation above and below the mean growth curves. Figure and caption modified from Tuson et al. [77].

architecture of gram-negative bacteria provide additional avenues for mechanotransduction? These questions remain largely unanswered due to the limited understanding of bacterial envelope proteins and their mechanosensory roles [70, 71].

In addition to external forces, bacterial growth can be significantly influenced by mechanical stresses arising from cell-cell interactions [72, 73]. When bacteria interact via their lateral sides or through single-point contacts, the impact on growth may be less pronounced. However, when both tips of the bacterial cell are involved in interactions, these forces appear to have a more substantial effect on their growth dynamics [74, 75]. This suggests that the spatial distribution and magnitude of mechanical forces within bacterial communities play a crucial role in regulating cellular behavior [76].

A clear example of how mechanical constraints influence bacterial growth is seen when bacteria are encapsulated in stiff environments, such as agarose gels. Both gram-negative and gram-positive species experience growth inhibition under such conditions. This effect is evident in the growth curves of *Pseudomonas aeruginosa* PAO1 (a gram-negative species) and Bacillus subtilis BB11 (a gram-positive species) when embedded in agarose gels of varying stiffness. As shown in Fig. 3.7, increasing agarose concentration leads to a significant reduction in bacterial elongation and division rates, demonstrating how mechanical confinement can limit growth.

Interestingly, the growth curves of *B. subtilis* BB11 displayed an upward curvature at longer time scales, suggesting a potential increase in growth rate due to mechanical tearing of the gel at high strains (15%). To prevent this effect from influencing our

conclusions, only data from the first five minutes of encapsulated growth were used to determine cell stiffness [77].

For gram-negative bacteria, the inhibition of *E. coli* and P. aeruginosa growth was observed at a similar stiffness threshold of the surrounding gel (Egel). This indicates that the mechanical properties of gram-negative peptidoglycan are largely conserved across species. Such consistency has important implications for molecular-level modeling of peptidoglycan organization, as it suggests that the same mechanical parameters can be applied across different gram-negative species. This simplifies theoretical models of cell wall mechanics by reducing the need for species-specific adjustments to peptide cross-link stiffness [78, 79, 80].

This phenomenon suggests that mechanical forces, whether from direct cell-cell contact or confinement within rigid environments, can significantly alter bacterial physiology. While previous studies have primarily focused on biochemical regulators of bacterial growth, these findings emphasize the necessity of considering mechanical constraints as a key factor in bacterial development.

Understanding bacterial mechanosensing will be critical for comprehending how bacteria adapt to physical stresses and interact with their environment, which has implications for fields ranging from infection biology to biotechnology. *Escherichia coli*, for example, frequently encounters mechanical stresses in its natural habitats, such as turbulent flow in aquatic environments, shear forces in host tissues, or mechanical compression within biofilms. Despite the ubiquity of these forces, the relationship between mechanical stress and bacterial growth dynamics remains poorly understood.

To address this gap, an experiment was conducted to evaluate how mechanical stress affects the growth of *E. coli* under controlled laboratory conditions. By systematically varying mechanical constraints, this study aims to elucidate the mechanisms by which bacterial growth adapts to physical stressors, ultimately contributing to a deeper understanding of bacterial behavior in real-world environments.

3.3.1 Experimental Investigation of Mechanical Stress on *E. coli* Growth Using a Microfluidic Device

To explore how mechanical stress affects bacterial growth, a novel air-driven microfluidic device was developed to apply controlled compressive forces on *Escherichia coli* cells. As it has shown in Fig. 3.8 the device features two chambers—a top air chamber and a lower cell culture chamber—separated by a thin polydimethylsiloxane (PDMS) layer, $200\mu m$ thick. By introducing positive pressure into the air chamber, the PDMS

layer deforms downward, exerting mechanical compression on the E. coli cells cultured below.

Hexagonally arranged micropillars, deposited onto the coverglass within the cell culture chamber, serve as structural supports during compression. These pillars, fabricated from a photoresist material, have a diameter of $6\mu m$, a height of approximately [0.8 - 0.9] μm, and are spaced $10\mu m$ apart. This design ensures precise control of compression while maintaining sufficient space for observing cellular responses.

Before compression, phase-contrast microscopy revealed that *E. coli* cells swam freely and diffused throughout the chamber. Some cells adhered to the chamber floor, coated with poly-ethylenimine to enhance surface interactions. Scanning electron microscopy (SEM) provided a closer look at the micropillar arrangement, confirming the uniformity and consistency of the fabricated structures. This sophisticated microfluidic setup enabled the investigation of mechanical stress effects on bacterial growth and behavior at a high level of precision.

Variation of the hight of the micropillar control the deformation of the bacteria and their growth rate. It has been shown in Fig. 3.9 as the hight of the micropillar is equal to half of the bacterial diameter the volume change of the bacteria goes to zero. One possible explanation is that due to the compression DNA segregation perturbed and leads the bacteria to stop growing [81].

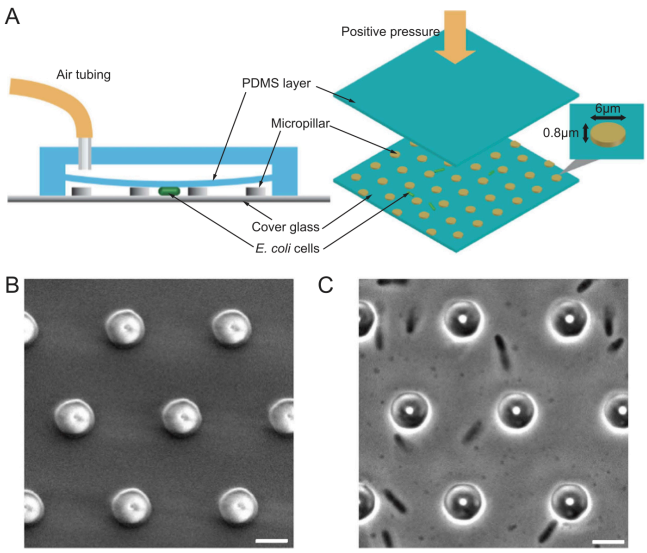

Figure 3.8: (A) Left: Side view of the device. The device contains two chambers. The upper air chamber and lower cell culture chambers are separated by a PDMS layer of $200\mu m$ in thickness. The PDMS layer is deformed downward to compress cells in the culture chamber when there is positive pressure in the air chamber. Micropillars made by a photoresist are deposited onto the coverglass, which support the PDMS layer when pressure is applied. Right: 3D view of the device. Mircopillars are patterned hexagonally with a distance of $10\mu m$ between pillars. Pillar diameter is $6\mu m$ and typical height is $0.8\breve{}0.9\mu m$. (B) Low vacuum scanning electron microscopy image of micropillars on the coverglass. (C) Phase contrast image of live *E. coli* cells distributed in the culture chamber between micropillars. Before compression, cells swim and diffuse within the chamber normally. Some cells adhere onto the bottom from the poly-ethylenimine coating. (Scale bars, $5\mu m$). Figure and the caption reprinted from Si et. al [81].

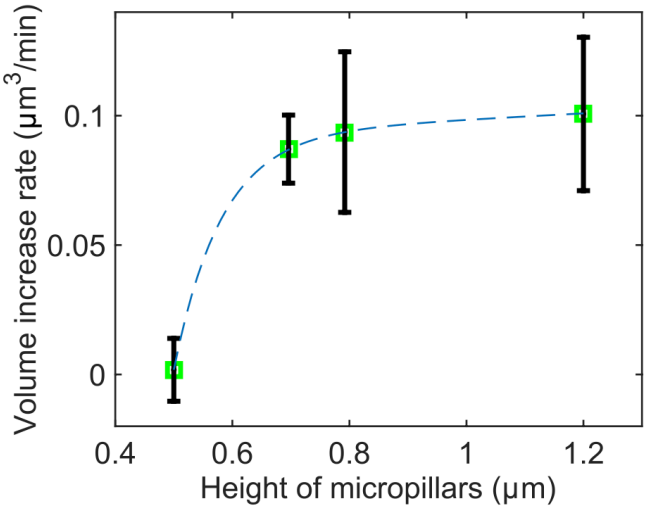

Figure 3.9: Volume growth rate as a function of mircopillar height (equal to the thickness of compressed cells). Cells no longer grows when the height is $0.5\mu m$. ($n \geq 7$ for each point. Error bars indicate standard deviation.) Figure and the caption reprinted from Si et. al. [81].

3.3.2 Experimental Investigation of Pressure and Temperature Dependence of Growth of *Escherichia Coli*

In natural environments, bacteria are frequently exposed to external mechanical pressures that influence their survival and growth. For instance, in aquatic ecosystems, bacterial colonies attached to surfaces such as rocks or plants experience shear forces from flowing water. In soil, bacterial communities within micropores face compressive forces from surrounding particles and shifting soil matrices due to moisture fluctuations or mechanical disturbances. Within host organisms, pathogenic bacteria [7] encounter external pressures from immune responses, such as macrophages [8] exerting physical forces during phagocytosis [9] , or compressive forces in confined tissues. These diverse scenarios illustrate how bacteria must adapt to varying mechanical challenges to sustain their growth and maintain their functions in dynamic environments.

To explore how bacterial cells adapt to extreme pressure and temperature, this study investigated the growth and phenotypic [10] changes of *Escherichia coli* under varying

[7] Pathogenic bacteria are bacteria that cause disease by producing toxins, evading immune defenses, or damaging host tissues, leading to infections and illnesses.

[8] Macrophages are immune cells that engulf and digest pathogens, dead cells, and other debris. They play a key role in the body's defense against infections and in initiating immune responses.

[9] Phagocytosis is the process by which immune cells, such as macrophages, engulf and digest pathogens, dead cells, and other foreign particles to protect the body from infection.

[10] Phenotypic refers to the observable traits or characteristics of an organism, such as appearance, behavior, and physiological functions, which result from the interaction of its genotype and environment.

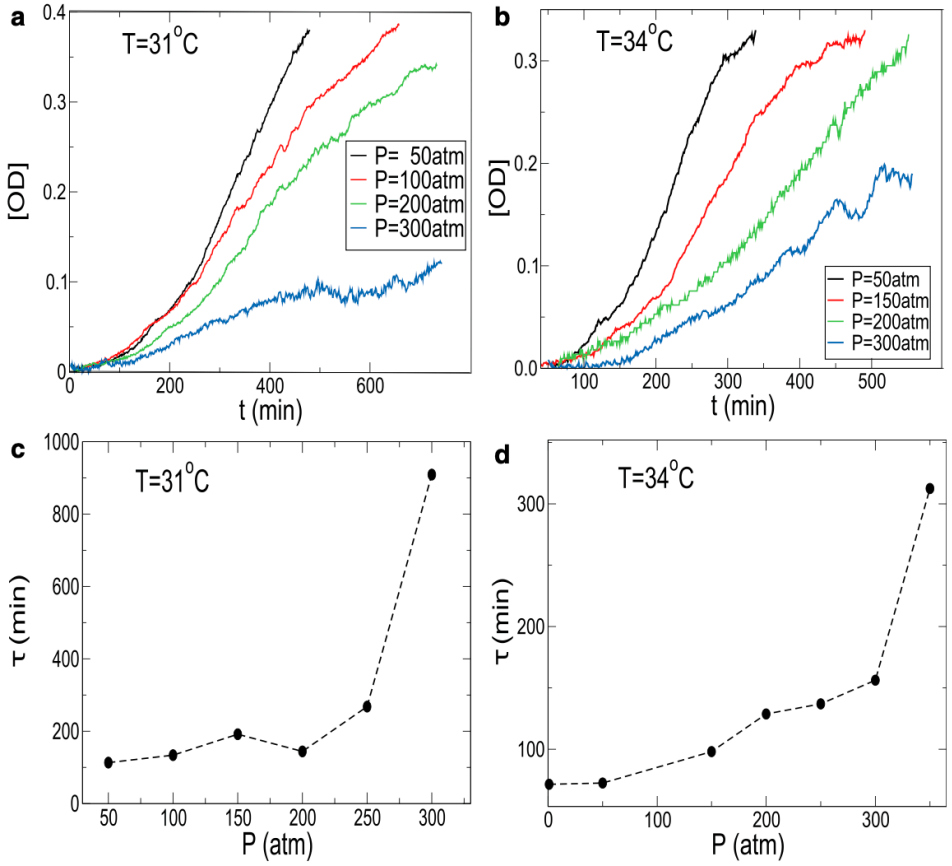

Figure 3.10: (a) Growth curves at different pressure for $T = 31^{\circ}$C. (b) Growth curves at different pressures for $T = 34^{\circ}$C. (c) Doubling time ζ(P) extracted from Fig. 3 a. (d) Doubling time ζ(P) extracted from Fig. 3 b. Pressure dependence of ζ(P) is marked by a sharp increase at high pressure where the cells still grow, but the growth is extremely slow. Figure and the caption reprinted from Kumar et. al. [82].

thermodynamic conditions. The researchers aimed to identify growth bottlenecks and understand physical changes induced by these conditions on a mesophilic bacterium. Using a real-time optical measurement method, they analyzed the pressure-temperature dependence of bacterial growth and morphological changes.

The experimental setup consisted of a high-pressure cell containing a bacterial sample in Luria Broth (LB) medium, housed within a fused silica rectangular cuvette. Pressure was applied using a piston, with water pressure monitored via a pressure gauge. Growth was measured by shining a 586-nm light beam through the sample and detecting the transmitted light intensity using a silicon photodiode-based photosensor. The system was regulated by a LABVIEW interface, and the temperature was controlled using a water-bath thermostat. Experiments, lasting 200 to 1000 minutes, were conducted in oxygen-limited conditions due to the closed design of the setup, with an oxygen partial pressure of 20 kPa in the LB medium.

As it is shown in Fig. 3.10(a-b) the effects of pressure on bacterial growth dynamics were investigated at two temperatures, $T = 31^{\circ}$C and $T = 34^{\circ}$C . Where saturation was achieved within the experimental timeframe, the growth profiles exhibited typical characteristics similar to those observed at $1atm$ and $T = 31^{\circ}$C.
Analysis of the extracted time parameter $\zeta(P)$, shown in Fig. 3.10(c) and Fig. 3.10(d), reveals that $\zeta(P)$ increases with rising pressure. This indicates a slower growth rate as pressure increases. Additionally, the optical density (OD) in the saturation phase decreases with increasing pressure, suggesting a reduction in total biomass production under higher pressure. These findings align with previous studies that observed similar declines in biomass production in response to elevated pressure across various bacterial species. It has also been shown that at both low and high temperature the doubling time increase by increasing the pressure. The study also examined the relationship between pressure and bacterial doubling time in the low-pressure regime. It was observed that the doubling time increases exponentially with pressure in this regime. Moreover, the rate of this exponential increase is temperature-dependent, with the exponent growing larger as the temperature decreases.
This finding highlights the interplay between pressure and temperature in influencing bacterial growth dynamics, suggesting that lower temperatures amplify the inhibitory effects of pressure on growth [82].

3.3.3 Self-Induced Collective Mechanical Stresses in Bacterial Colonies

Bacterial colonies are dynamic systems where mechanical interactions among cells play a crucial role in shaping their structure and function. As colonies grow, these interactions give rise to self-induced mechanical stresses that influence cellular behavior. Far from being passive byproducts of growth, such stresses actively affect cell size distribution, colony morphology, and overall growth dynamics. However, the precise mechanisms by which bacterial cells sense and respond to these collective stresses remain poorly understood.
To address these gaps, this study investigates the phenomena arising from self-induced collective mechanical stresses in expanding bacterial colonies. Growth experiments on a nutrient-rich agarose substrate, combined with a microscopic model based on dynamical density functional theory (DDFT), were used to explore how mechanical interactions regulate cell size distribution and growth behavior.
The growth of bacterial colonies in a nutrient-rich environment at 30° is influenced by bacterial population density. As the colony becomes denser, the elongation rate of

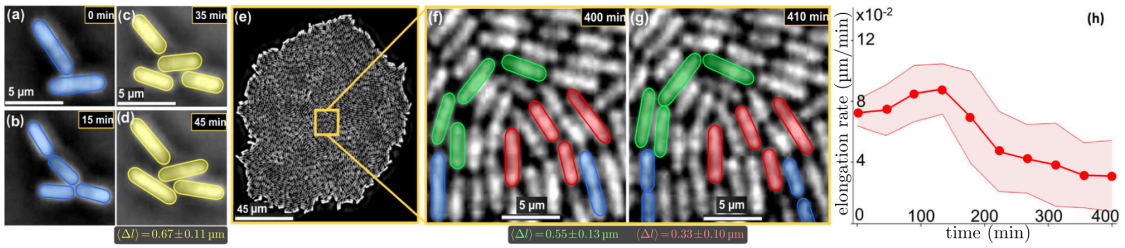

Figure 3.11: Experiments on a monolayer of cells dividing every ≈ 30 min on a nutrient-rich agarose substrate, reaching a cell count of ≈ 4500 bacteria after 450 minutes. **a, b** Division of cells (hued in blue) in the early stage of the colony. **c, d** Growth of cells (hued in yellow) during the early phase over an interval of ten minutes. The average cell elongation rate (determined from the average length $\langle l \rangle$ grown in 10 min) is $0.067 \pm 0.011 \mu m/min$. **e** Micrograph of a well-developed bacterial monolayer comprising about 2600 cells. **f, g** Division and growth of cells over an interval of 10 minutes within the dense colony. Dividing cells are hued in blue. Fast and slowly growing cells are hued in green or red, respectively, as identified from a large or small free area near the ends visible in (f). The average elongation rates resulting from this selection are $0.055 \pm 0.013 \mu m/min$ and $0.033 \pm 0.01 \mu m/min$. **h** Cell elongation rate of all bacteria as a function of time (red dots) with standard deviation (red shaded area), determined from three distinct biological replicates. Figure and the caption reprinted from Wittmann et. al. [83]

cells decreases, especially when their ends come into close contact with neighboring cells, even though nutrients remain abundant Fig. 3.11. This behavior is attributed to the cells' response to mechanical stresses during growth. The elongation rate of well-nourished Escherichia coli cells was found to decrease over time, depending on the availability of free space around each individual cell. Using a cell-resolved model that incorporates the feedback of collective forces on individual cell growth, the study quantifies how this mechano-response shapes the structure and composition of bacterial colonies, including the local microenvironment of each cell [83].

4 Bacterial Self-Organization in Isotropic and Anisotropic Confinement

Sections 2.4.1 and 2.4.2 have highlighted the role of mechanical interactions on the growth of bacterial colony and spatial organization. While previous studies have explored how geometric constraints influence bacterial alignment, the combined effects of bacterial properties, surface characteristics, and mechanosensitivity in confined environments remain less understood. By addressing these factors together, my work provides a unique perspective on the interplay between bacterial mechanics and confinement.

In this work, I investigate how mechanical forces arising from cell-cell and cell-substrate interactions shape bacterial self-organization within colonies confined by different geometries. By varying bacterial characteristics, surface properties, and mechanosensitivity, I analyze their collective influence on colony alignment and structural evolution. Through molecular dynamics simulations, this study provides new insights into the complex interplay between bacterial properties, confinement, and mechanosensitivity in determining bacterial behavior. By examining these factors together, my work offers a unique perspective on how mechanical interactions govern microbial organization in diverse environments, advancing our understanding of microbial dynamics in confined spaces.

This chapter is based on the preprint **Effect of mechanical interactions on bacterial self-organization and growth rate inside an isotropic and anisotropic confinement**, available on arXiv, authored by **Samaneh Rahbar**, **Ludger Santen**, and **Reza Shaebani**.

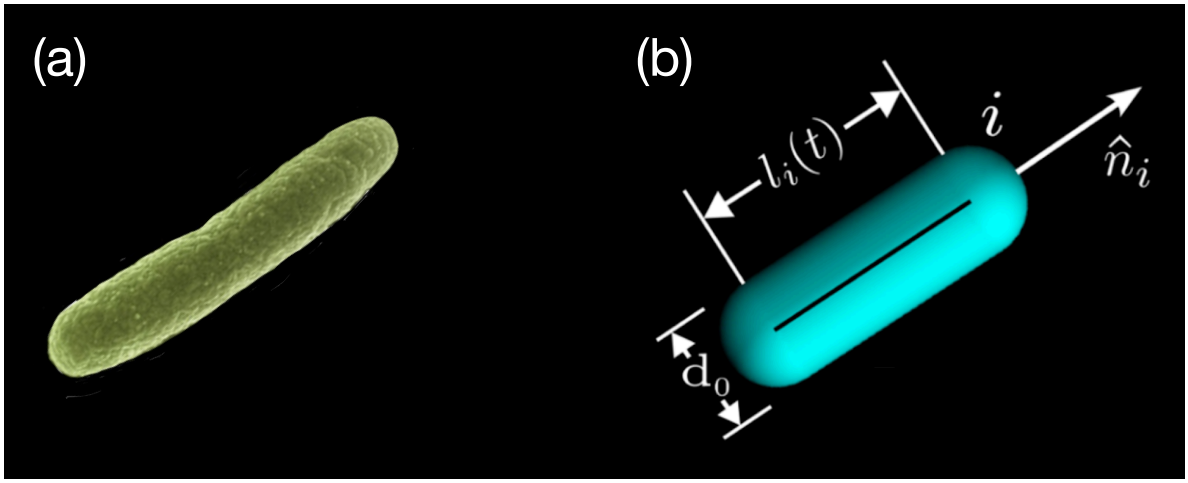

Figure 4.1: (a) High-resolution image of *E. coli*. (b) Presentation of a rod-shaped bacteria with a constant diameter d_0, variable length l, and the unit vector $\hat{n}$.

4.1 Model

4.1.1 Bacterial Mechanical Interactions

The geometry of a rod-shaped bacterium, such as *Escherichia coli (E. coli)*, can be characterized by two distinct length scales as it has shown in Fig.4.1(a) . To model these bacteria, I represent each elastic rod with a constant diameter d_0 and a time-dependent length l with major axis cross from the center of the bacteria to its both ends, shown in Fig, 4.1(b). These geometric parameters are crucial for describing their mechanical interactions, growth, and behavior within confined environments.The mechanical force between two spherocylinders is approximated by the force between two spheres placed along the major axis of the rods at such positions that their distance is minimal

$$\vec{f}_{ij}(h) = E d_0^{\frac{1}{2}} (h_{ij})^{\frac{3}{2}} \hat{e}_{c_{ij}}, \tag{4.1.1.1}$$

where E represents the Young's modulus of the bacterium, and h_{ij} is the overlap distance between bacteria i and j Fig. 4.2 (a). This force acts along the major axis of the bacterium and is normal to its surface in the direction of $\hat{e}_{c_{ij}}$, and $\vec{r}_{c_{ij}}$ is the contact vector from bacteria j to bacteria i, as illustrated in Fig. 4.2(b) .

Calculations of the minimum distance created between two contacting bacteria pose a significant challenge in this modeling approach. As I will delve into the details, this calculation is essential for determining the exact points of contact and the direction of the forces acting between bacteria. Therefore, I propose a calculations which is practical in both two and three dimensions.

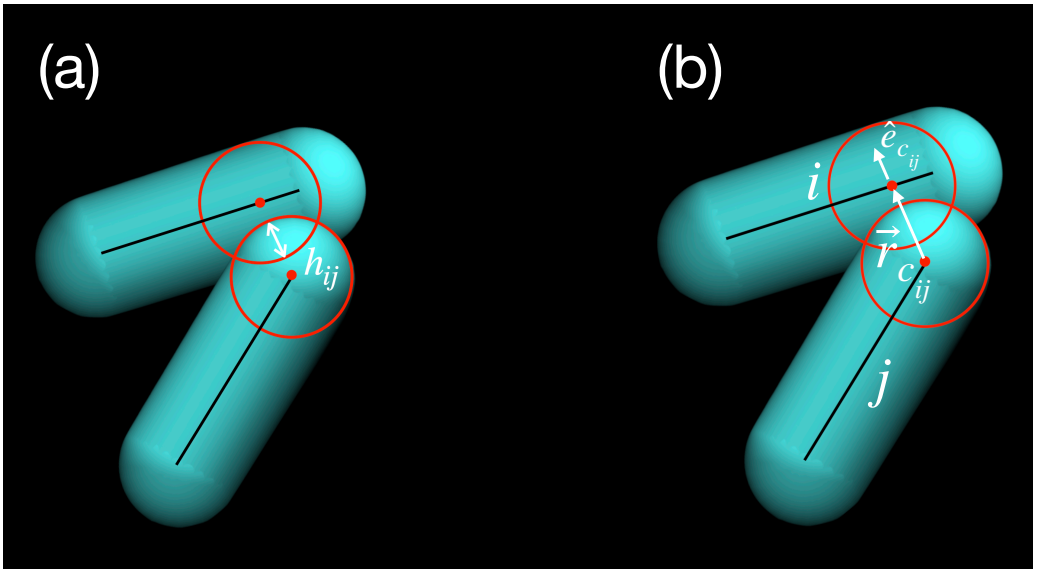

Figure 4.2: Two circle (red) along the major axis of the rod-shaped bacteria. (a) Presentation of the length scale as an overlap h_{ij} between two contact bacteria. (b) $\vec{r}_{c_{ij}}$ is the contact vector between two bacteria, $\hat{e}_{c_{ij}}$ the direction of the contact vector, and correspondingly the force interaction.

As I mentioned above, the mechanical interaction between two contacting bacteria is approximated by the force between two spheres placed along the major axis of the rods at such positions that their distance is minimal. To determine this minimum distance, I focus on the major axis of each individual rod. For this purpose, for a given bacterium i, I define the length vector $\vec{l}_i$, which spans from one end to the other, two distinct position vectors representing the endpoints $\vec{r}_{l_i}, \vec{r}_{r_i}$, and a position vector for the center of mass $\vec{r}_{CM_i}$. Similarly, for a bacterium j in contact with bacterium i, I define the same set of vectors for its major axis Fig. 4.3. These vectors use as the foundational elements for calculating the minimum distance between the two bacteria.
If I consider bacteria i and j, by defining the equations of line for any given bacteria I can find each point on the major axis which the distance between two contact bacteria is minimum.

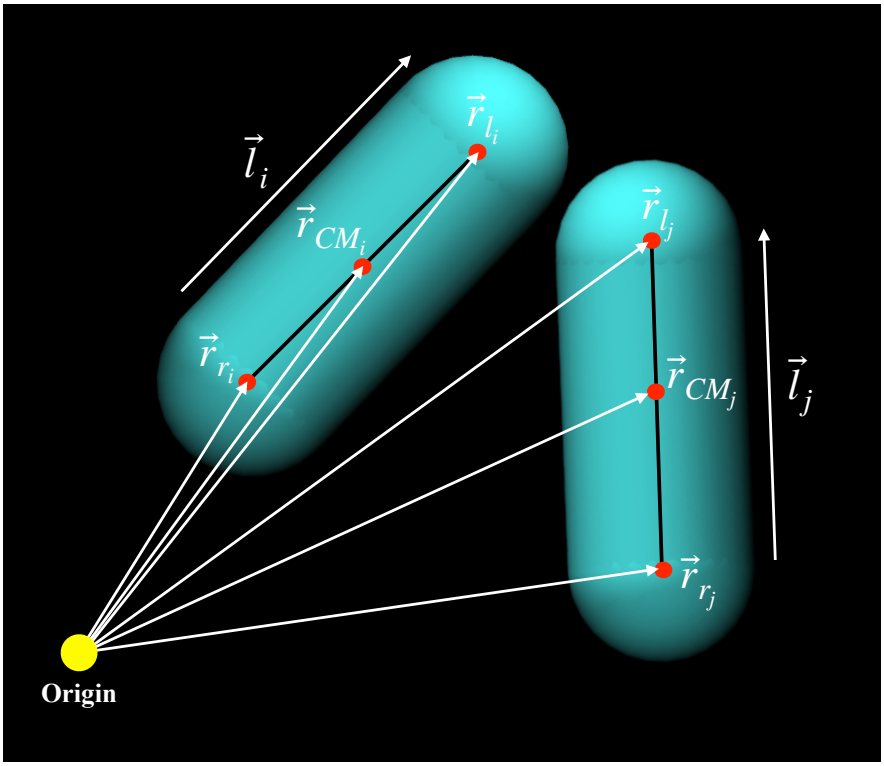

Figure 4.3: Illustration of vectors characterizing different points along the major axis of a given bacterium.

$$\vec{r}_i(\lambda) = \vec{r}_{\mathrm{CM}_i} + \lambda\vec{l}_i \tag{4.1.1.2}$$

$$\vec{r}_j(\mu) = \vec{r}_{\mathrm{CM}_j} + \mu\vec{l}_j \tag{4.1.1.3}$$

where λ and μ are scalar parameters, which belong to $\left[\frac{-1}{2}, \frac{1}{2}\right]$. If I consider the distance between these two bacteria, it corresponds to

$$d \approx |\vec{r}_i(\lambda) - \vec{r}_j(\mu)|, \tag{4.1.1.4}$$

$$d^2 = (\vec{r}_i(\lambda))^2 + (\vec{r}_j(\mu))^2 - 2\vec{r}_i(\lambda) \cdot \vec{r}_j(\mu). \tag{4.1.1.5}$$

By substituting Eq. (4.1.1.2), (4.1.1.3) in Eq. (4.1.1.5),

$$d^2 = \left(\vec{r}_{\mathrm{CM}_i} + \lambda\vec{l}_i\right)^2 + \left(\vec{r}_{\mathrm{CM}_j} + \mu\vec{l}_j\right)^2 - 2\left(\vec{r}_{\mathrm{CM}_i} + \lambda\vec{l}_i\right) \cdot \left(\vec{r}_{\mathrm{CM}_j} + \mu\vec{l}_j\right) \tag{4.1.1.6}$$

I can open this equation and introduce the terms which are independent of λ and μ as Cte and I keep the rest of the terms which are dependent on λ and μ

$$d^2 = Cte + \left(\lambda\vec{l_i} - \mu\vec{l_j}\right)^2 + 2\left(\vec{r}_{\mathrm{CM}_i} - \vec{r}_{\mathrm{CM}_j}\right)\cdot\left(\lambda\vec{l_i} - \mu\vec{l_j}\right) \tag{4.1.1.7}$$

I want to see for which values of λ and μ d^2 becomes minimum

$$\frac{\partial(d^2)}{\partial\lambda} = 0 \tag{4.1.1.8}$$
$$\frac{\partial(d^2)}{\partial\mu} = 0 \tag{4.1.1.9}$$

By taking the derivatives

$$\frac{\partial(d^2)}{\partial\lambda} = 2\vec{l_i}\cdot\left(\lambda\vec{l_i} - \mu\vec{l_j}\right) + 2\vec{R}\cdot\vec{l_i} = 0 \tag{4.1.1.10}$$
$$\frac{\partial(d^2)}{\partial\mu} = -2\vec{l_j}\cdot\left(\lambda\vec{l_i} - \mu\vec{l_j}\right) - 2\vec{R}\cdot\vec{l_j} = 0 \tag{4.1.1.11}$$

which $\vec{R} = \left(\vec{r}_{\mathrm{CM}_i} - \vec{r}_{\mathrm{CM}_j}\right)$.
To solve this problem, I have a system of two equations with two unknowns. By introducing some parameter like $\vec{l_i}\cdot\vec{l_j} \equiv l_{ij}$, $\vec{l_i}\cdot\vec{l_i} = l_i^2$, and $\vec{l_j}\cdot\vec{l_j} = l_j^2$ I solve these equation to find corresponding λ and μ which the distance is minimum. By solving the equations 4.1.1.10 and 4.1.1.11 I can find the values for λ and μ.

$$\lambda = \frac{l_{ij}\vec{l_j}\cdot\vec{R} - l_j^2\vec{l_i}\cdot\vec{R}}{l_i^2 l_j^2 - l_{ij}^2} \tag{4.1.1.12}$$
$$\mu = \frac{l_{ij}\vec{l_i}\cdot\vec{R} - l_i^2\vec{l_j}\cdot\vec{R}}{l_{ij}^2 - l_i^2 l_j^2} \tag{4.1.1.13}$$

As long as the scalar parameters are in the range of $\left[\frac{-1}{2}, \frac{1}{2}\right]$ I get the exact points on bacteria i and j which are along the major axis. But there are conditions that either one scalar parameter or both are out of the range or when the contact bacteri are parallel. Once they are out of range or are parallel I use the following method to find the contact points.
Condition one: If $\lambda > \frac{1}{2}$ and $\mu = \left[\frac{-1}{2}, \frac{1}{2}\right]$, I consider $\lambda = 0.5$, and find the values for μ in which gives us the contact point on the bacterium j which has minimum distance from bacterium i.

$$\vec{r_i}(\lambda) = \vec{r}_{\mathrm{CM}_i} + 0.5\vec{l_i} \tag{4.1.1.14}$$

$$\vec{r_j}(\mu) = \vec{r}_{\mathrm{CM}_j} + \mu\vec{l_j} \tag{4.1.1.15}$$

Ba finding the square distance $d^2 = \left(\vec{R} + 0.5\vec{l_i} - \mu\vec{l_j}\right)^2$ and making the derivative $\frac{\partial d^2}{\partial \mu} = 0$, the corresponding μ will be

$$\mu = \frac{\vec{l_j} \cdot \vec{R} + 0.5\vec{l_i} \cdot \vec{l_j}}{l_j^2} \tag{4.1.1.16}$$

Condition two:

If $\lambda < \frac{1}{2}$ and $\mu = \left[\frac{-1}{2}, \frac{1}{2}\right]$, I consider $\lambda = -0.5$, and find the values for μ in which gives us the contact point on the bacterium j which has minimum distance from bacterium i.

$$\vec{r_i}(\lambda) = \vec{r}_{\mathrm{CM}_i} - 0.5\vec{l_i} \tag{4.1.1.17}$$

$$\vec{r_j}(\mu) = \vec{r}_{\mathrm{CM}_j} + \mu\vec{l_j} \tag{4.1.1.18}$$

Ba finding the square distance $d^2 = \left(\vec{R} - 0.5\vec{l_i} - \mu\vec{l_j}\right)^2$ and making the derivative $\frac{\partial d^2}{\partial \mu} = 0$, the corresponding μ will be

$$\mu = \frac{\vec{l_j} \cdot \vec{R} - 0.5\vec{l_i} \cdot \vec{l_j}}{l_j^2} \tag{4.1.1.19}$$

Condition three:

If $\mu > 0.5$ and $\lambda = \left[\frac{-1}{2}, \frac{1}{2}\right]$, I consider $\mu = 0.5$ and find the corresponding λ, based on the pervious calculations,

$$\vec{r_i}(\lambda) = \vec{r}_{\mathrm{CM}_i} - \lambda\vec{l_i} \tag{4.1.1.20}$$

$$\vec{r_j}(\mu) = \vec{r}_{\mathrm{CM}_j} + 0.5\vec{l_j} \tag{4.1.1.21}$$

Ba finding the square distance $d^2 = \left(\vec{R} + \lambda\vec{l_i} - 0.5\vec{l_j}\right)^2$ and making the derivative $\frac{\partial d^2}{\partial \lambda} = 0$, the corresponding λ will be

$$\mu = \frac{-\vec{l_i} \cdot \vec{R} + 0.5\vec{l_i} \cdot \vec{l_j}}{l_i^2} \tag{4.1.1.22}$$

Condition four:
If $\mu < -0.5$ and $\lambda = \left[\frac{-1}{2}, \frac{1}{2}\right]$, I consider $\mu = -0.5$ and find the corresponding λ, based on the pervious calculations,

$$\vec{r_i}(\lambda) = \vec{r}_{\mathrm{CM}_i} - \lambda\vec{l_i} \tag{4.1.1.23}$$
$$\vec{r_j}(\mu) = \vec{r}_{\mathrm{CM}_j} - 0.5\vec{l_j} \tag{4.1.1.24}$$

Ba finding the square distance $d^2 = \left(\vec{R} + \lambda\vec{l_i} + 0.5\vec{l_j}\right)^2$ and making the derivative $\frac{\partial d^2}{\partial \lambda} = 0$, the corresponding λ will be

$$\mu = \frac{-\vec{l_i} \cdot \vec{R} - 0.5\vec{l_i} \cdot \vec{l_j}}{l_i^2} \tag{4.1.1.25}$$

Substitution of the corresponding λ and μ in the equations 4.1.1.2 and 4.1.1.3 give us the exact contact points on the major axis of bacteria i and j.
When bacteria are aligned in parallel, the denominator in equations 4.1.1.12 and 4.1.1.13 becomes undefined. In such cases, I directly apply all four conditions by choosing $\lambda \pm 0.5$, finding the corresponding μ, and vice versa.
By the exact calculations of λ and μ I can substitute them in the equations 4.1.1.2 and 4.1.1.3 correspondingly I can find the contact point on the bacteria i and bacteria j. Hence, I can calculate the minimum distance between bacteria i and j as $d_{min} = |\vec{r_i}(\lambda) - \vec{r_j}(\mu)|$ and I can find the overlap created between two contact bacteria as

$$h_{ij} = d_0 - |\vec{r_i}(\lambda) - \vec{r_j}(\mu)| \tag{4.1.1.26}$$

4.1.2 Over-Damped Dynamics of Bacterial Motion

The motion of rod-shaped bacteria is governed by the principles of Newtonian dynamics, adapted for the overdamped regime. In this regime, inertial forces are negligible compared to frictional forces. This simplification is particularly appropriate for the microscale dynamics of bacteria moving on a surface with effective friction, where their motion is dominated by contact and frictional forces .
The translational motion of each bacterium is modeled using the following equation:

$$\frac{d\vec{r}_i}{dt} = \frac{1}{\zeta l_i} \sum_{j}^{N_c^i} \vec{f}_{ij}, \tag{4.1.2.1}$$

- $\vec{r}_i$ is the position of the center of mass of bacterium i,

- ζ is the effective friction per unit length, which accounts for the resistance due to the both bacterial membrane and surface properties,
- l_i is the length of bacterium i,
- f_{ij} represents the interaction force between bacteria i and j,

This equation reflects the balance between contact forces exerted by neighboring bacteria and the frictional forces arising from their interaction with the environment. The scaling factor $\frac{1}{\zeta l_i}$ensures that the effect of forces diminishes with increased friction and bacterial length.
The rotational dynamics of the bacteria are described by the following equation,

$$\frac{d\theta_i}{dt} = \frac{12}{\zeta l_i^3} \sum_{j}^{N_c^i} \left((\vec{r}_{c_{ij}} - \vec{r}_i) \times \vec{f}_{ij} \right) \cdot \hat{z}, \tag{4.1.2.2}$$

- θ_i the orientation angle of bacterium i with respect to the x axis,
- $\vec{f}_{ij}$ is the force vector exerted by bacterium j on i,
- $\hat{z}$ represents the unit vector perpendicular to the plane of motion (out-of-plane direction),

This equation highlights the torque experienced by each bacterium due to the forces exerted by its neighbors. The torque is proportional to the cross product of the lever arm $(\vec{r}_{c_{ij}} - \vec{r}_i)$ and the interaction force $\vec{f}_{ij}$. The cubic dependence on length reflects the reduces sensitivity of rotational dynamics to forces for longer bacteria. In this model, the friction coefficient ζ is assumed to be isotropic, meaning that the frictional resistance experienced by a bacterium is the same regardless of its orientation. This assumption simplifies the model and is valid for rod-shaped bacteria whose resistance is dominated by the cross-sectional diameter rather than the specific direction of motion. The overdamped nature of bacterial dynamics ensures that the system rapidly reaches mechanical equilibrium, with motion directly responding to external forces and torques without oscillations or inertial delays. This is a key feature when modeling dense bacterial colonies or biofilms, where mechanical interactions between cells and with the substrate dominate their collective behavior.

4.1.3 Bacterial Interactions With the Confinement

The interaction between bacteria and confinement follows Hertzian contact mechanics, where the rigid wall is treated as an impenetrable boundary. In the case of square

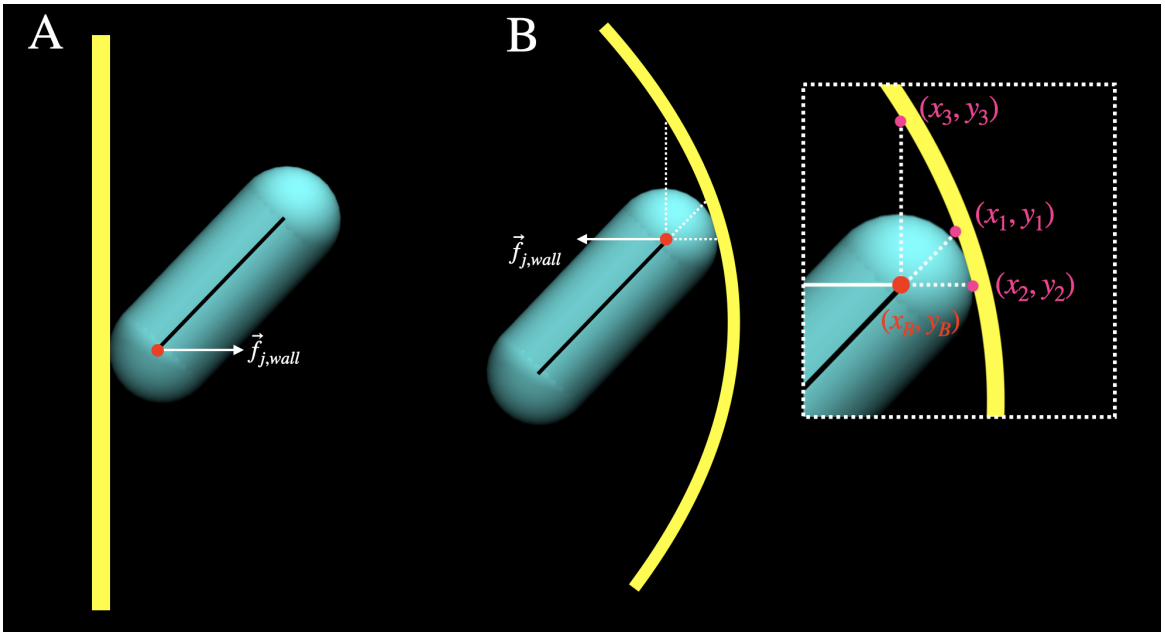

Figure 4.4: Interaction between bacteria and the confinement. (A) Interaction with the boundaries of a square wall. (B) Interaction with the boundaries of a circular wall.

confinement Fig. 4.4(A), the minimum distance between the bacterial major axis and the wall can be determined by defining the wall boundaries. Interaction occurs when the overlap is less than $d_0/2$, which is expressed as $h = \frac{d_0}{2} - d_{min}$. In square confinement, the calculation of d_{min} is straightforward since it is simply the shortest distance from a line to the wall.

However, for circular confinement, determining the minimum distance between the bacterial major axis and the curved boundary requires identifying the quadrant in which the bacterium is located.I define the left and right coordinates of the bacterial major axis as $(x_l, y_l), (x_r, y_r)$, with the circular confinement having a radius of $r_{circle} = d_c/2$.

First I compute the distance of both bacterial tips from the center of the circular confinement $O = (x_0, y_0)$:

$$r_1 = \sqrt{((x_l - x_0)^2 + (y_l - y_0)^2)} \tag{4.1.3.1}$$

$$r_2 = \sqrt{((x_r - x_0)^2 + (y_r - y_0)^2)} \tag{4.1.3.2}$$

By comparing 4.1.3.1 and 4.1.3.2 I identify the bacterial tip closest to the confinement boundary, denoted as (x_B, y_B), with its distance from the center given by r_B.

T o find the points $(x_1, y_1), (x_2, y_2), (x_3, y_3)$ on the circular boundary I first determine the bacterial orientation by $\theta = \tan((y_B - y_0)/(x_B - x_0))^{-1}$, In simulations, I use the `atan2` function to correctly compute θ while avoiding miscalculations.
The coordinates of (x_1, y_1) which represents a point along the bacterial orientation, are calculated as:

$$x_1 = x_B + (r_{circle} - r_B)\cos\theta \tag{4.1.3.3}$$
$$y_1 = y_B + (r_{circle} - r_B)\sin\theta \tag{4.1.3.4}$$

For different quadrants, the coordinates (x_2, y_2) and (x_3, y_3) are determined as follows:
First Quadrant:

$$x_2 = x_0 + \sqrt{r_{circle}^2 - (y_B - y_0)^2} \tag{4.1.3.5}$$
$$y_2 = y_B \tag{4.1.3.6}$$

and:

$$x_3 = x_B \tag{4.1.3.7}$$
$$y_3 = y_0 + \sqrt{r_{circle}^2 - (x_B - x_0)^2} \tag{4.1.3.8}$$

Second Quadrant:

$$x_2 = x_0 + (-1)\sqrt{r_{circle}^2 - (y_B - y_0)^2} \tag{4.1.3.9}$$
$$y_2 = y_B \tag{4.1.3.10}$$

and:

$$x_3 = x_B \tag{4.1.3.11}$$

$$y_3 = y_0 + \sqrt{r_{circle}^2 - (x_B - x_0)^2} \tag{4.1.3.12}$$

Third Quadrant:

$$x_2 = x_0 + (-1)\ \sqrt{r_{circle}^2 - (y_B - y_0)^2} \tag{4.1.3.13}$$

$$y_2 = y_B \tag{4.1.3.14}$$

and (x_3, y_3):

$$x_3 = x_B \tag{4.1.3.15}$$

$$y_3 = y_0 + (-1)\ \sqrt{r_{circle}^2 - (x_B - x_0)^2} \tag{4.1.3.16}$$

Fourth Quadrant:

$$x_2 = x_0 + \sqrt{r_{circle}^2 - (y_B - y_0)^2} \tag{4.1.3.17}$$

$$y_2 = y_B \tag{4.1.3.18}$$

and (x_3, y_3):

$$x_3 = x_B \tag{4.1.3.19}$$

$$y_3 = y_0 + (-1)\ \sqrt{r_{circle}^2 - (x_B - x_0)^2} \tag{4.1.3.20}$$

Finally, I calculate the distance from the bacterial tip (x_B, y_B) to each of the three points $(x_1, y_1), (x_2, y_2), (x_3, y_3)$ and select the minimum distance. The corresponding overlap is then given by $h = d_0/2 - d_{min}$. Using Eq. 4.1.1.1 I determine the resulting force interactions between the bacteria and the confinement.

4.1.4 Growth Dynamics

As discussed in the chapter one, mechanical interactions play a pivotal role in determining bacterial growth and division, especially under confined conditions where spatial constraints impose mechanical stress. These interactions influence the elongation rate

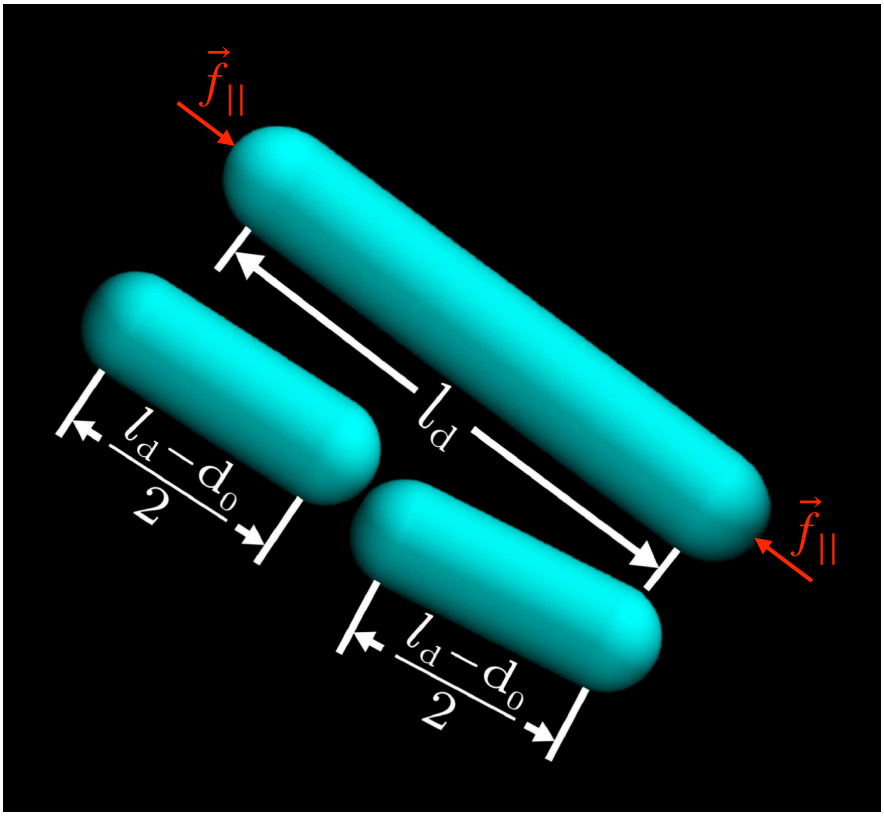

Figure 4.5: Representation of a bacterium reaching the division length l_d and dividing into two daughter bacteria. Red vectors indicate the projected forces along the major axis of the bacterium. The daughter bacteria inherit slightly deviated orientations from the mother bacterium.

of individual bacteria, which is modeled as a function of both time and the forces acting along their major axis Fig. 4.5.

The growth of an individual bacterium is described by the following equation:

$$\frac{dl_i}{dt} = \begin{cases} r_{g_i} - \beta|f_{||_i}|, & r_{g_i} > \beta|f_{||_i}| \\ 0, & r_{g_i} < \beta|f_{||_i}|, \end{cases} \tag{4.1.4.1}$$

where:

- r_{g_i} is the intrinsic growth rate of the bacterium i,
- β is the mechanosensitivity parameter, quantifying how robustly or weakly bacteria respond to the mechanical forces,
- $|f_{||_i}|$ represents the total force projected along the major axis of the bacterium i, capturing the experienced mechanical stress,

This equation highlights that growth ceases entirely when the mechanical force surpasses a threshold proportional to β. The inhibition reflects the energy redistribution within the bacterium, where growth-related activities are compromised by physical stress.
To quantify $|f_{||_i}|$, the mechanical forces acting on the bacterium are resolved along its major axis, as follows:

$$|f_{||_i}(t)| = \sum_{j=1}^{N_c^i} |\vec{f_{ij}}(t) \cdot \hat{n}_i|, \tag{4.1.4.2}$$

where:

- $\hat{n}_i$ is the unit vector aligned with the major axis bacterium i,
- $\vec{f_{ij}}$ represents the force exerted by the bacterium j on bacterium i,
- the summation extends over all contacting bacteria (N_c),

This formulation ensures that only the forces aligned with the bacterial axis contribute to growth inhibition, accurately capturing the mechanosensitivity nature of bacterial elongation.
Based on the experimental observations discussed in Chapter One, I assume that when the deformation of the bacterial envelope exceeds half its diameter, the growth rate becomes zero.

$$\frac{dl}{dt} = 0 \quad \text{if } h > \frac{d_0}{2} \tag{4.1.4.3}$$

where h represents the total overlap value applied on a given bacteria, and d_0 is the bacterial diameter. This condition reflects the physical limitation of the bacterial cell wall to sustain growth under extreme stress.

Estimation of β

The parameter β governs the sensitivity of growth rate to mechanical forces and is estimated based on experimental observations of growth inhibition. For example, with a threshold force (corresponds to the deformation around the half of the bacterial diameter) of approximately 35 kPa $\cdot$ μm^2 and an average growth rate of 4 μm $\cdot$ h^{-1}, β is computed as:
$\beta = 0.11 \ \frac{1}{\text{kPa}\cdot\mu\text{m}\cdot\text{h}}$.
This value captures the relationship between applied mechanical stress and bacterial growth, facilitating quantitative predictions of growth dynamics under varying conditions.

As the applied pressure increases due to mechanical interactions, the doubling time of bacteria is observed to lengthen significantly. This behavior highlights the sensitivity of bacterial growth and division to mechanical stresses in their environment. Division occurs when a bacterium reaches a threshold length l_d, signaling the completion of its growth cycle. At this stage, the bacterium divides into two daughter cells Fig. 4.5, which inherit the orientation of the mother cell. To account for natural variability, the orientations of the daughter cells deviate slightly from that of the mother cell, with random angular deviations within the range $(0, 0.1745]$ radians (approximately $0° - 10°$). To capture biological heterogeneity, the growth rates of the daughter cells are drawn randomly from a uniform distribution $\left[\frac{r_g}{2}, \frac{3r_g}{2}\right]$ [84, 85]. This randomization reflects experimental observations of variability in bacterial growth rates due to genetic and environmental factors.

4.1.5 Numerical Implementation

The equations of motion and growth, represented in Eqs. 4.1.2.1, 4.1.2.2, and 4.1.4.1, are solved numerically using the forward Euler time-stepping algorithm. This method is selected for its simplicity and computational efficiency, particularly when addressing the over-damped dynamics of bacterial motion. The discretized forms of these equations are used to compute the translational, rotational, and growth dynamics of the bacteria, ensuring a consistent and accurate numerical solution. Specifically, the translational and rotational equations take the forms:

Here, the superscripts n and $n+1$ represent the current and next time steps, respectively.

$$\vec{r_i}^{\,(n+1)} = \vec{r_i}^{\,(n)} + \Delta t \cdot \frac{1}{\zeta l_i} \sum_{j=1}^{N_c^i} \vec{f}_{ij}, \tag{4.1.5.1}$$

$$\theta_i^{(n+1)} = \theta_i^{(n)} + \Delta t \cdot \frac{12}{\zeta l_i^3} \sum_{j=1}^{N_c^i} \left((\vec{r}_{c_{ij}} - \vec{r}_i) \times \vec{f}_{ij} \right) \cdot \hat{z}. \tag{4.1.5.2}$$

$$l_i^{(n+1)} = l_i^{(n)} + \Delta_t \cdot \left(r_{g_i} - \beta |f_{||_i}| \right) \tag{4.1.5.3}$$

The time step, Δt, is calculated as:

$$\Delta t = \frac{\zeta}{E} \tag{4.1.5.4}$$

where ζ is the friction coefficient per unit length, and E is the Young's modulus. This choice ensures numerical stability by maintaining the condition Δt small enough to avoid undamped or oscillatory behavior in the over-damped regime.
Each simulation begins with bacteria randomly positioned and oriented within a confined geometry. The confinement can take the form of:

- **Square boundaries** with dimensions $L_x \times L_y$
- **Circular boundaries** with a diameter d_c

The forward Euler method, while straightforward, requires careful monitoring of numerical accuracy. To enhance stability:

- The time step Δt is adjusted based on the Young's modulus and the friction coefficient to prevent excessively large displacements in a single step.
- Force calculations are optimized using efficient neighbor search algorithms to reduce computational complexity in systems with many bacteria.

By employing this numerical approach, the model captures the dynamic interplay between bacterial growth, mechanical interactions, and spatial confinement, enabling robust simulation of bacterial behaviors under a variety of conditions.
The model is grounded in experimental data to ensure realistic simulations of bacterial dynamics. The key parameter used in the simulations are included in Table. 4.1.

Parameter	Symbol	Value
Bacterial diameter	d_0	$0.5\,\mu m$
Average growth rate	r_g	$4\,\mu m/h$
Threshold length for division	l_d	$[2-4]\,\mu m$
Friction coefficient	ζ	$200\,\mathrm{Pa}\cdot\mathrm{h}$
Young's modulus of the bacteria	E	$400\,\mathrm{kPa}$
Young's modulus of the confinement	E_{wall}	$1000\,\mathrm{kPa}$
Confinement's diameter (circular)	d_c	$60\,\mu m$
Confinement's length (square)	L_x, L_y	$60\,\mu m$

Table 4.1: Default parameter values used in the simulations.

This parameterization enables the model to simulate bacterial division dynamics under varying mechanical stresses and environmental conditions. By integrating experimentally validated parameters, the model provides insights into how bacteria adapt their growth and division in response to physical constraints, such as crowding and surface interactions.

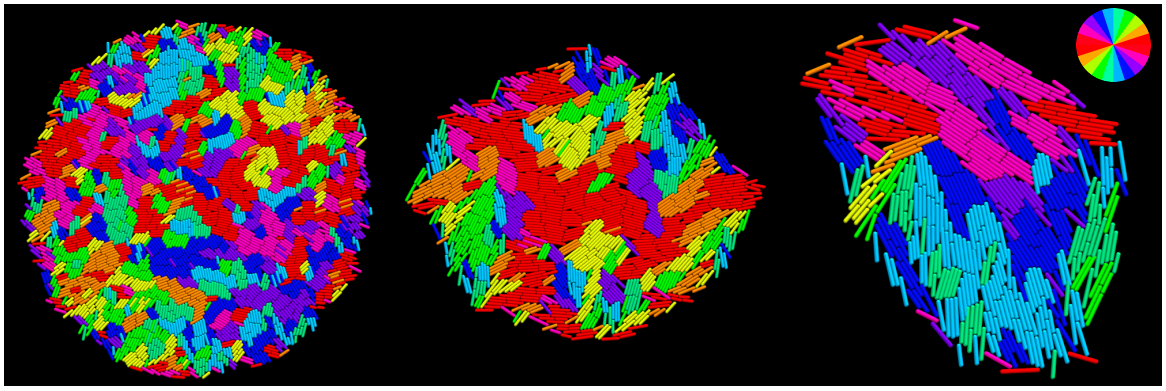

Figure 4.6: Visualizing bacterial colony dynamics: simulated configurations at concurrent times steps. From left to right, the division length l_d increases, resulting in changes in the number of bacteria: $l_d = 2\mu m, N = 2853$, $l_d = 3\mu m, N = 1265$, $l_d = 4\mu m, N = 505$. Color circle shows the orientational distribution.

4.2 Results

In this section, I present the outcomes of my molecular dynamics simulations investigating bacterial colony growth under varying confinement geometries and substrate properties. Initially, simulations are conducted for bacterial colonies with different division lengths l_d growing within distinct confinement shapes, including square domains $(60 \times 60)\mu m^2$ and circular domains ($d_c = 60\mu m$). These simulations aim to understand how confinement geometry influences the ordering and self-organization of the bacterial colony.

Once the impact of confinement shape on the colony's dynamics is established, I shift focus to a single division length within circular confinement. Here, I systematically vary substrate properties, such as the frictional coefficient and the degree of mechanosensitivity, to analyze their effects on the self-organization, alignment, and growth dynamics of the colony. This approach allows us to explore the interplay between mechanical forces, spatial constraints, and environmental conditions in shaping bacterial collective behavior.

This analysis provides key insights into the mechanical and spatial factors that regulate bacterial colony growth in confined environments, offering a deeper understanding of their self-organization mechanisms under varying conditions.

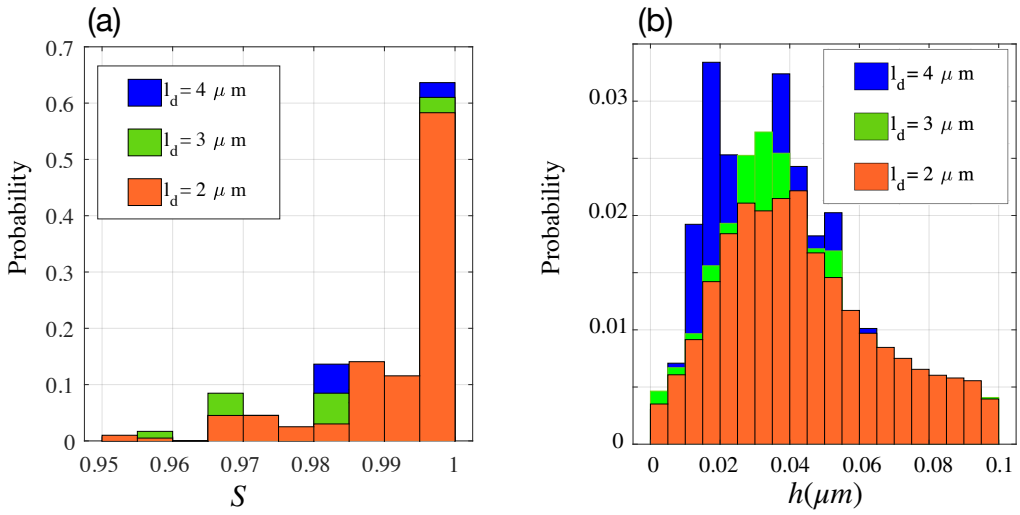

Figure 4.7: Probability distribution of the orientational order parameter S for domains within the colony at different division lengths l_d. (b) Probability distribution of the overlap between contacting bacteria for different division lengths l_d.

4.2.1 Bacterial Free Growth

I begin the simulations for different division lengths l_d , as shown in Fig. 4.6. At the early stages of the simulation, the bacteria within the colony are able to grow freely, forming an initial configuration.

As the colony expands, the bacteria tend to locally align in a common direction due to contact forces and mechanical interactions. These local alignments arise from mechanical constraints imposed by neighboring cells, where contact forces influence bacterial orientation, promoting alignment along a shared axis. I can analytically compare the degree of ordering among the three bacterial colonies. As shown in Fig. 4.6, distinct domains emerge, with different colors representing different bacterial orientations. By analyzing each individual domain, I can calculate the corresponding order parameter S and determine which colony, based on aspect ratio, exhibits the highest degree of ordering.

From the colony configurations in Fig. 4.6, I compute the order parameter S, to quantify bacterial alignment. The probability distribution of the orientational order parameter, S for the domains, is shown in Fig. 4.7(a), reveals that these domains are highly ordered, with S being close to 1. Moreover, as the aspect ratio increases (corresponding to smaller l_d), the probability of achieving $S \approx 1$ becomes higher compared to colonies with a smaller aspect ratio.

These preliminary results motivate us to examine the overlap between contacting bacteria Fig. 4.7(b). Since my model considers only mechanical interactions, the observed

ordering may stem from the mechanical forces at play. Given that Hertz contact forces depend on the extent of overlap, I analyze the distribution of overlaps within these colonies to further understand their structural organization.
From the results Fig. 4.7(b), I observe that the range of overlap at contact points is more concentrated for colonies with a larger aspect ratio. This means that for all aspect ratios, a given bacterium typically has at least eight neighboring bacteria in contact. However, in colonies with a larger aspect ratio, the overlap between almost all eight neighboring bacteria falls within a narrower range of $[0.02-0.05]$.
However, at the scale of the entire colony, particularly in conditions where bacteria grow without confinement, the orientational distribution remains isotropic, exhibiting no discernible preferential alignment. This distinction between local alignment and global isotropy highlights the dynamic balance between mechanical interactions at the microscopic scale and the overall structural randomness that arises in the absence of spatial constraints. In the following sections, I delve into more details regarding the higher-order organization of bacteria at larger aspect ratios, even when they are freely growing.

4.2.2 Bacterial Growth Inside an Isotropic and Anisotropic Confinement

I established two types of confinements: square and circular, both of which act as rigid boundaries for bacterial growth. The interaction between the hard walls and bacteria is governed by the Hertz contact force, as described in section 4.1.5.
Simulations were conducted for varying division lengths (l_d), starting with a single bacterium placed at the center of the square and circular confinement.
The simulations were allowed to evolve over time, with the bacterial colonies gradually growing and reaching the boundary and afterward filling the confinement, as shown in Fig. 4.8. This setup enabled us to monitor the dynamics of bacterial growth and organization within the confinements. A primary focus was on quantifying the nematic ordering, and the memory of the bacterial orientation to the initial orientation (OCF), which emerges from the alignment of bacteria along a common direction. The nematic order parameter was tracked for different division lengths l_d as the colonies reached high densities within the confined spaces.
The results, depicted in Fig. 4.9, reveal how division length influences the bacterial ordering since they are freely growing to a time point they fill in the confinement.
By considering the scalar order parameter $\langle 2\cos^2\theta_{ij} - 1\rangle_{ij}$, I can evaluate the degree of bacterial alignmet across different aspect ratio.

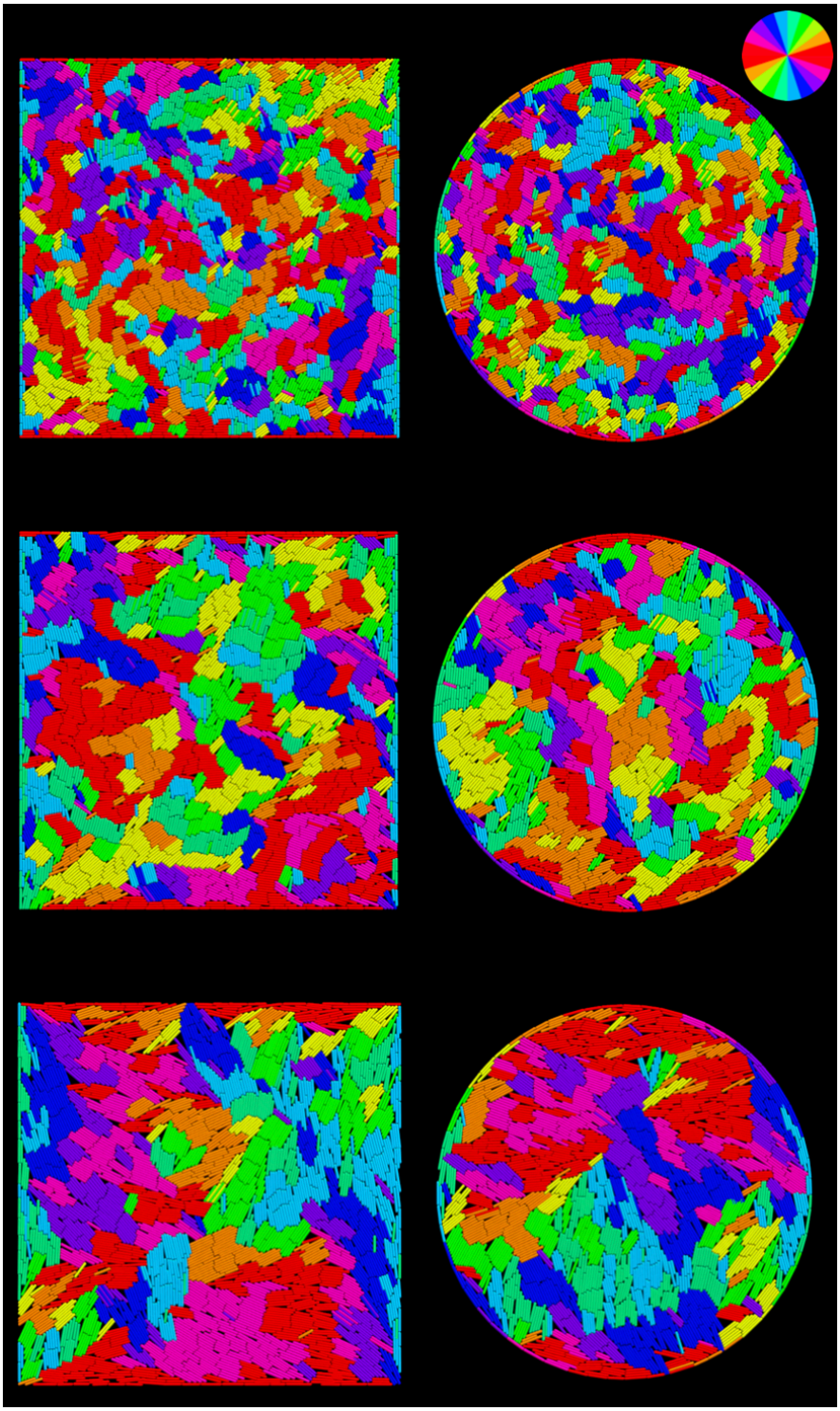

Figure 4.8: Visual representation of bacterial colonies at the time step when the confinement becomes fully populated. The figure shows both square and circular confinements, with division lengths increasing from top to bottom $l_d = [2, 3, 4]\mu m$. The color map shows the different orientation of the bacteria.

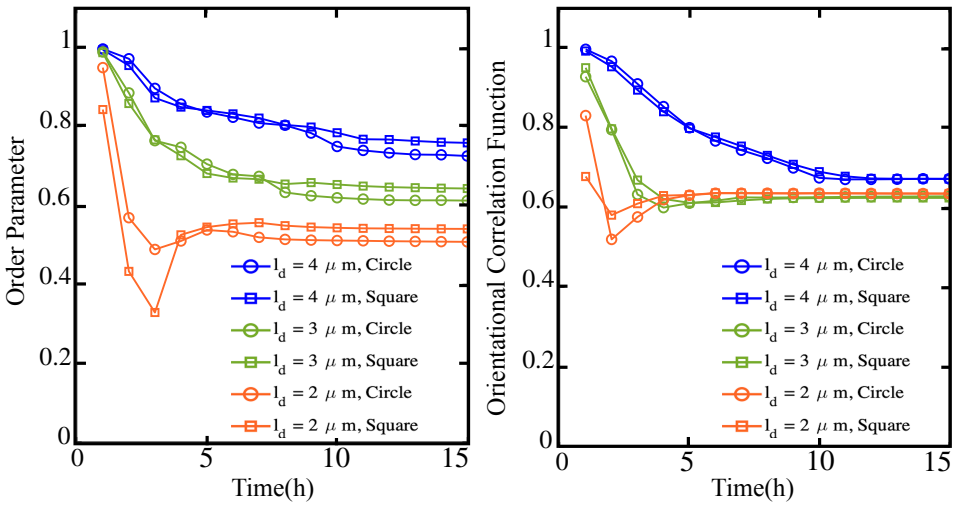

Figure 4.9: Sample-averaged orientational order parameter and orientational correlation function for both square and circular-like confinement. (a) The orientational order parameter is shown for different division lengths $l_d = [2, 3, 4]\mu m$. (b) The orientational correlation function is displayed for the same division lengths $l_d = [2, 3, 4]\mu m$.

In this way, I start the simulation with a single bacterium at an initial orientation and allow it to evolve, observing how the order parameter, S, and the orientational correlation function, $OCF(t) = \frac{1}{N_t}\sum_{i=1}^{N_t} |\cos(\theta_i(t) - \theta_0)|$, (where θ_0 is the reference angle for the initial bacterium, and N_t is the total number of bacteria at time t), change over time. As shown in the figures, S decreases as the colony grows, reflecting a reduction in overall alignment, while OCF also declines, indicating increased randomness in bacterial orientations Fig. 4.9. As the colony reaches the confinement boundary, both S and OCF stabilize at a constant value.

In order to delve into the details and thoroughly compare the results for the orientational correlation function and the order parameter for different division lengths, I focus on bacterial colony growth within circular confinement. I can define a characteristic time as $\tau = \frac{l_d + d_0}{2r_g}$ to determine the generation, given by $\frac{t}{\tau}$, of the colony for each specific division length.

Fig. 4.10 presents the evolution of S and OCF during bacterial growth inside circular confinement. As time and generation count increase, OCF continues to decline Fig. 4.10(a-b), a trend mirrored by S Fig. 4.10(c-d). Colonies with smaller aspect ratios divide more rapidly, reaching higher generations sooner. Interestingly, for these smaller aspect ratios, S and OCF exhibit a slight increase, suggesting possible realignment, though not necessarily to the initial reference.

This decline in S Fig. 4.10(c-d) and OCF Fig. 4.10(a-b) is primarily driven by anisotropic bacterial growth, which disrupts mechanical equilibrium, leading to buckling instabili-

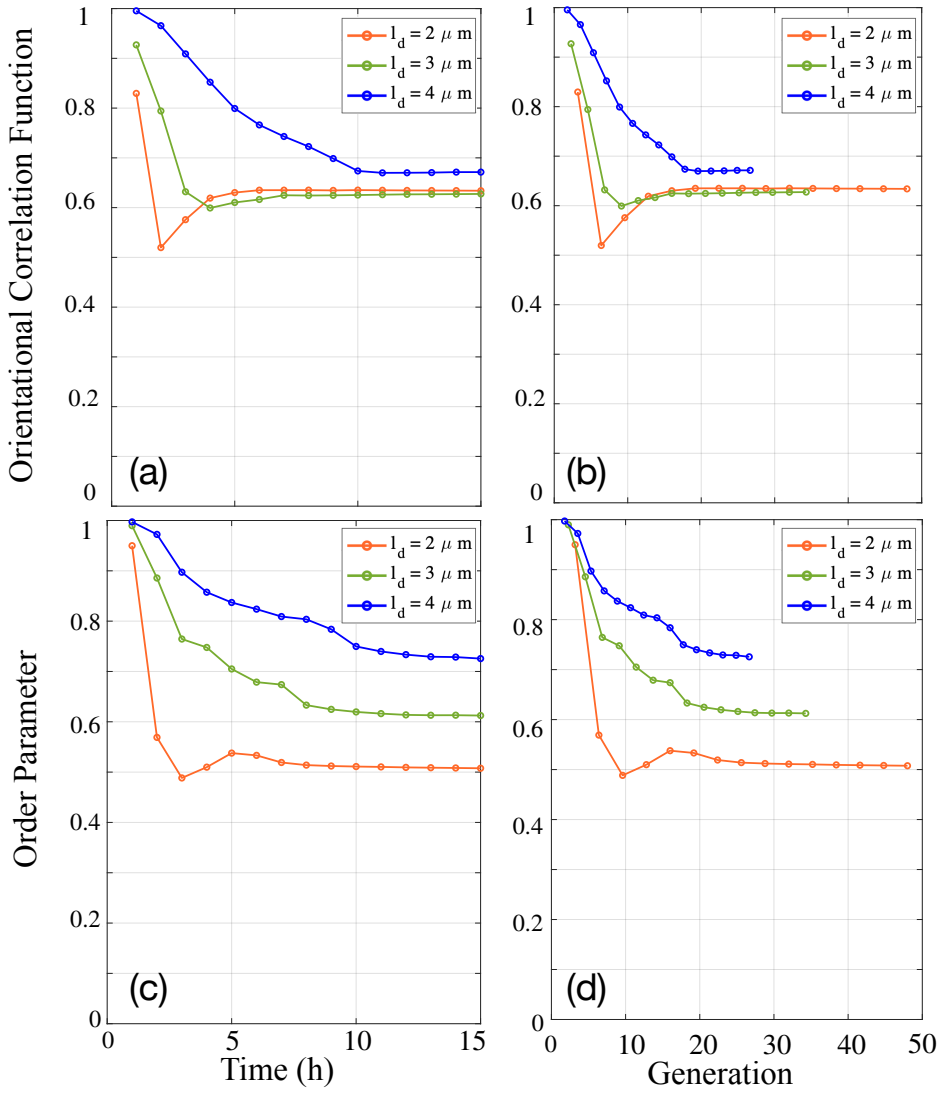

Figure 4.10: (a) time evolution of the orientational correlation function OCF over time for different division lengths. (b) The evolution of the orientational correlation function OCF versus generation evolution. (c) The time evolution of the order parameter S for different division lengths l_d. (d) The evolution of the orientational correlation function OCF versus generation evolution for different division lengths l_d.

ties. Stochastic effects such as cell division and increasing bacterial count further amplify these instabilities. Additionally, analyzing OCF relative to the initial bacterium orientation allows us to quantify the degree of alignment and ordering within the colony. The rate of decline in S and OCF is slower in colonies with larger aspect ratios, indicating a more gradual evolution. This slower change can be attributed to their smaller population size, which experiences fewer instabilities from cell division and mechanical forces. Consequently, these colonies are structurally stiffer and more resistant to deformation. Furthermore, cell division introduces anisotropic stress, reinforcing stability in larger aspect ratio colonies.
At a specific time point, when the colony reaches the confinement boundary, S and OCF stabilize. This occurs around 5.5 hours for $l_d = 2\mu m$, 7.5 hours for $l_d = 3\mu m$, and 10 hours for $l_d = 4\mu m$. The distinct edges and corners of square confinement provide alignment cues, leading to higher nematic ordering, whereas circular confinement, lacking these structural features, results in lower alignment.
Taken together, colonies with higher aspect ratios exhibit greater nematic ordering and orientational correlation, primarily due to increased overlap between contacting cells—a topic explored further in the following sections. Even within the same generation, a larger aspect ratio still results in higher ordering and a greater orientational correlation function.

By understanding how individual contact forces distributed for the colonies with different aspect rations I gain a deeper insight what factor is controling the ordering and self-organization of the colonies. By accessing to individual overlap between contact bacteria and the individual contact forces in the simulations I can plot the the probability distribution functions.
The colony takes approximately 15 hours to grow, reach confinement, and fill the available space. I analyze the system at $t = 3$h and $t = 5$h, when the colony is still free and has not yet reached the confinement. By examining individual overlap and contact forces between neighboring bacteria, their probability distribution provides insight into how mechanical forces are distributed within the colony at different aspect ratios.
As shown in Fig. 4.11(a-b), a decrease in aspect ratio increases the probability of larger overlaps and higher contact forces. However, as discussed earlier, for colonies with a larger aspect ratio, the probability of overlap within the interval $[0 - 0.05]$ is higher. This suggests that if a given bacterium has 10 neighboring cells, most of its overlaps fall within this range, leading to a greater average force exerted on an individual bacterium. This trend is also evident in Fig. 4.12. At $t = 3$h, for smaller aspect ratios, I observe that once the bacterial population within the colony exceeds

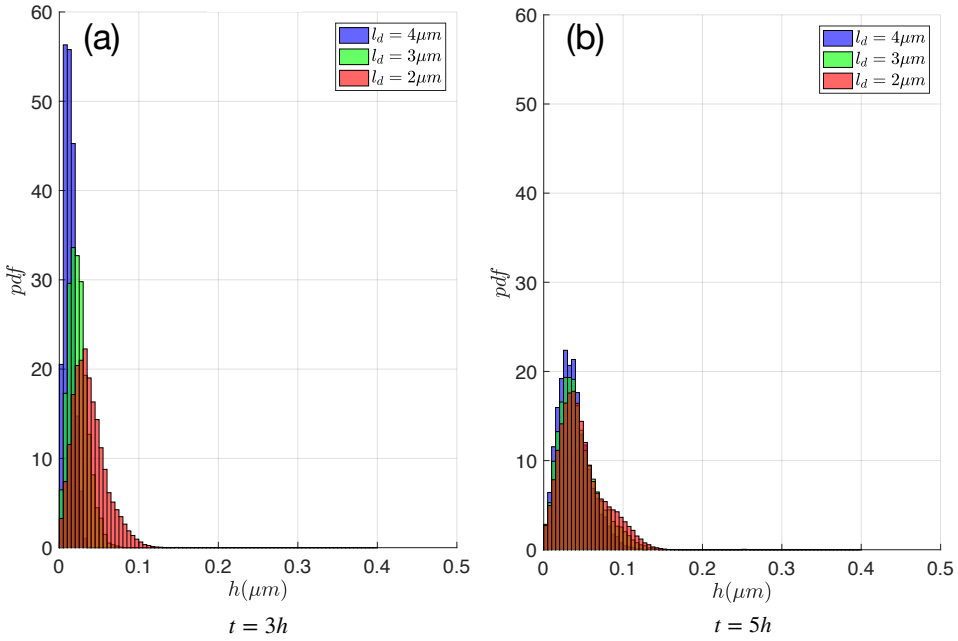

Figure 4.11: Probability distribution function of the overlap between contacting bacteria for different division lengths l_d.(a) $t = 3$h and (b) $t = 5$h.

200, the individual contact forces begin to rise. Similarly, in Fig. 4.12 and Fig. 4.11, as the number of bacteria increases across all three colonies, they transition into a regime characterized by higher contact forces.

These observations indicate that during unrestricted growth, higher nematic ordering in this active system depends on the aspect ratio. This dependency is linked to the moment of inertia and the resistance of bacterial orientation against external perturbations. Moreover, on average, the total contact force exerted on an individual bacterium is greater for colonies with a higher aspect ratio.

Finally, findings suggest that as bacteria continue to grow freely, increasing population size can drive the colony into a higher-force regime, reinforcing the role of mechanical interactions in shaping the collective behavior of the system.

After examining the force and overlap distribution between contacting bacteria, I now analyze how contact forces are affected once the colony reaches full confinement at $t = 15$h. As shown in Fig. 4.13, when the confinement is fully occupied, bacteria with a larger aspect ratio exhibit a higher probability of experiencing stronger contact forces compared to those with a smaller aspect ratio. This is attributed to their reduced flexibility and the pronounced volume exclusion effects, which result in a stronger mechanical response within the confined environment.

Bacteria with smaller aspect ratios divide more rapidly, leading to larger colony sizes and higher initial contact forces due to frequent cell-cell interactions. However, their

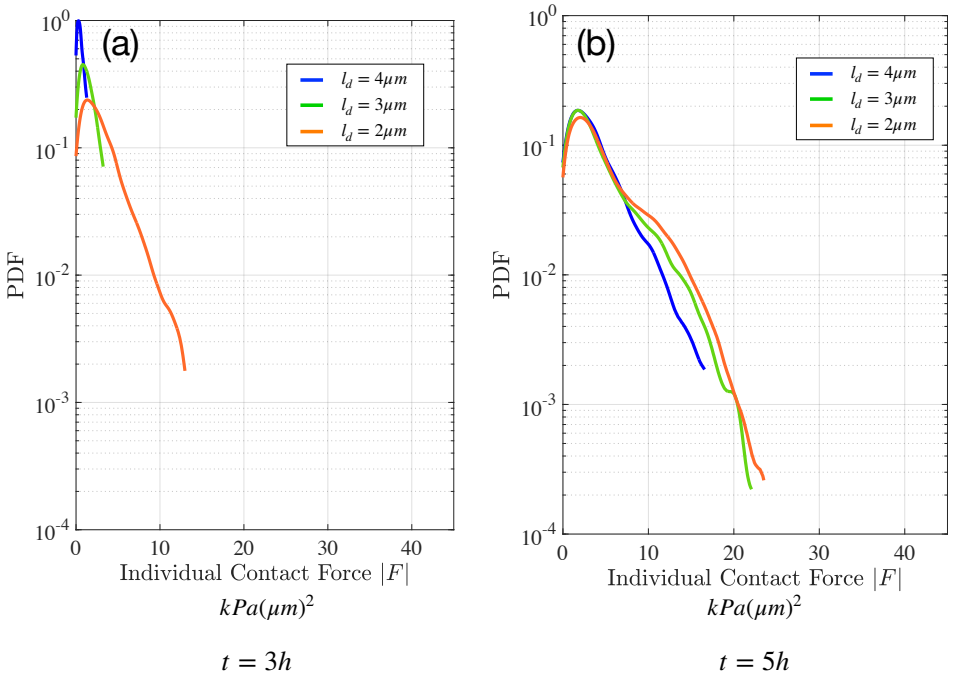

Figure 4.12: Probability distribution function of the individual contact force for different division lengths l_d.(a) $t = 3$h and (b) $t = 5$h.

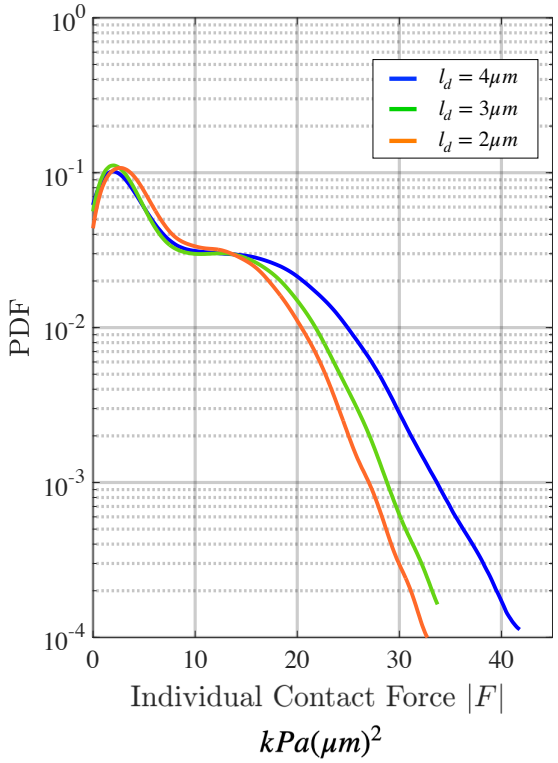

Figure 4.13: Probability distribution function of the individual contact force for different division lengths at time $t = 15$ h.

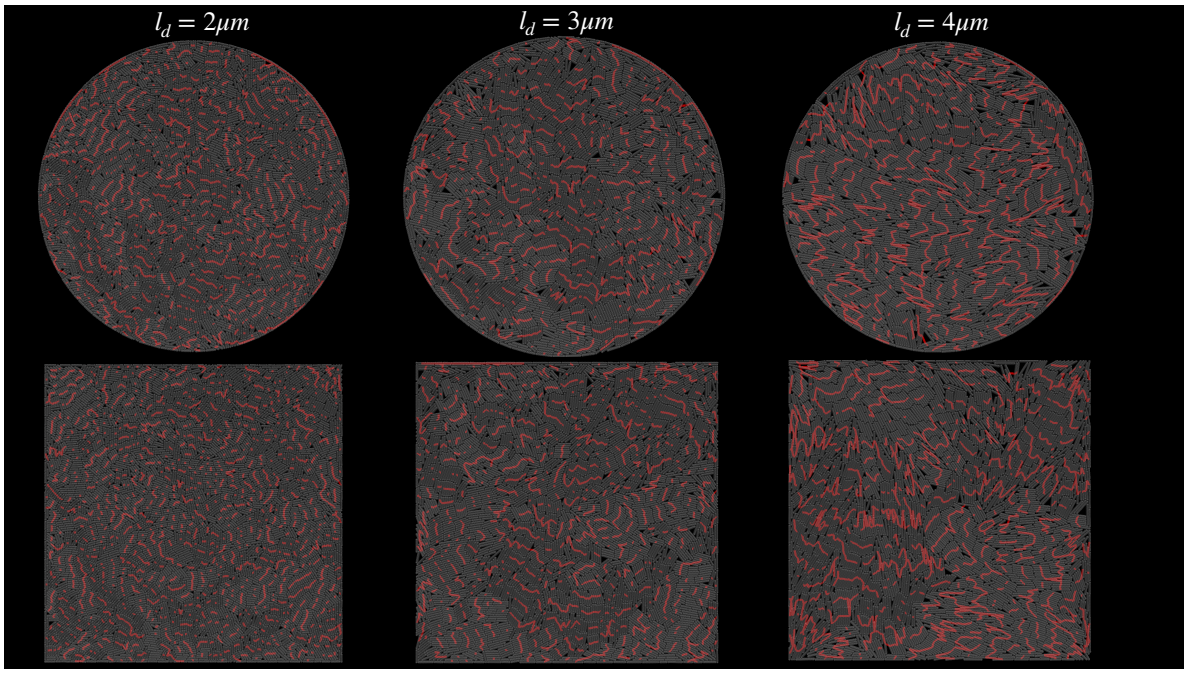

Figure 4.14: Force network (red lines) for individual contact forces exceeding $|F| = 13$ $(kPa \cdot \mu m^2)$, overlaid on the bacterial colony configuration for each division length under square and circular confinement for different division length l_d.

compact shape allows for greater flexibility in rearranging under mechanical stress, enabling them to redistribute forces more effectively as they grow. In contrast, bacteria with larger aspect ratios experience lower initial contact forces due to slower division and a smaller colony size. However, as the colony reaches the confinement boundary, these elongated bacteria face greater steric constraints, limiting their ability to reposition. This forced alignment amplifies contact forces, as the elongated cells press more rigidly against each other and the boundary, leading to a buildup of mechanical stress. As a result, while smaller aspect ratio colonies initially experience stronger contact forces, larger aspect ratio bacteria ultimately exhibit greater force accumulation once confined due to their restricted mobility and increased excluded volume.

In Fig. 4.14, I visualize the spatial distribution of contact forces exceeding $|F| = 13(kPa \cdot \mu m^2)$, mapping the centers of mass of the contacting bacteria to highlight the force network. The force chains predominantly form along the lateral sides of bacteria, connecting neighboring cells aligned side by side or at small relative angles. In contrast, forces acting along the end-to-end direction are significantly weaker and less frequent, as interactions at bacterial tips contribute minimally to the overall mechanical response.

This lateral force concentration is a direct consequence of bacterial growth and division patterns. As bacteria elongate and pack together, steric interactions favor alignment along their major axis, leading to anisotropic force transmission. Growth-induced compressive stresses cause localized rearrangements, minimizing force buildup at the tips while reinforcing lateral contact forces. This trend is evident across different division lengths l_d, suggesting that the dominant force pathways are dictated by bacterial geometry rather than just population size or confinement effects.

The observed lateral force distribution is also linked to mechanical stability. By aligning side by side, bacteria reduce internal stress and enhance colony coherence, facilitating collective motion and structural integrity. This arrangement minimizes orientational frustration and maximizes space efficiency, further supporting the self-organized nature of bacterial colonies under confinement.

4.2.3 Evolution of Colony Shape: From Early Growth to Circular Boundary Contact

The formation and evolution of bacterial colony shape in circular confinement are significantly influenced by the division length l_d of individual bacteria. To investigate this process, I simulate the time evolution of the colony for different division lengths and analyze its morphology from the early stages of growth to the point where the colony reaches the circular boundary.

A key metric used to quantify the shape of the expanding colony is the ratio of the minor axis to the major axis. This metric increases as the colony becomes more circular, offering a direct measure of how closely the colony approximates an isotropic shape. Two figures summarize my findings: the first tracks how the minor-to-major axis ratio changes as the number of bacteria N increases, and the second illustrates the time evolution of the colony's shape for all division lengths.

For colonies with smaller division lengths, the minor-to-major axis ratio remains higher throughout the simulation, indicating a more circular shape. This observation is consistent both over time and as the number of bacteria increases. The more isotropic interactions and uniform packing of bacteria in these colonies contribute to their near-circular morphology. In contrast, colonies with larger division lengths exhibit a lower minor-to-major axis ratio, reflecting greater elongation and anisotropy in their growth patterns. Even for the same number of bacteria, colonies with larger division lengths are noticeably more elongated, suggesting that the division length strongly influences the collective organization of bacterial populations Fig. 4.15.

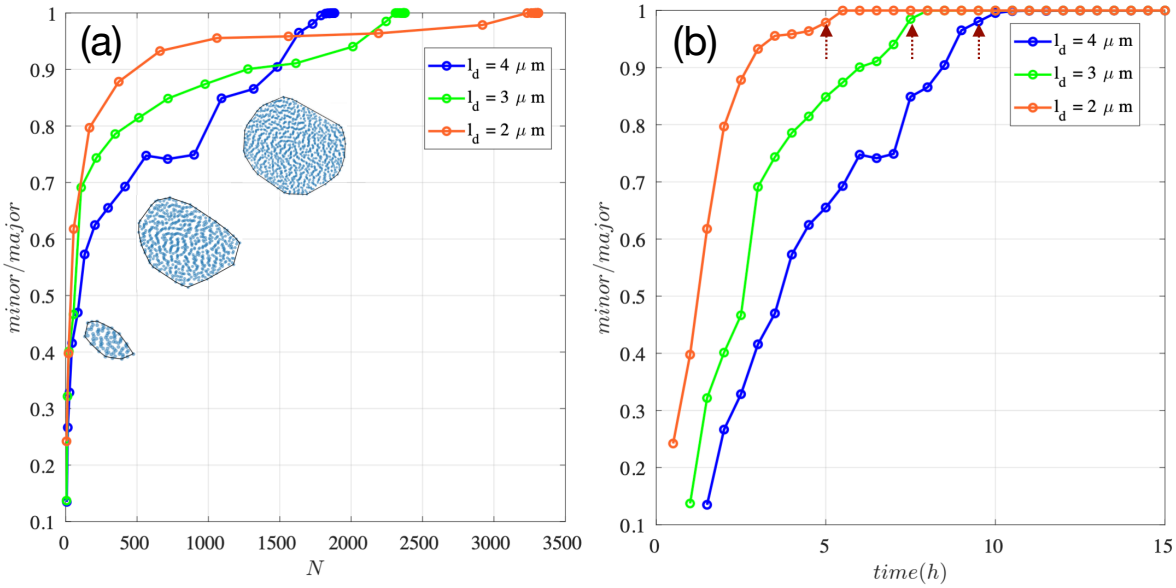

Figure 4.15: (a) Variation of the minor-to-major axis ratio of the bacterial colony over time as a function of the number of bacteria within the colony. The data is presented for different aspect ratios, illustrating how colony shape evolves with bacterial growth. (b) Time evolution of the minor-to-major axis ratio of the bacterial colony for different division lengths l_d. The arrows indicate the time steps at which the colony reaches circular confinement.

As the colonies grow and approach the boundaries of the circular confinement, the minor-to-major axis ratio converges to 1 for all division lengths. This convergence arises from the uniform constraints imposed by the circular geometry, which effectively counterbalances the inherent anisotropy of colonies with larger division lengths. Fig. 4.15 vividly captures this time evolution, showing how the colony shape evolves from its initial stages to the point where the confinement boundary imposes a uniform circular morphology.

Taken together, these findings emphasize the interplay between individual bacterial properties, such as division length, and external geometric constraints. Smaller division lengths promote isotropic growth, resulting in a more circular colony shape, while larger division lengths favor anisotropic growth and elongation. However, the circular confinement imposes a boundary-driven shape uniformity, demonstrating the significant influence of environmental geometry on the emergent morphology of bacterial colonies.

4.2.4 Influence of Substrate Properties on Self-Organization and Ordering

The substrate on which a bacterial colony grows plays a critical role in shaping its self-organization and overall ordering. Variations in substrate properties, such as stiffness, friction, and surface topography, can significantly influence the spatial arrangement and dynamics of bacterial cells within a colony. To explore this, I systematically varied substrate properties in my simulations and analyzed their impact on the colony's structure and alignment.

Frictional forces between bacteria and the substrate have a profound impact on colony organization. On low-friction substrates, bacteria can slide more freely, reducing stress accumulation and facilitating smoother reorientation, which contributes to higher levels of nematic ordering. In contrast, high-friction substrates inhibit bacterial movement, leading to greater stress accumulation and buckling instabilities. These instabilities disrupt the alignment of bacteria and increase orientational entropy, resulting in a more disordered colony. The relationship between friction and colony order highlights the delicate balance between stability and adaptability in bacterial populations.

Directional Distribution of Domains and the Effect of Friction

The frictional coefficient between the substrate and bacteria plays a pivotal role in shaping the local alignment and organization of bacterial colonies. To investigate this effect, I focus on the domain areas for specific division length $l_d = 3\mu m$, within a circular confinement where bacteria exhibit similar orientations. Domains are defined as regions in which neighboring bacteria align closely, forming clusters with minimal orientational variation, as show in Fig. 4.16.

By analyzing individual domains within the bacterial colony, I define a directional vector for each domain to study their orientation distribution under varying frictional coefficients ζ. This approach enables us to quantify the degree of alignment and identify patterns in the directional organization of domains.As shown in Fig. 4.17, the probability distribution of these directional vectors was calculated and compared for both low and high frictional coefficients, revealing distinct trends.

For lower frictional coefficients ($\zeta = 200\ Pa \cdot h$), the directional vectors exhibit a more peaked distribution, indicating a higher degree of alignment among the domains. This behavior reflects smoother alignment facilitated by the reduced substrate resistance, allowing bacteria within the colony to align more effectively. At higher frictional coefficients ($\zeta = 1000\ Pa \cdot h$), the distribution of directional vectors becomes more uniform.

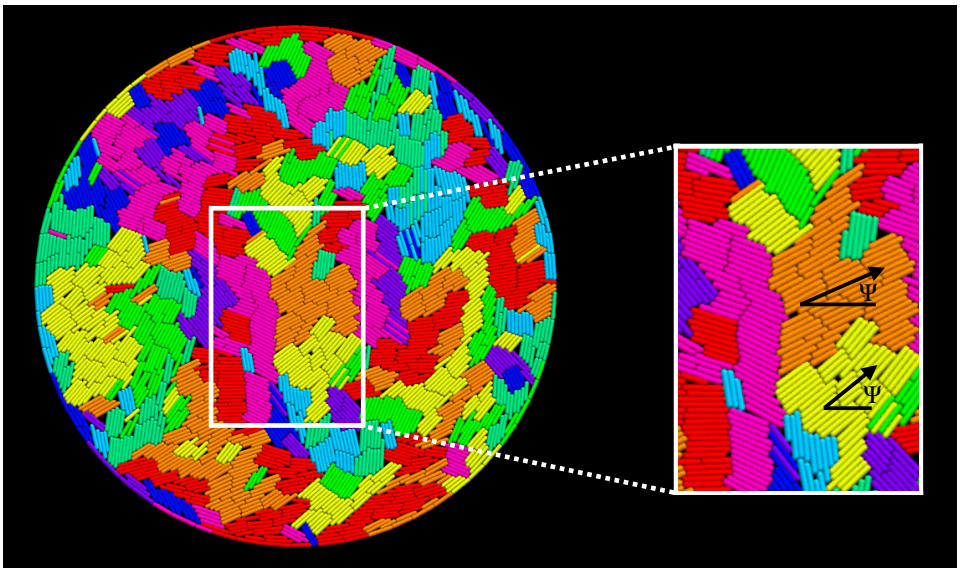

Figure 4.16: Visualization of a bacterial colony within a confinement, highlighting local domains where bacterial orientations are uniform. A zoomed-in view illustrates these domains, with each assigned an average orientation denoted as Ψ.

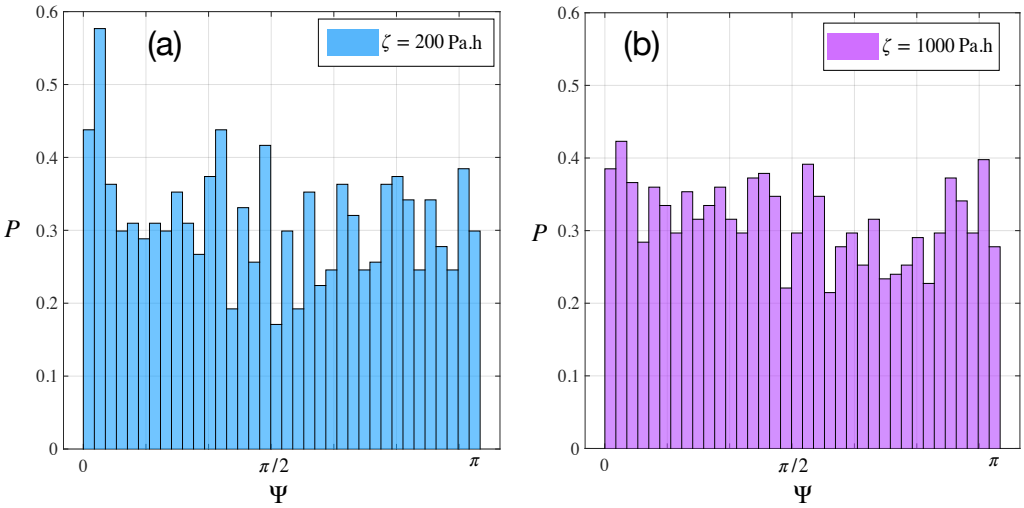

Figure 4.17: Probability distribution of the domains orientation Ψ for different values of frictional coefficient.

The increased resistance inhibits smooth alignment and induces greater angular variability in the domain orientations, contributing to a broader, flatter distribution.

To quantitatively assess the variability in the directional distribution, I define a fluctuation parameter (η) as the ratio of the standard deviation (σ) to the mean value (μ) of the bin heights in the probability distribution:

$$\eta = \frac{\sigma}{\mu}. \tag{4.2.4.1}$$

For the case of low frictional coefficient ($\zeta = 200\ Pa \cdot h$):

$$\begin{aligned} \mu &= 0.3157, \\ \sigma &= 0.0798, \\ \eta &= \frac{0.0798}{0.3157} \approx 0.2528. \end{aligned}$$

For the case of high frictional coefficient ($\zeta = 1000\ Pa \cdot h$):

$$\begin{aligned} \mu &= 0.3157, \\ \sigma &= 0.0574, \\ \eta &= \frac{0.0574}{0.3157} \approx 0.1753. \end{aligned}$$

The fluctuation parameter demonstrates that the distribution for lower friction ($\zeta = 200$) exhibits greater variability, as indicated by $\eta = 0.2528$. In contrast, the higher frictional coefficient ($\zeta = 1000$) results in reduced fluctuations, with $\eta = 0.1753$. This analysis underscores the relationship between substrate friction and the directional organization of bacterial domains, where higher friction leads to a more uniform distribution of orientations.

These results highlight the influence of substrate friction on the directional organization of bacterial colonies. Lower friction allows for more consistent alignment within domains, while higher friction disrupts this organization, promoting greater randomness in domain orientations. The fluctuation parameter serves as a robust metric for characterizing these differences, offering valuable insights into how environmental factors regulate self-organization in bacterial populations.

The probability distribution of the cross product magnitude between the unit length vectors of contacting bacteria in Fig. 4.18 reveals that alignment is slightly higher for lower frictional coefficients. Reduced substrate resistance enables bacteria to reorient

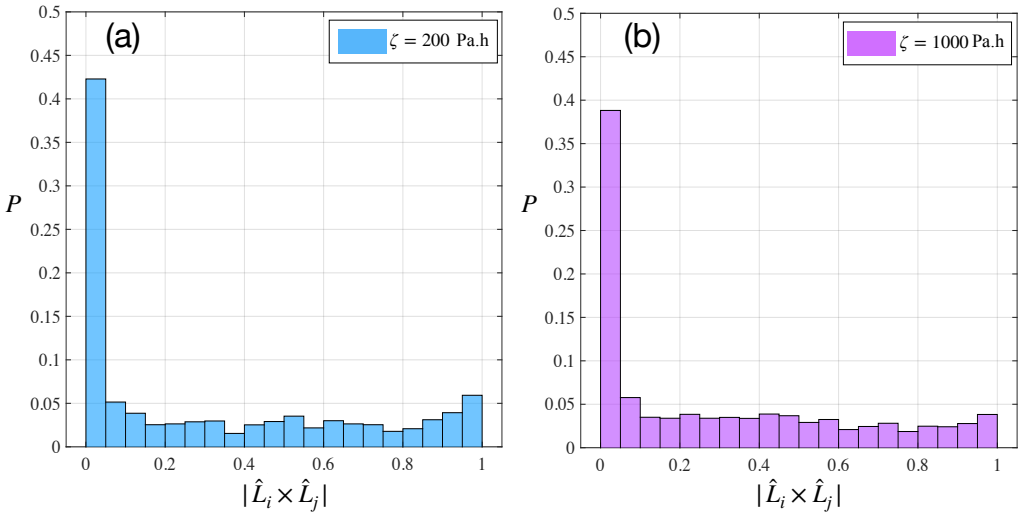

Figure 4.18: Probability distribution of the cross product magnitude between the unit length vectors of contacting bacteria for different frictional coefficients. Lower friction facilitates better alignment, while higher friction results in a more isotropic orientation distribution.

more effectively, minimizing angular deviations. In contrast, higher friction hinders alignment, leading to a more isotropic orientation distribution.

Impact of Frictional Coefficient on Domain Areas within Circular Confinement

For each simulation, I calculate the area of every individual domain and average these values to obtain a measure of the average domain area for different frictional coefficients. This approach allows us to quantify how the degree of alignment and clustering changes as substrate friction varies.

As it is shown in Fig. 4.19(a) at lower frictional coefficients, bacteria can move and reorient more freely. This mobility promotes smoother local alignment and larger, more contiguous domains. The reduced stress and lower accumulation of anisotropic forces facilitate the formation of well-aligned clusters, resulting in a higher average domain area.

As the frictional coefficient increases, bacterial motion is restricted, leading to higher stress accumulation at localized regions. This stress induces buckling instabilities, which disrupt local alignment and fragment the domains Fig. 4.19(b). Consequently, the average domain area decreases with increasing friction, reflecting the heightened disorder within the colony Fig. 4.20.

Across the range of frictional coefficients studied, the average domain area exhibits a decreasing trend with increasing friction. This behavior underscores the destabilizing

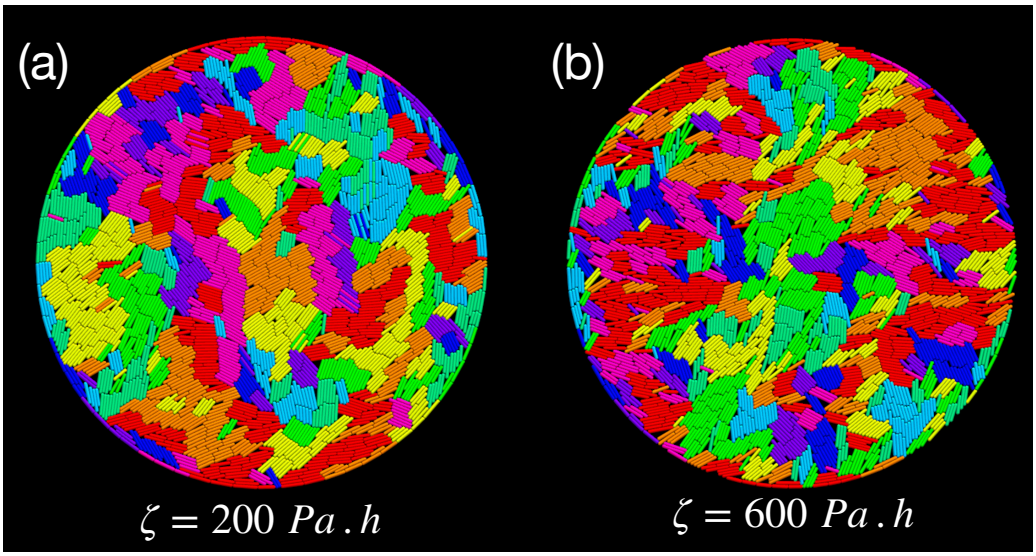

Figure 4.19: Configuration of the bacterial colony within a circular confinement under different frictional coefficients ($\zeta = 200\ Pa \cdot h$ and $\zeta = 1000\ Pa \cdot h$).

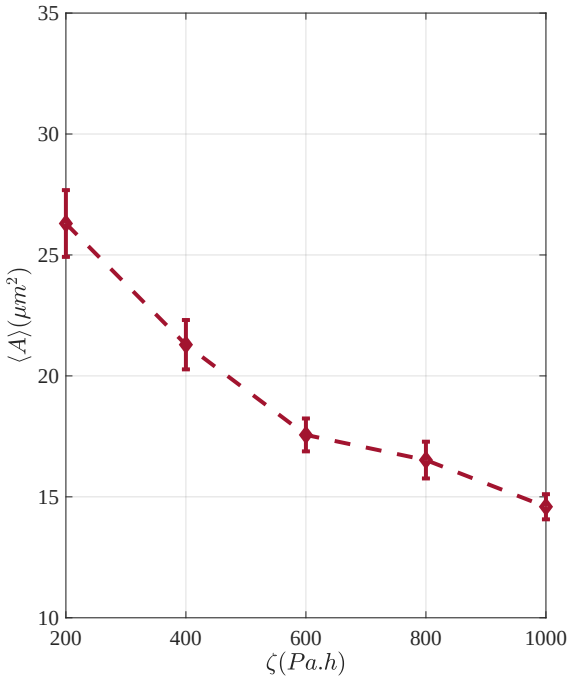

Figure 4.20: Variation of the average domain area for different frictional coefficients, with error bars representing the standard error of the mean.

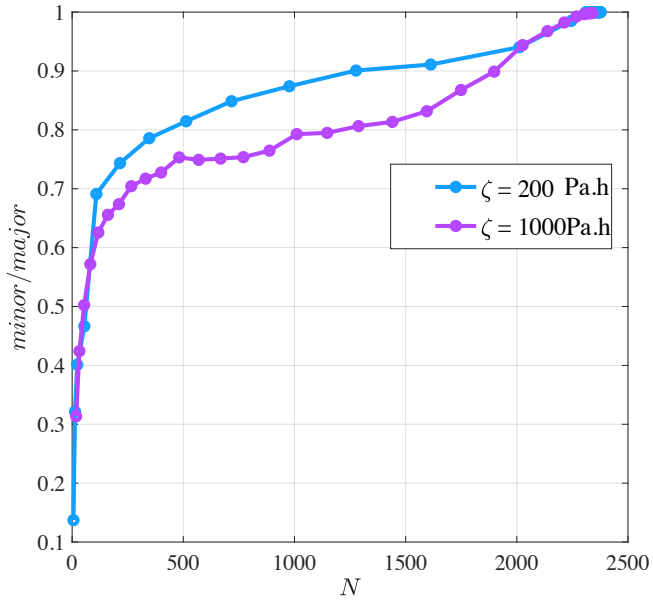

Figure 4.21: Evolution of the minor-to-major axis ratio as a function of bacterial population size for both frictional coefficients.

effect of high friction on bacterial self-organization, as increased substrate resistance inhibits smooth alignment and promotes stress-induced domain fragmentation.

Impact of Frictional Coefficient on Colony Shape and Organization

As it has shown in the Fig. 4.21 lower friction reduces resistance to bacterial movement and reorientation. This allows the bacteria to redistribute more evenly within the confinement, minimizing directional growth anisotropy. As a result, the colony tends to grow in a more isotropic (circular) manner.
Instead, higher friction increases resistance to bacterial movement and alignment. This can lead to directional biases where bacteria experience difficulty spreading laterally and instead elongate preferentially along one axis. Consequently, the colony becomes more elongated, reducing the minor-to-major axis ratio.

- **Alignment in low friction:** With reduced friction, bacterial cells can more easily adjust their orientations to align with neighbors. This promotes uniform packing and reduces anisotropic effects, resulting in a colony that expands more symmetrically.

- **Disruption in high friction:** High friction disrupts this alignment, as bacteria struggle to reorient against the increased substrate resistance. This misalignment contributes to anisotropic growth and elongation.

In circular confinements, the shape of the boundary naturally guides the colony toward a circular configuration. However, when friction is high, the internal stresses and misalignments override the boundary-induced symmetry, leading to a more elongated shape. At lower friction, the colony can more effectively conform to the confinement, maintaining a shape closer to the circular geometry of the boundary. The larger minor-to-major axis ratio (more circular colony) for smaller frictional coefficients results from reduced resistance to bacterial movement and alignment. This promotes isotropic stress distribution, uniform growth, and better conformance to the circular confinement. Higher friction disrupts these dynamics, causing stress buildup, misalignment, and anisotropic growth that elongates the colony.

4.3 Conclusion

This study has provided an in-depth examination of the mechanical interactions that govern the self-organization of rod-shaped bacterial colonies under isotropic and anisotropic confinement. By employing molecular dynamics simulations, I have demonstrated that both the confinement geometry and the aspect ratio of bacterial cells play crucial roles in shaping the structural and dynamical properties of colonies. The results highlight how spatial constraints and mechanical forces interact to determine bacterial alignment, growth dynamics, and force distributions within confined environments.

One of the key findings is the significant effect of bacterial aspect ratio on nematic ordering. Colonies composed of cells with higher aspect ratios exhibit stronger nematic alignment, highlighting the critical influence of cell shape on self-organization. The degree of ordering is particularly pronounced in environments where confinement enhances alignment through mechanical constraints. Additionally, the impact of confinement geometry—whether square or circular—was shown to alter the degree of order, illustrating the interplay between external spatial constraints and intrinsic bacterial properties. Square confinements promote more structured ordering due to their rigid boundaries, while circular confinements encourage more isotropic distributions, demonstrating how geometry can dictate colony morphology.

Furthermore, this study revealed that mechanical compression within confined bacterial colonies influences force magnitudes and growth dynamics. Cells with longer division lengths experience greater internal stress, which in turn affects their spatial organization and growth efficiency. The force network analysis demonstrated that bacterial interactions lead to anisotropic force distributions, with lateral forces dominating over end-to-end interactions, particularly in dense colonies. These findings suggest that

growth-induced mechanical forces play a substantial role in shaping bacterial behavior, affecting how colonies evolve over time and respond to spatial limitations.
The influence of substrate properties, particularly friction, was also evident in the simulations. Lower friction coefficients facilitated smoother bacterial alignment and increased domain sizes, whereas higher friction induced local stress accumulation, leading to disrupted ordering and increased disorder within the colony. This highlights the importance of environmental conditions in regulating bacterial self-organization and suggests that surface properties play a crucial role in determining the collective dynamics of bacterial populations.
Beyond fundamental bacterial self-organization, these findings have broader implications for fields such as microbial ecology, where understanding bacterial collective behavior is essential, and biotechnology, where optimizing bacterial growth in constrained environments is a key objective. The results underscore the importance of mechanical interactions and confinement effects in shaping bacterial colonies, providing insights that could inform biofilm formation studies, microbial engineering applications, and theoretical models of bacterial population dynamics. Ultimately, this work lays the foundation for further exploration into the complex interplay of mechanics, geometry, and biology in microbial systems, offering new perspectives on the physical principles that drive bacterial organization in confined environments.

5 Growth of Stress-Responsive Bacteria in 3D Under Confining Pressure

In Sections 3.3.1 and 3.3.2, research on bacterial growth in both two and three dimensions has demonstrated that mechanical stress from an external source plays a crucial role in the structural evolution of colonies, with even weak stresses driving morphological transitions and self-organization. Prior studies have investigated bacterial growth under various forms of confinement and mechanical forces, revealing how spatial constraints and stress influence colony expansion.
However, a comprehensive understanding of how confining isotropic pressure specifically affects stress-responsive bacteria, their growth dynamics, and population behavior remains incomplete. My work addresses this gap by examining the interplay between mechanosensitivity and external pressure, shedding light on how these factors dictate bacterial colony expansion, intercellular force distribution, and overall structural evolution. By integrating theoretical modeling with computational simulations, my research provides a deeper mechanistic understanding of bacterial adaptation to mechanical stress in confined environments.

This chapter is based on the **Growth of nonmotile stress responsive bacteria in three dimensional colonies under confining pressure** published in Biophysical Journal (2025) by **Samaneh Rahbar**, **Farshid Mohammad-Rafiee**, **Ludger Santen**, and **Reza Shaebani** [86].

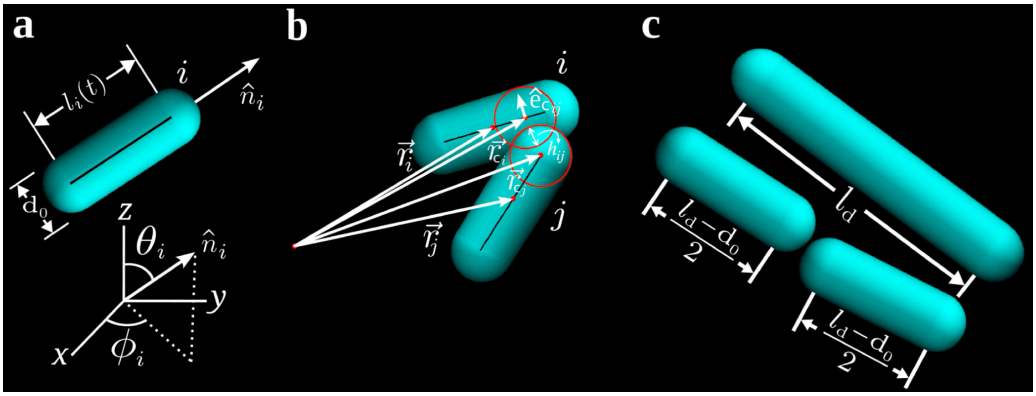

Figure 5.1

5.1 Model

5.1.1 Bacterial Motion and Growth

The dynamics of bacteria under confining isotropic pressure are governed by over-damped Newtonian equations that model their positions, orientations, and interactions. Each bacterium is represented as a spherocylinder with a constant diameter d_0 and a time-dependent length $l(t)$, show in Fig. 5.1(a), growing and dividing in three-dimensional space.

The translational motion of each bacterium, influenced by contact and frictional forces, is described by:

$$\frac{dr}{dt} = \frac{1}{\zeta l_i} \sum_{j=1}^{N_c^i} \vec{f}_{ij} \tag{5.1.1.1}$$

where $\vec{r}_i$ is the position of the center of the bacterial center of the mass, $\vec{f}_{ij}$ represents the force exerted on bacterium i by the bacterium j, ζ is the effective drap per unit of length. For computation of the contact vectors $\vec{r}_{c_i}$, $\vec{r}_{c_j}$, and the overlap h_{ij}, and correspondingly, mechanical forces $\vec{f}_{ij}$, I employ the modeling described in Chapter four, section 4.1.1. These quantities are depicted in Fig. 5.1(b).

As shown in Fig. 5.1, the orientation of each bacterium in three-dimensional space can be fully represented using two angles, the azimuthal angle ϕ (azimuthal angle) and the polar angle θ.

Since the bacterium is symmetric around its long axis and the mechanical interactions do not couple with self-rotation, rotations about the bacterium's own axis are negligible and can be ignored.

The time evolution of the ϕ could be given by:

$$\frac{d\phi}{dt} = \frac{12}{\zeta l_i^3} \sum_{j=1}^{N_c^i} ((\vec{r}_{c_i} - \vec{r}_i) \times \vec{f}_{ij}) \cdot \hat{z} \tag{5.1.1.2}$$

where $\vec{r}_{c_i}$ is the position of the contact point for bacterium i, and $\hat{z}$ is the unit vector along the $z-$axis.

The torque in the direction of the unit vector $\hat{\phi}$ lies in changing θ in spherical coordinates. In Cartesian coordinates, it can be expressed as:

$$\hat{\phi} = (-\sin\phi\hat{x} + \cos\phi\hat{y}) \tag{5.1.1.3}$$

Therefore, the projection of the torque in the direction of $\hat{\phi}_i$ gives us the time evolution of θ as

$$\frac{d\theta}{dt} = \frac{12}{\zeta l_i^3} \sum_{j=1}^{N_c^i} ((\vec{r}_{c_i} - \vec{r}_i) \times \vec{f}_{ij}) \cdot \hat{\phi}_i \tag{5.1.1.4}$$

This equation captures how the forces and torques acting on the bacterium influence its motion associated with changes in the polar angle θ.

As it has shown in Fig. 5.1(c), the growth and division dynamics of the bacteria are modeled following the method detailed in Chapter four, section 4.1.4.

5.1.2 Implementation of Periodic Boundary Conditions

To eliminate boundary effects and enable realistic modeling, I can implement periodic boundary conditions (PBC) in all directions. This approach poses challenges for imposing isotropic pressure, as moving walls or physical pistons cannot be utilized. Instead, an imaginary piston could be employed, where the system volume becomes a dynamic variable.

As illustrated in Fig. 5.2, this work considers a large three-dimensional phase space discretized into a grid. Gridding is particularly effective for molecular dynamics simulations, enabling efficient computation and spatial organization of particles or system states. As detailed in the previous chapter, this structured framework facilitates the implementation of PBC, ensuring continuity and consistency across the edges of the simulation domain. The size of each grid cell L is chosen to be slightly larger than both the bacterial length scale l and the interaction range, which is in order of d_0, ensuring accurate capture of interactions within each cell. Additionally, this setup prevents over-

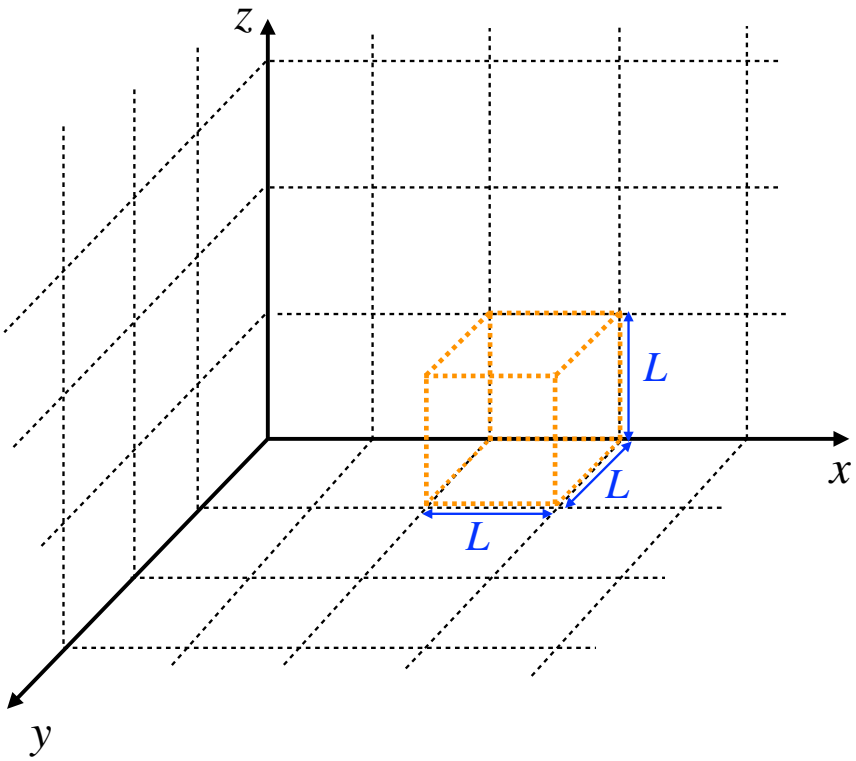

Figure 5.2: Representation of a cubic box with periodic boundary conditions applied, within a defined grinding space, to simulate continuous cell interactions in the system. L represents the dimension of the box.

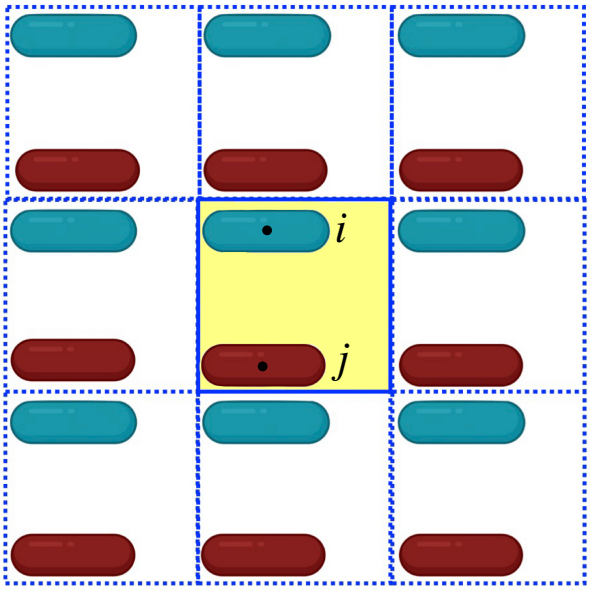

Figure 5.3: Illustration of a 2D square box (colored yellow) containing bacteria i and j, along with all possible imaginary positions of these bacteria under periodic boundary conditions, to model their interactions in the system.

lap or distortions in the representation of bacterial dynamics, as the minimum distance between bacteria satisfies $d_{min} < d_0$.

The logic behind PBC relies on the concept of **imaginary interactions**, which replicate the system's behavior as if it existed in an infinite space. Bacteria near the boundaries interact with their periodic images to maintain continuity across the simulation domain. However, only particles within the interaction range near the boundaries contribute to these imaginary interactions, as particles farther away have no influence.

In the simulation, a list of bacteria near the boundaries is maintained. Given the defined length scale and interaction range, it is unnecessary to generate all 27 possible periodic images of a given bacterium j relative to i to compute the pair interactions. Instead, the calculations are limited to interactions within the relevant range, significantly reducing computational complexity while maintaining accuracy using the **minimum image convention**[1].

The **minimum image convention** ensures that only the closest periodic image of a bacterium is considered during interaction calculations, eliminating the need to compute all 27 periodic images in a three-dimensional cubic box.

[1]The minimum image convention, used in this work, ensures that only the nearest periodic images are considered for interactions between bacteria.

As shown in Fig. 5.3, consider two bacteria within a periodic box. To find the nearest image of bacterium j relative to bacterium i, at the first step the displacement vector between them is calculated as:

$$\vec{r}_{ij} = \vec{r}_j - \vec{r}_i \tag{5.1.2.1}$$

Under the minimum image convention, the displacement vector is wrapped into the rangee $-L/2$ to $L/2$ (where L is the box dimension in each direction). This is achevied using the following:

$$\vec{r}_{ij,wrapped} = \vec{r}_{ji} - L \cdot round\left(\frac{r_{ij}}{L}\right) \tag{5.1.2.2}$$

This ensures that the displacemesnt vector $\vec{r}_{ij,wrapped}$ corresponds the displacement vector for the nearest image of bacterium j relative to i.

Two conditions determine how the displacement vector is wrapped into the simulation box:

1. If the displacement vector component satisfies $r_{ij} > L/2$, the wrapped displacement is:

$$r_{ij} > \frac{L}{2} \quad \text{if } r_{ij,wrapp} = r_{ij} - L \tag{5.1.2.3}$$

2. If the displacement vector component satisfies $r_{ij} < -L/2$, the wrapped displacement is:

$$r_{ij} < \frac{L}{2} \quad \text{if } r_{ij,wrapp} = r_{ij} + L \tag{5.1.2.4}$$

These conditions ensure that the displacement vector always corresponds to the shortest distance between bacteria i and j, accounting for periodic boundaries.

Using the wrapped displacement vector $\vec{r}_{ij,\text{wrapped}}$, the coordinates of the **nearest image** of bacterium j, denoted as $\vec{r}'_j$, can be computed relative to the position of bacterium i:

$$\vec{r}'_j = \vec{r}_i + \vec{r}_{ij,\text{wrapped}} \tag{5.1.2.5}$$

This equation provides the exact position of the nearest image of bacterium j within the simulation box. By employing this method, the computational burden is reduced while preserving the accuracy of interaction calculations under periodic boundary conditions.

5.1.3 Time Evolution of Volume and Scalar Pressure

To model bacterial colonies within periodic boundary conditions, it is essential to determine the time evolution of the periodic boundaries' volume and their positions. Mechanical forces generated by bacterial interactions are used to calculate the scalar pressure within the colony, capturing the effects of these interactions. The scalar pressure is calculated using the contact forces and vectors between bacteria, as introduced in chapter two section 2.2:

$$p_{\text{in}}(t) = \frac{1}{3V}\left(\frac{1}{2}\sum_{i=1}^{N}\sum_{j=1}^{N_c^i}\vec{r}_{c_{ij}} \cdot \vec{f}_{ij}\right) \tag{5.1.3.1}$$

Here $p_{in}(t)$ represents the scalar internal pressure, V is the volume of the system, $\vec{r}_{c_{ij}}$ is the contact vector, and $\vec{f}_{ij}$ is the contact force between bacteria i and j. The volume of the system V, is treated as a dynamic variable whose evolution is governed by the interplay between the constant external pressure p_{out} and the evolving internal pressure p_{in} of the system. The change in volume, mediated by the inertia of the piston M, is expressed as [87, 88]:

$$M\frac{d^2V(t)}{dt^2} = p_{in}(t) - p_{out} = \Delta p(t) \tag{5.1.3.2}$$

In this study, I assume that the mass of the piston M, is significantly large. Consequently, the piston moves very slowly, allowing us to approximate its velocity as zero $\frac{dV}{dt} = 0$. By properly rescaling bacterial positions to account for changes in the system volume, the dynamics of bacterial motion can be expressed as:

$$\frac{d\vec{r}_i}{dt} = \frac{1}{\zeta l_i}\sum_{j=1}^{N_c^i}\vec{f}_{ij} + \frac{1}{3}\vec{r}_i(t)\frac{d\ln V(t)}{dt} \tag{5.1.3.3}$$

where the last term on the right rescales the position according to the relative volume change. This method has been demonstrated to produce isotropic and homogeneous jammed packings of grains, as shown in prior studies [88, 89].

5.2 Numerical Implementation

In this study, the time evolution of the bacteria's translational motion, orientation, and system dynamics is numerically solved using the forward Euler method. This method, chosen for its simplicity and computational efficiency, is applied to discretize the governing equations.

Translational Motion

The equation governing the translational motion of bacterium i Eq. 5.1.3.3 is descretized as:

$$\vec{r}_i{}^{(n+1)} = \vec{r}_i{}^{(n)} + \Delta t \left[\frac{1}{\zeta l_i} \sum_{j=1}^{N_c^i} \vec{f}_{ij} + \frac{1}{3} \vec{r}_i{}^{(n)} \frac{d \ln V(t)}{dt} \right] \tag{5.2.0.1}$$

where:

- $\vec{r}_i{}^{(n)}$ is the position of bacterium i at the $n-$th time step,
- Δt is the time step size.

Azimuthal angles (ϕ) dynamics

The time evolution of ϕ, Eq. 5.1.1.2 is descritized as:

$$\phi^{n+1} = \phi^n + \Delta t \left[\frac{12}{\zeta l_i^3} \sum_{j=1}^{N_c^i} \left[(\vec{r}_{c_i} - \vec{r}_i) \times \vec{f}_{ij} \right] \cdot \hat{z} \right] \tag{5.2.0.2}$$

Polar angle (θ) dynamics

Similarly, the time evolution of θ, Eq. 5.1.1.4 is descritized as:

$$\theta^{n+1} = \theta^n + \Delta t \left[\frac{12}{\zeta l_i^3} \sum_{j=1}^{N_c^i} \left[(\vec{r}_{c_i} - \vec{r}_i) \times \vec{f}_{ij} \right] \cdot \hat{\phi} \right] \tag{5.2.0.3}$$

To ensure the stability of the forward Euler method, the time step Δt is chosen to be sufficiently small, based on the characteristic time scales of bacterial motion and interactions. The numerical integration is performed iteratively, with each time step updating the positions, orientations, and angles of all bacteria in the system.

By employing the forward Euler method, the computational framework is kept straightforward and efficient, allowing for the simulation of large systems of interacting bacteria under isotropic pressure.

To model the dynamic volume changes while maintaining computational stability, the governing equations are discretized. The volume evolution from Eq. 5.1.3.2 is updated as follows by considering $\frac{dV}{dt} = 0$:

$$V(t + \Delta t) = V(t) + \frac{1}{2} \frac{\Delta P}{M} \Delta t^2 \tag{5.2.0.4}$$

Here Δt represents the time step, and is the pressure difference driving the volume change.

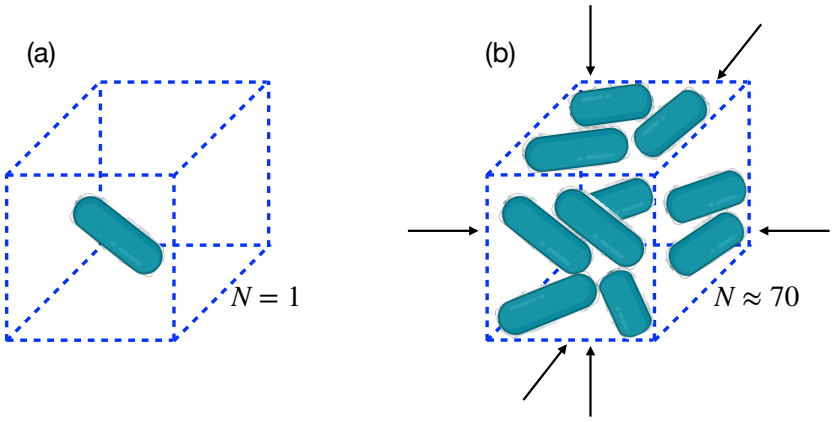

Figure 5.4: Illustration of the cubic box with a periodic boundaries. (a) $N = 1$ at the middle of the box at the early stage of the simulation. (b) $N \approx 70$ in the cubic box with periodic boundaries, and implementing isotropic external pressure (denoted by black arrows).

At each time step, the volume of the cubic box with periodic boundaries is known, and from this, the lengths in all three directions, as well as the coordinates of the boundaries, are determined. The coordinates are expressed as $r_{\min}$ and $r_{\max}$, representing the minimum and maximum points along each axis. When the system evolves to the next time step $t + \Delta t$, the volume of the cubic box changes. This results in a new length for the box, which can be computed as $V^{1/3}$, where V is the updated volume. To account for this change in the box size, the length difference $\Delta L = L(t + \Delta t) - L(t)$ is isotropically distributed around the initial boundary coordinates. The updated boundary coordinates at time $t + \Delta t$ are given by:

$$r_{\min}(t + \Delta t) = r_{\min}(t) - \frac{\Delta L}{2}, \quad r_{\max}(t + \Delta t) = r_{\max}(t) + \frac{\Delta L}{2} \tag{5.2.0.5}$$

This ensures that the boundaries shift symmetrically, maintaining the periodicity of the box while adjusting to the new dimensions.

To investigate the behavior of stress-responsive bacterial colonies under confining pressure, I perform simulations based on the bacterial growth, division, and dynamics models described in the earlier sections. The default parameter values used in the simulations are show in the Table. 5.1.

The simulations begin with the growth of a single elongated bacterium, as illustrated in Fig. 5.4(a). The initial simulation volume is $V = 27\mu m^3$. Applying isotropic confining pressure at this early stage leads to anisotropic behavior in the system's linear size across different directions.

To address this issue, the volume is kept constant during the early stages of the simulation, allowing bacteria to grow freely. Once the colony reaches $N = 70$ bacteria (where the individual volume of a single bacterium at the onset of division is $\propto 0.46\mu m^3$, isotropic external pressure is applied. Alternatively, simulations can be initialized with a compact, randomly arranged multicellular colony that is equilibrated before the introduction of confining pressure.
For ease of comparison, all measured quantities are nondimensionalized using the units provided in Table. 5.2.

Table 5.1: Default parameter values used in the simulations.

Parameter	**Symbol**	**Value**
bacterial diameter	d_0	$0.5\,\mu\text{m}$
Growth rate	r_g	$(2, 4)\,\mu\text{m} \cdot \text{h}^{-1}$
Division length	l_d	$2\,\mu\text{m}$
Viscous drag coefficient	ζ	$200\,\text{Pa} \cdot \text{h}$
Young's modulus of the bacteria	E	$400\,\text{kPa}$
Young's modulus of the wall	E	$1000\,\text{kPa}$
Piston inertia	M	$10^{-4}\,\text{kg} \cdot \text{m}^{-4}$
Mechanosensitivity	β	$0.4\,(\mu\text{m} \cdot \text{kPa} \cdot \text{h})^{-1}$
Time step	Δt	$5 \times 10^{-4}\,\text{h}$

Table 5.2: Non-dimensionalized parameters used in the simulations.

Parameter	**Symbol**	**Non-dimensionalized Value**
Time unit	t_0	$1\,\text{h}$
Growth rate	r_{g_0}	$2\,\mu\text{m} \cdot \text{h}^{-1}$
Volume scale	V_0	$125\,\mu\text{m}^3$
Mechanosensitivity	β_0	$0.02\,(\mu\text{m} \cdot \text{kPa} \cdot \text{h})^{-1}$

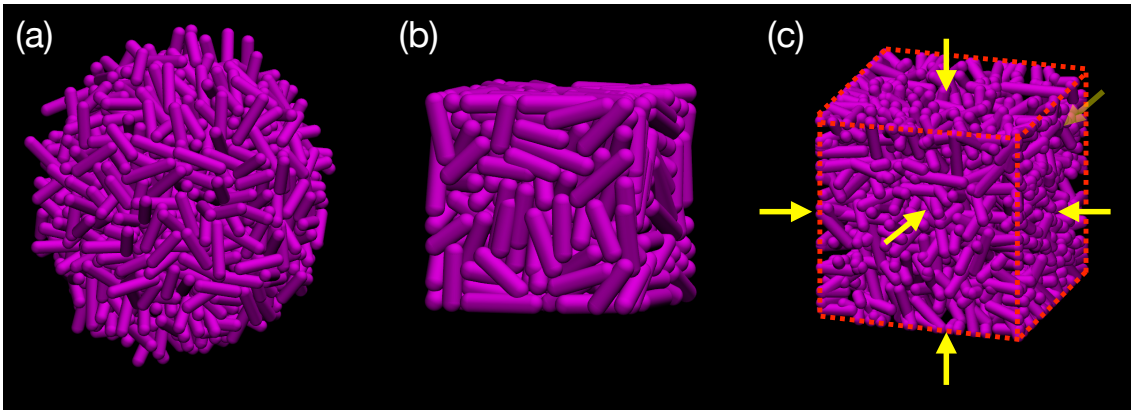

Figure 5.5: (a) Bacteria freely growing in a nutrient-rich environment, expanding without physical constraints. (b) Bacteria growing within a rigid cubic confinement, experiencing spatial restrictions and mechanical constraints. (c) Bacterial growth inside a cubic periodic boundary conditions (red dashed lines), in presence of external isotropic pressure (yellow arrows).

5.3 Results

5.3.1 Modeling Bacterial Proliferation: Growth in Unconfined vs. Confined Environments

As the first step in modeling bacterial growth under confining pressure, I performed simulations where bacteria grow freely in a large, unconfined space Fig. 5.5(a), mimicking a nutrient-rich environment. In the absence of external pressure, bacterial proliferation leads to the formation of a freely exponential growth Fig. (5.5 (a), 5.6(a)), which gradually adopts a spherical shape.

Before implementing periodic boundary conditions, I first consider bacterial growth within a rigid cubic confinement Fig. 5.5(b). As the bacteria proliferate and reach the boundaries, they begin to align along the walls of the enclosure. Due to the increasing population density, significant overlaps between bacteria are created, resulting in mechanical stress and localized crowding effects, shown in Fig. 5.6(b).

I expect that growth under confinement will lead to denser bacterial colonies and significantly influence the population dynamics of stress-responsive bacteria due to the development of internal stresses. In particular, confinement affects space-filling properties and proliferation statistics of the colonies, as shown in Fig. 5.5(b), the colony saturates 5.6(b) and bacteria are not able to grow. In the following sections, I explore the effects of key parameters such as imposed pressure, mechanosensitivity, and bacterial growth rate in the following sections.

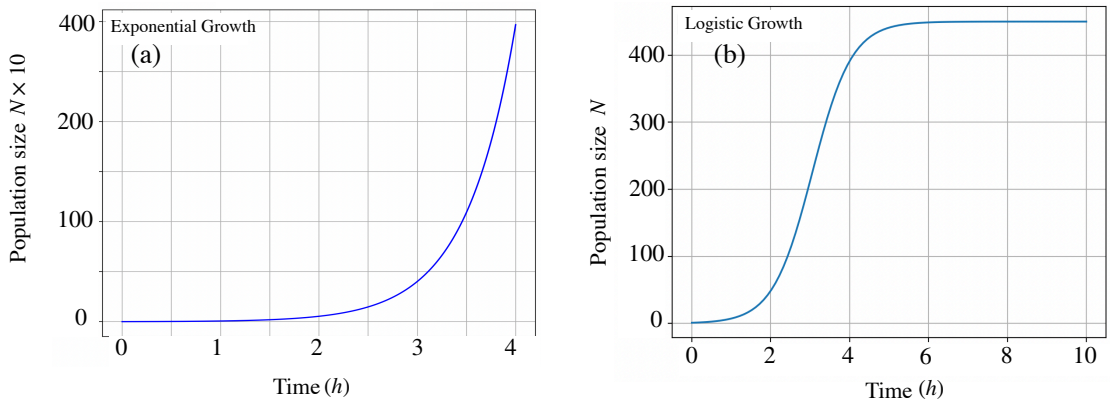

Figure 5.6: (a) Time evolution of the freely growing bacteria, which is given from Fig. 5.5(a). (b) Time evolution of the bacteria inside a hard cubic wall, which is given in Fig. 5.5(b).

5.3.2 Impact of Confining Pressure on Bacterial Growth and Population Dynamics

To more accurately represent bacterial growth in natural confined environments—such as human tissues or soil [90, 91]—I implement periodic boundary conditions to simulate isotropic confining pressure. This approach brings the model closer to real-world conditions, where bacterial colonies must adapt to spatial constraints and mechanical stresses within their surroundings [92, 93, 94].

I first investigate the pressure dependence of the population dynamics. Fig. 5.7 shows the time evolution of the total number of bacteria for two different growth rates r_g, and various values of the imposed confining pressure, p_{out}. As explained earlier, the simulation initially starts with $p_{\text{out}} = 0$ until the number of the bacteria $N \approx 70$ is reached, which occurs at approximately $t \sim 12t_0$ or $t \sim 6t_0$ for a bacterial colony with the growth rate of r_{g_0} or $2r_{g_0}$, respectively. During this initial growth phase, the colonies exhibit nearly exponential growth.

Due to the mechanosensitivity of bacteria ($\beta \neq 0$), the instantaneous growth rate of each bacterium fluctuates over time based on the local forces exerted by neighboring bacteria during growth and division. Once the external pressure is applied, the population dynamics slow considerably. Extremely high pressures can even completely inhibit population growth Fig. 5.7, similar to the effects observed in simulations with rigid boundaries.

Interestingly, at long times, the population growth under pressure appears nearly linear rather than exponential, with the slope decreasing as p_{out} increases. While the growth rate r_g affects the quantitative results, the qualitative behavior remains consis-

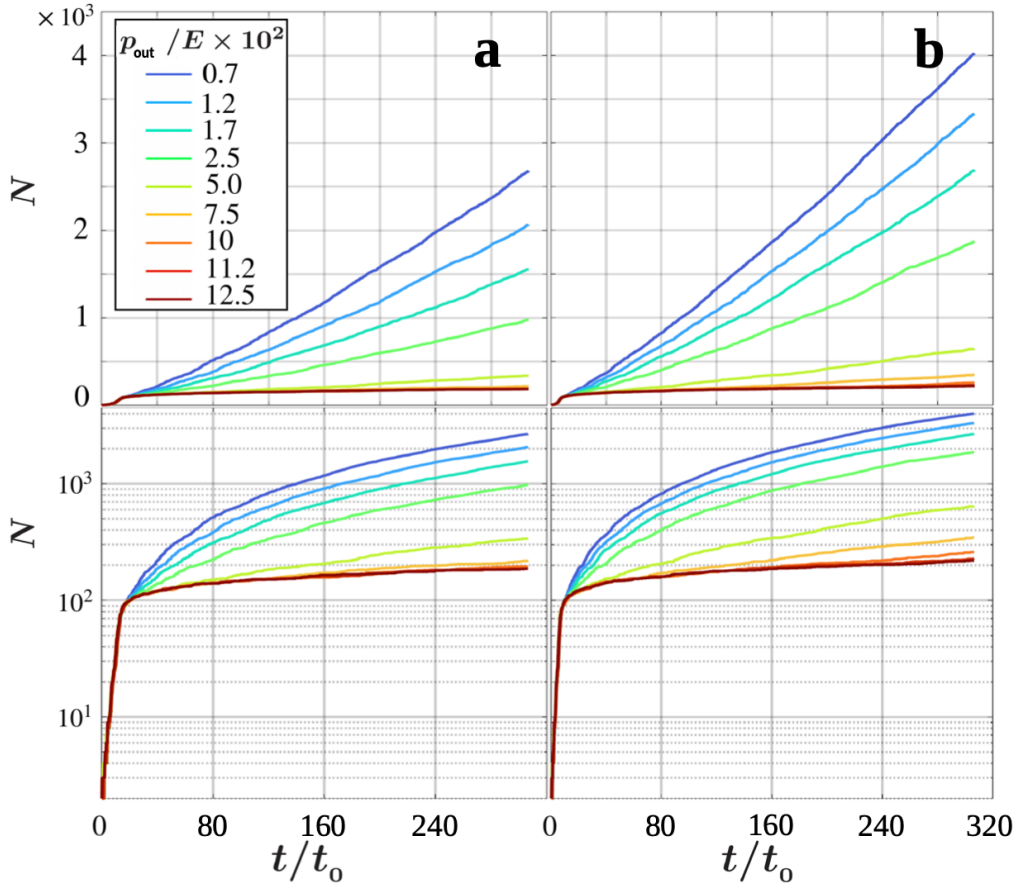

Figure 5.7: Time evolution of the total number of bacteria N for different values of p_{out} and (a) $r_g = r_{g_0}$ and (b) $r_g = 2r_{g_0}$. The upper and lower panels represent the same plots in linear and log-lin scales, respectively. Figure and the caption reprinted from Rahbar et al. [86].

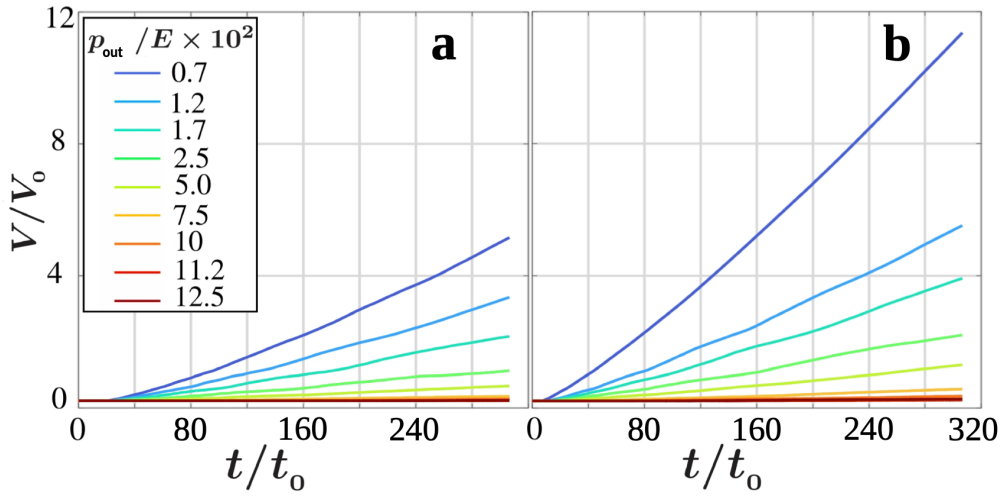

Figure 5.8: Volume of the bacterial colony as a function of time for different values of p_{out} and (a) $r_g = r_{g_0}$ and (b) $r_g = 2r_{g_0}$. Figure and the caption reprinted from Rahbar et al. [86].

tent Fig. 5.7. This pressure dependence aligns with experimental observations of E. coli colonies [82]. Notably, similar power-law dynamics have been reported for biofilms growing near surfaces [95], although in those cases, the slowed dynamics were attributed to mechanisms such as cell death and localized growth inhibition rather than mechanosensitivity.

The reduction in the population growth rate with increasing p_{out} directly affects the expansion of the bacterial colony's volume. As illustrated in Fig. 5.8, the rate of volume expansion decreases inversely with p_{out}. The bacterial growth rate r_g also plays a significant role. For instance, while an external pressure smaller than $0.07E$ is sufficient to halt the expansion of a colony with $r_g = r_{g_0}$ Fig. 5.8(a), a higher pressure $p_{\text{out}} \geq 0.1E$ is necessary to stop the expansion of a colony with $r_g = 2r_{g_0}$ Fig. 5.8(b).

5.3.3 The Role of Mechanosensitivity in Bacterial Growth Under Confinement

The degree of bacterial mechanosensitivity, captured by the parameter β, significantly impacts the growth dynamics of individual bacteria and the overall development of the bacterial colony under confinement. By systematically varying β over a broad range, I analyze the total number of bacteria N_f and the final colony volume V_f at a long time $t_f \approx 300t_0$. A larger β slows the growth dynamics of individual bacteria, leading to a slight reduction in both N_f and V_f, as shown in Fig. 5.9.

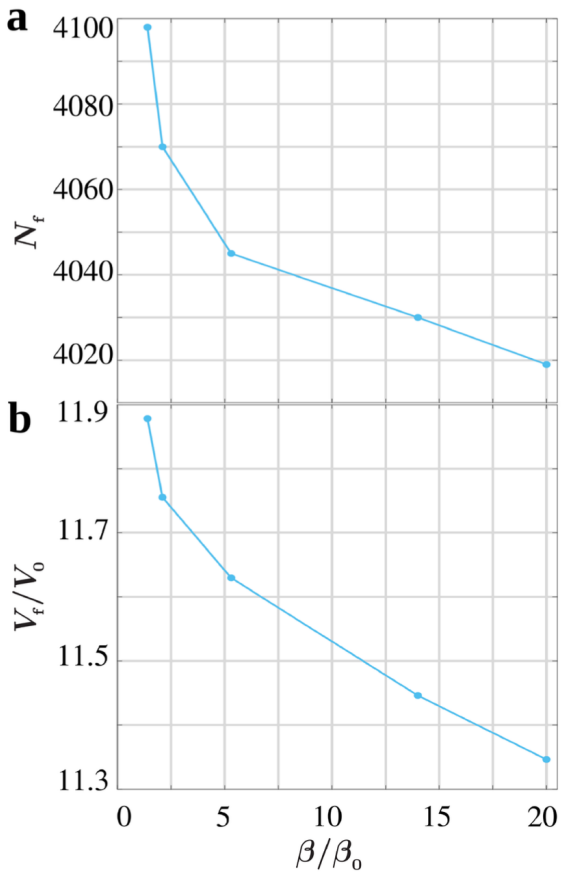

Figure 5.9: (a) Total number of bacteria and (b) volume of the colony at $t_f \approx 300t_0$ as a function of the mechanosensitivity β . Figure and the caption reprinted from Rahbar et al. [86].

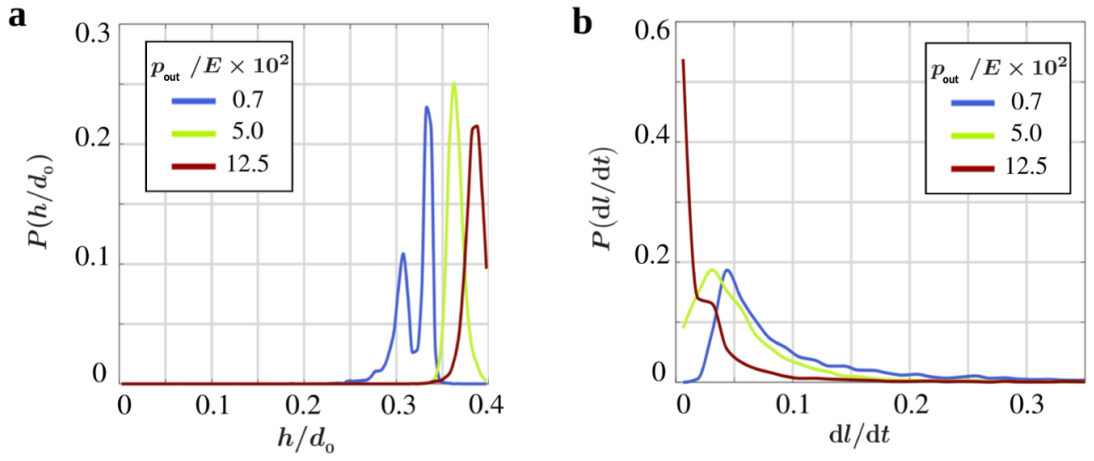

Figure 5.10: (a) Probability distribution of the scaled overlap $h/d0$ and (b) probability distribution of the instantaneous growth rate $\frac{dl}{dt}$ at $t \approx 300t_0$ for different values of p_{out}. Figure and the caption reprinted from Rahbar et al. [86].

For the biologically relevant parameter set chosen as a reference, the sensitivity of bacterial growth to β is relatively modest. Specifically, a tenfold increase in β (from $\beta = 2\beta_0$ to $\beta = 20\beta_0$) results in approximately 1% and 3% reductions in N_f and V_f, respectively. These findings highlight the limited yet measurable influence of mechanosensitivity on colony growth under the given conditions.

5.3.4 Pressure-Induced Changes in Bacterial Deformation and Growth Dynamics

To gain deeper insights into population dynamics under confining pressure, I analyze the probability distribution of bacterial overlaps h and instantaneous growth rates $\frac{dl}{dt}$ across the colony at a long time $t_f \approx 300t_0$. Increasing external pressure results in denser colonies, where bacteria experience greater deformations. As shown in Fig.5.10(a), the peak position and mean value of the overlap distribution shift toward higher h values with increasing p_{out}.

Consequently, as the forces exerted on bacteria intensify, the instantaneous growth rates $\frac{dl}{dt}$ are expected to decrease. This trend is confirmed in Fig. 5.10(b), where higher p_{out} correlates with smaller growth rates for individual bacteria. The probability distribution P transitions from a broad shape, with a mean at intermediate $\frac{dl}{dt}$ values, to a narrower profile centered at lower growth rates. These slower growth rates under higher external pressure result in extended division times for the bacteria.

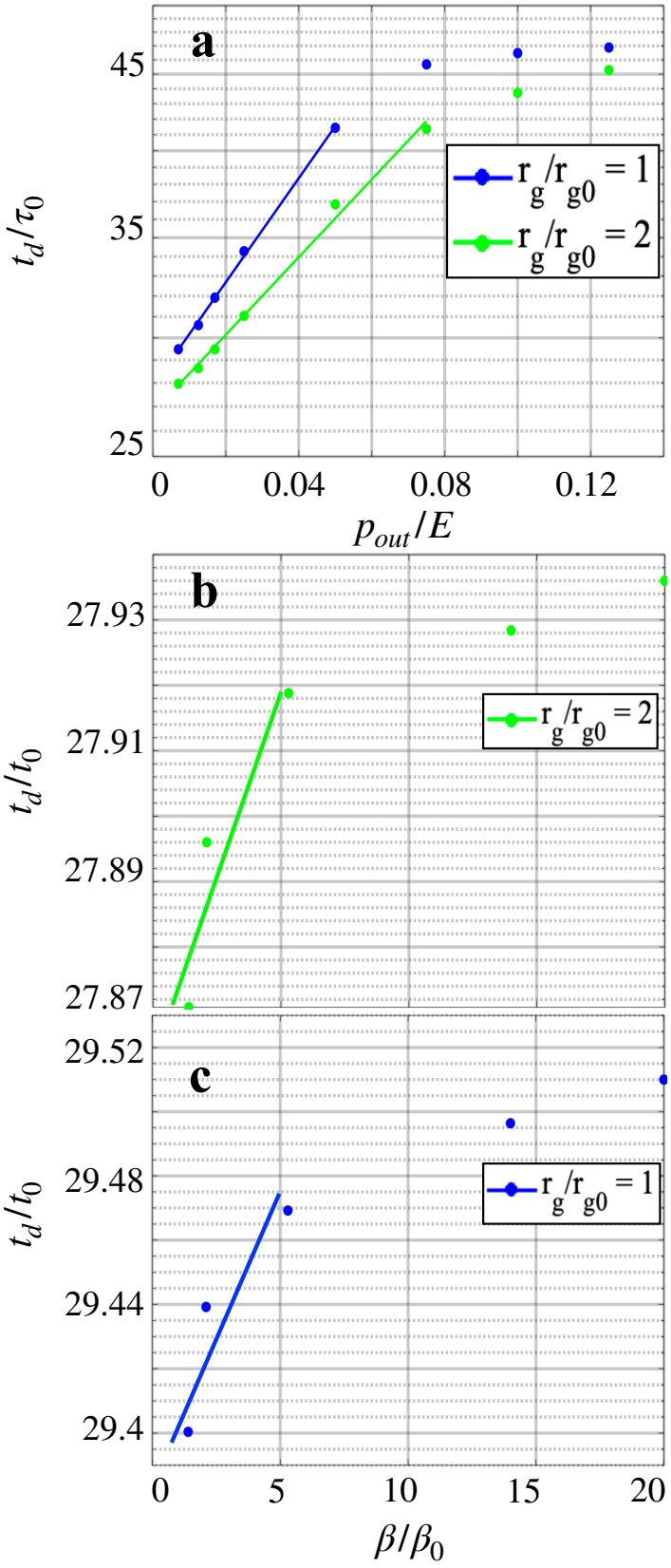

Figure 5.11: Log-in plots of doubling time of bacteria t_d versus (a) p_{out} and (b) β, for two different growth rates, r_g. Other parameters: (a) $\beta/\beta_0 = 20$, (b) $p_{out}/E = 0.007$. The lines represent exponential fits according to Eq. 5.3.6.4.

5.3.5 Division Dynamics Under Pressure: How Confinement Affects Bacterial Doubling Time

To analyze the effects of confinement on bacterial division dynamics, I extract the division time t_d using the relation $N = N_0 2^{\frac{t}{t_d}}$. Fig. 5.11(a) illustrates how t_d varies with the external pressure p_{out}. Initially, t_d increases with p_{out} and eventually plateaus. At small p_{out}, the increase in t_d is nearly exponential, with a slope inversely related to the growth rate r_g. Previous experiments on *E. coli* colonies [82] similarly observed an exponential rise in t_d with p_{out}. Notably, in those experiments, the slope decreased with higher temperatures, corresponding to increased growth rates. As p_{out} increased further, t_d diverged, indicating the cessation of growth and division dynamics under extremely high stress, leading to an infinite division time for a growing fraction of bacteria.

In my numerical study, the simulation time window $t_{\max}$ is finite. Consequently, for non-growing bacteria, I record $t_d \leq t_{\max}$ instead of ∞, resulting in the saturation of t_d at large p_{out} rather than its divergence. Fig. 5.11(b) shows the variation of t_d with the mechanosensitivity parameter β. Although the range of variation is limited, t_d follows a similar trend as observed for p_{out}: t_d grows exponentially at small β values and saturates at larger β.

5.3.6 Effective- Medium Estimate of the Doubling Time

The doubling time t_d can be analytically estimated by approximating the fluctuating stress field across the colony at long times (when the internal pressure equals p_{out}) as an isotropic, homogeneous stress field characterized by p_{out}. In this approximation, the discrete contact force network between bacteria is replaced with an effective uniform stress medium. Consequently, Eq. 4.1.4.1 for bacterial growth dynamics can be simplified as

$$\frac{dl(t)}{dt} = r_g - 2\beta\sigma p_{out} \tag{5.3.6.1}$$

where $\sigma = \frac{\pi d_0^2}{4}$ represents the cross-sectional area perpendicular to the major axis of each bacterium. Then, the average length of bacteria at time t becomes

$$l(t) = \frac{l_d}{2} + (r_g - 2\beta\sigma p_{out})t \tag{5.3.6.2}$$

from which the doubling time t_d can be extracted as

$$t_d = \frac{l_d}{2(r_g - 2\beta\sigma p_{out})} \tag{5.3.6.3}$$

According to this approximation, the doubling time diverges at the threshold confining pressure $p_{\text{out}}^{\max} = \frac{r_g}{2\sigma\beta}$, where the mean stresses exerted along the major axis of bacteria reach the required value to fulfill $\frac{dl}{dt} = 0$.

However, even below the $p_{\text{out}}^{\max}$ threshold, individual cells in a bacterial colony may randomly experience large forces, which prevent their length growth and division (leading to an infinite doubling time). The increase of p_{out} enhances the frequency of such stochastic singular events in the system. Therefore, the approximation in Eq.5.3.6.3 underestimates t_d at larger values of p_{out} and predicts a pressure threshold $p_{\text{out}}^{\max}$ higher than observed in simulations.

Nevertheless, in the limit of small p_{out}, the analytical prediction in Eq.5.3.6.3 successfully captures the behavior.

By expanding Eq. 5.3.6.3 around $p_{\text{out}} = 0$, I can extract an exponential approximation for t_d at small confining pressures as

$$t_d \sim \exp\left[\frac{2\sigma}{r_g}\beta p_{out}\right] \tag{5.3.6.4}$$

Fig. 5.11(a) shows that the behavior of t_d at small p_{out} is well-captured by the exponential relation in Eq. 5.3.6.4. Expansion of Eq.5.3.6.3 around $\beta = 0$ similarly leads to Eq.5.3.6.4, i.e., t_d also grows exponentially with β in the limit of small β. The fit to Eq.5.3.6.4, shown in Fig. 5.11(b), verifies that the agreement is satisfactory.

5.3.7 Population Growth Model

To quantitatively describe bacterial population growth under confining pressure, I propose a minimal theoretical model that captures the time evolution of the bacterial population N during the development of internal pressure. Initially, in the absence of external pressure ($p_{out} = 0$), the bacterial colony is free to expand, allowing it to relax internal stresses caused by growth and division. This freedom prevents the internal pressure, p_{in}, from increasing beyond a small baseline level, p_{in}^{free}, despite continuous population growth.

When external pressure p_{out} is applied ($p_{out} > p_{in}^{free}$), the colony's expansion becomes constrained, leading to an increase in intercellular interactions and a gradual buildup of internal pressure. Assuming that these interactions are primarily dominated by binary

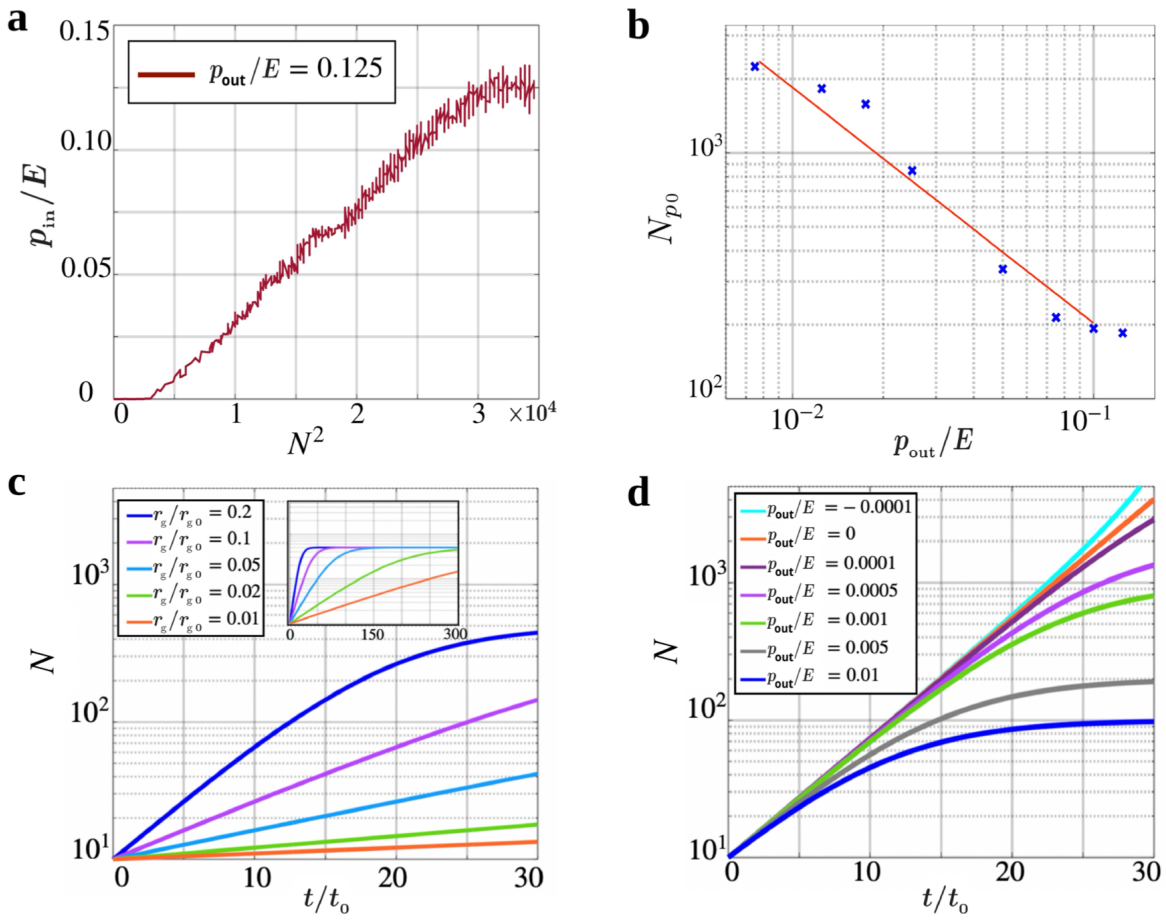

Figure 5.12: (a) Internal pressure p_{in} , scaled by the Young's modulus E, versus the square of the increasing number of bacteria at the given external pressure p_{out}. (b) Population of bacteria N_{p0} at the onset of $p_{in} = p_{out}$ in terms of the external pressure p_{out} . The line is a fit to $N_{p0} \propto 1/p_{out}$. (c),(d) Time evolution of the number of bacteria via Eq. 5.3.7.2 for $N_0 = 10$ and (c) $p_{out}/E = 0.002$ and different values of r_g and (d) $r_g/r_{g0} = 0.1$ and different values of p_{out}/E. The inset of the panel (c) represents the long time behavior of N. Figure and the caption reprinted from Rahbar et al. [86].

contacts between neighboring bacteria, I hypothesize that the internal pressure p_{in} grows proportionally to the square of the bacterial population, $p_{in} \propto N^2$, for $p_{in} \leq p_{out}$. Simulation results, as shown in Fig. 5.12(a), validate this assumption. During the initial phase of exponential growth at $p_{out} = 0$, the internal pressure remains negligible ($p_{in} \sim p_{in}^{free}$) despite an increase in bacterial population. However, upon applying an external pressure $p_{out} > p_{in}^{free}$, the internal pressure begins to grow linearly with N^2 until it approaches equilibrium with p_{out}. Once this balance is achieved, further bacterial division and growth dynamics no longer contribute to a rise in p_{in}, as the system effectively relaxes excess internal stresses to maintain $p_{in} \approx p_{out}$. Under these conditions, the population continues to grow despite the confining pressure.

To clarify how the magnitude of p_{out} influences population dynamics, I extract the population size at the onset of $p_{in} = p_{out}$, denoted as N_{p_0}, from the simulations. As shown in Fig. 5.12(b), N_{p_0} decreases with increasing p_{out}, and their relationship is approximately captured by $N_{p_0} \propto \frac{1}{p_{out}}$ within the studied range of p_{out}. This observation leads to the simplifying assumption that the strength of the imposed constraint is linearly proportional to the external pressure.

Building on this, I propose the following master equation to describe the time evolution of the bacterial population:

$$\frac{dN}{dt} = r_g N - \frac{p_{out} r_g}{E} N^2 \tag{5.3.7.1}$$

The first term on the right-hand side represents exponential population growth, where the growth rate is proportional to the current population. The second term introduces a constraint that slows the growth rate by accounting for the increasing number of binary interactions ($\propto N^2$) under external pressure. This equation suggests that the population dynamics are fully governed by the external pressure, Young's modulus E, and the mean growth rate. The solution of this logistic growth model is given by:

$$N(t) = \frac{N_\infty}{1 + \left(\frac{N_\infty}{N_0} - 1\right) \exp^{(-r_g t)}} \tag{5.3.7.2}$$

Here, $N_\infty = \frac{E}{p_{out}}$ represents the carrying capacity of the system, while N_0 is the initial population size when p_{out} is applied.

Figures 5.12(c) and 5.12(d) illustrate the time evolution of N as predicted by Eq. 5.3.7.2, for various values of the mean growth rate r_g, and external pressure p_{out}. Notably, this simple model qualitatively reproduces the behavior observed in simulations, particularly the time evolution of N following the initial exponential growth phase (see the lower panels of Fig. 5.7 for comparison). It is worth noting that when $p_{out} = 0$, Eq.

5.3.7.1 reduces to a pure exponential growth model, while a negative external pressure ($p_{out} < 0$) would accelerate population growth, as shown in Fig. 5.12(d).
The asymptotic behavior of $N(t)$ is depicted in the inset of Fig. 5.12(c), showing that $N(t)$ approaches a plateau at long times. This behavior contrasts with the simulation results in Fig. 5.7, where $N(t)$ continues to grow indefinitely at long times, with a slope inversely related to the external pressure. In the logistic growth model (Eq. 5.3.7.1), the maximum possible number of bacteria, N_∞, is determined by the ratio $\frac{E}{p_{out}}$, making the carrying capacity a fixed value. However, as previously demonstrated in Fig. 5.12(a), the carrying capacity of the system grows indefinitely beyond the onset of $p_{in} = p_{out}$. This is because the system can expand and relax the excess internal pressure generated by bacterial division and growth dynamics.
To incorporate this effect into my model, I modify Eq. 5.3.7.1 by introducing a linearly growing term, $\frac{A}{p_{out}}t$, to the maximum possible number of bacteria. Here, A is a constant that accounts for the gradual increase in the system's capacity over time. The revised master equation for the time evolution of the bacterial population under confining pressure becomes:

$$\frac{dN}{dt} = r_g N \left(1 - \frac{N}{(E + At)/p_{out}}\right) \tag{5.3.7.3}$$

This equation can be numerically solved for a given set of parameters r_g, p_{out}, E, A to predict $N(t)$. The results, shown in Fig. 5.13, demonstrate that the asymptotic continuous growth of $N(t)$ is successfully captured by the modified master equation Eq. 5.3.7.3. Moreover, the model accurately reproduces the inverse dependence of the growth slope on p_{out} at long times, consistent with the simulation observations.

5.4 Discussion

I have numerically studied the evolution of colonies of stress-responsive bacteria under confining isotropic pressure. To generate homogeneous colonies, boundary effects were eliminated by employing periodic boundary conditions, which posed challenges in imposing a confining pressure. To address this, I developed a method based on rescaling the momenta and positions of cells, adapting it to the overdamped dynamics of bacteria. The imposed pressure influences colony growth dynamics by affecting intercellular interactions and the growth of individual stress-responsive bacteria. By introducing mechanosensitivity into my model, I enabled tuning of bacterial growth responses to applied stresses. The validity of this approach is supported by the remarkable agreement between my numerical predictions and experimental observations of evolving *E.*

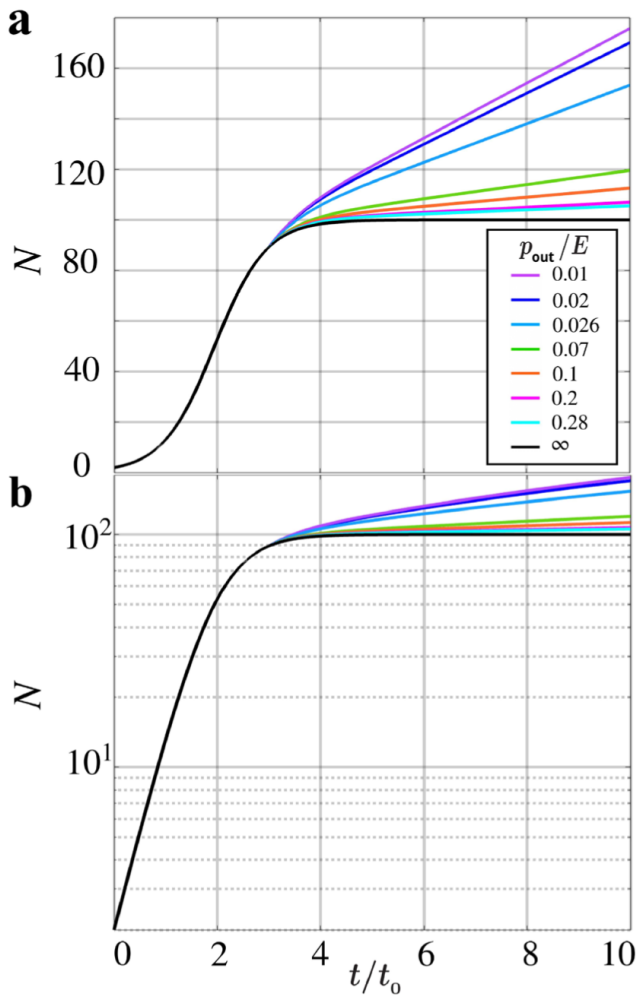

Figure 5.13: Time evolution of N according to Eq. 5.3.7.3 in (a) linear and (b) log-lin scales for $N_0 = 2$, $r_g/r_{g_0} = 1$, $A/E = 10^{-4}h^{-1}$, and different values of the external pressure. Figure and the caption reprinted from Rahbar et al. [86].

coli colonies under confining pressure [82]. Furthermore, the simulation method presented here can be efficiently parallelized for large-scale simulations, as the varying volume method is compatible with adaptive hierarchical domain decomposition and dynamic load balancing [96]. This method can also be straightforwardly generalized to model assemblies of motile cells.

For simplicity, I chose constant values for the model parameters, including bacterial structural and mechanical properties (such as cell diameter d_0 and Young's modulus E), growth parameters (growth rate r_g and division length l_d), and environmental properties (e.g., drag per unit length ζ and temperature). However, these choices do not fully reflect the diverse phenotypic characteristics of bacteria, such as morphological variability or differentiation. Experimentally derived distributions of these quantities could be incorporated into simulations to produce quantitatively comparable statistics. Adapting the mechanical interactions and equations of motion in my model would require minor modifications to accommodate these real-world distributions.

The exponential growth of bacterial and other populations under ideal conditions can be significantly impacted by environmental and biological constraints. Factors such as limited resources, competition, toxic metabolite accumulation, or mechanical interactions (as in my system) disrupt exponential growth, resulting in alternative patterns like power-law, logistic, or plateaued dynamics [82], [95], [97]. Conversely, suboptimal nutrient distribution or intrinsic genetic and metabolic limitations may reduce growth rates while preserving the exponential nature of the dynamics. Thus, the choice of modeling approach depends on the specific constraints within a given system.

Introducing mechanosensitivity into the model has complex implications for the structure and dynamics of bacterial colonies. For the parameter set chosen in this study, the results were only modestly sensitive to the choice of β. However, in general, reduced growth rates due to mechanosensitivity can influence bacterial length diversity and spatial organization, altering the stress state of the system. This feedback loop could enable stress-responsive bacteria to adapt to environmental changes. Exploring the effects of mechanosensitivity on colony structure, dynamics, and adaptation across biologically relevant parameter ranges would be an intriguing avenue for future research.

In the absence of quantitative experimental data, I assumed a simple linear force-dependence for mechanosensitivity. This functional form could be refined to reflect the specific stress responses of different bacterial types. Stress-responsive bacteria in the model experience time-dependent instantaneous growth rates due to mechanical stress variations. Extensions of the model could account for spatial and temporal variations in growth rates caused by local nutrient availability [98, 99] or viscoelasticity changes [100]. Experimental studies [77, 82, 101] also show that imposed stresses may affect bac-

terial division length thresholds, cell shapes, and even induce aging of cell mechanical properties. Quantitative data would be necessary to algorithmically implement these effects.

The generalized overdamped Newtonian dynamics approach, commonly used to model bacterial dynamics in viscous environments, was employed to study non-motile bacterial colonies under confining pressure. However, this method assumes the environment exerts a purely viscous drag, ignoring memory or elasticity effects. Consequently, it cannot capture the time-dependent mechanical responses characteristic of viscoelastic media, such as biofilms embedded in extracellular polymeric substances (EPS). Accurately modeling bacterial dynamics within viscoelastic EPS matrices would require viscoelastic frameworks, such as Maxwell models. These models combine reversible elastic responses with irreversible dissipative deformations, capturing memory effects that govern how stress evolves with strain over time. Incorporating these effects would enable a more realistic representation of bacterial behavior in environments where deformations do not relax instantaneously. While my current approach effectively models the influence of confining pressure on bacterial population growth, further developments are needed to consider the effects of confining pressure on EPS matrix structure.

Experimental evidence [102, 103] indicates that high confining pressures alter bacterial activity, affecting biofilm structural characteristics. Addressing this aspect would provide a more comprehensive understanding of the interplay between confining pressure and biofilm mechanics.

In summary, I have developed methods and conducted numerical simulations to study evolving 3D colonies of stress-responsive bacteria under confining pressure. The findings demonstrate how physical interactions regulate biological processes at the microscale and highlight the intricate feedback between mechanical stimuli and bacterial growth dynamics. Understanding the interplay of mechanosensitivity, bacterial structural characteristics, and mechanical interactions offers valuable insights into adaptive responses under varying environmental conditions. These insights may inspire novel strategies for controlling bacterial infections.

6 Summary and Conclusion

I constructed a molecular dynamics simulation framework in C++ from the ground up, designed to accommodate various bacterial shapes and species. This tool allows for the detailed investigation of how mechanical interactions, confinement, and environmental factors influence bacterial population dynamics in both two- and three-dimensional contexts. My work specifically examines how the intrinsic properties of bacteria, including geometry, mechanosensitivity, and growth rate, shape bacterial responses to environmental confinement.

I numerically studied the evolution of bacterial colonies under different mechanical and environmental constraints, focusing on the role of confinement, bacterial properties, and mechanosensitivity. My investigations covered two primary research directions: bacterial self-organization in confinement and the effects of isotropic pressure on the growth dynamics of the stress-responsive bacteria.

In my study of bacterial self-organization, I demonstrated that confinement geometry and bacterial aspect ratio significantly influence colonies' nematic ordering and structural organization. Colonies composed of bacteria with higher aspect ratios exhibited stronger nematic alignment, while the degree of ordering was further modulated by the shape of the confinement. Square confinements promoted more structured ordering due to their rigid boundaries, whereas circular confinements encouraged more isotropic distributions. Furthermore, mechanical compression within confined bacterial colonies influenced force distributions and growth dynamics. Cells with longer division lengths in a confined environment experienced greater internal stress, revealing the profound impact of growth-induced mechanical forces on colony organization. The role of substrate properties was also examined, with lower friction facilitating smoother alignment and higher friction inducing stress accumulation, disrupting bacterial organization.

In investigating stress-responsive bacteria, I developed a method to impose a confining isotropic pressure while eliminating boundary effects using periodic boundary conditions. This required adapting a rescaling technique to the overdamped dynamics of bacteria, enabling the study of how pressure influences colony growth dynamics. The imposed pressure affected intercellular interactions and the growth of individual bacteria, with mechanosensitivity allowing bacterial responses to be tuned based on

applied stresses. The validity of my approach was confirmed by its strong agreement with experimental observations of E. coli colonies under confining pressure. Additionally, I demonstrated that this simulation framework could be efficiently parallelized for large-scale simulations, making it compatible with adaptive hierarchical domain decomposition and dynamic load balancing.

Mechanosensitivity played a crucial role in shaping bacterial growth and colony structure. While my results indicated only modest sensitivity to the mechanosensitivity parameter β within the chosen parameter set, more generally, reduced growth rates due to mechanosensitivity influenced bacterial length diversity and spatial organization. This feedback loop between stress-induced growth inhibition and bacterial structural adaptation suggests potential mechanisms for environmental adaptation. Furthermore, my model provided insights into alternative growth patterns, showing how mechanical constraints can shift bacterial population dynamics away from purely exponential growth toward power-law, logistic, or plateaued behavior.

The findings of my work have significant implications for understanding bacterial self-organization, stress response, and biofilm dynamics. By incorporating mechanical interactions and mechanosensitivity into bacterial models, I have provided a framework for exploring bacterial adaptation under various environmental constraints. These insights are relevant to microbial ecology, where understanding collective bacterial behavior is essential, and biotechnology, where optimizing bacterial growth in constrained environments is a key objective. The results also have potential applications in medical and industrial microbiology, particularly in understanding biofilm formation and developing strategies to control bacterial populations.

Future research could refine the mechanosensitivity model by incorporating experimentally derived distributions for bacterial properties such as division length thresholds, cell shape variability, and metabolic responses to stress. My current model assumes a linear force-dependence for mechanosensitivity, but future work could explore alternative functional forms that better reflect bacterial stress responses. Additionally, while my study focused on overdamped Newtonian dynamics in viscous environments, extending the model to include viscoelastic effects would allow for a more accurate representation of bacterial behavior in biofilms embedded within extracellular polymeric substances (EPS). Such extensions would enable the study of stress evolution within biofilms, where time-dependent mechanical responses and memory effects play a crucial role in bacterial adaptation.

Experimental evidence suggests that high confining pressures alter bacterial activity and biofilm structure, an aspect that warrants further computational exploration. Addressing this in future models could provide deeper insights into how confinement and

mechanical stress shape microbial communities in natural and artificial environments. Furthermore, incorporating more biologically realistic constraints, such as nutrient limitations and metabolic feedback mechanisms, would enhance the predictive power of the simulations.

In summary, I developed a molecular dynamics simulation framework from scratch to study bacterial colony dynamics under various mechanical and environmental constraints. My numerical studies highlight the intricate feedback between mechanical stimuli and bacterial growth dynamics. I explored bacterial self-organization in confined environments, revealing the role of geometry and substrate interactions in shaping colony structure. I also examined the effects of isotropic pressure on stress-responsive bacteria, showing how mechanosensitivity can influence growth dynamics and adaptation. These findings contribute to a deeper understanding of bacterial collective behavior and provide a foundation for future research into adaptive responses under varying environmental conditions. Ultimately, my work offers valuable insights into microbial dynamics that may inspire novel strategies for controlling bacterial populations and optimizing bacterial cultures in both natural and engineered settings.

Bibliography

[1] Popov, V.L., Hess, M. and Willert, E., 2019. *Handbook of contact mechanics: exact solutions of axisymmetric contact problems*. Springer Nature.

[2] Hertz, H. "Über die Berührung fester elastischer Körper," *Journal für die reine und angewandte Mathematik*, 1881.

[3] Johnson, K. L. *Contact Mechanics*, Cambridge University Press, 1985.

[4] E. R. Smith, D. M. Heyes, D. Dini; Towards the Irving-Kirkwood limit of the mechanical stress tensor. *J. Chem. Phys.* 14 June 2017; 146 (22): 224109.

[5] Brown, D., Neyertz, S. (1995). A general pressure tensor calculation for molecular dynamics simulations. *Molecular Physics*, 84(3), 577–595.

[6] M. J. Louwerse and E. J. Baerends, *Chem. Phys. Lett.* **421**, 138 (2006).

[7] Heinz, Hendrik, Wolfgang Paul and Kurt Binder. "Calculation of local pressure tensors in systems with many-body interactions." *Physical review. E, Statistical, nonlinear, and soft matter physics* 72 6 Pt 2 (2003): 066704 .

[8] Thomas W Lion and Rosalind J Allen 2012 *J. Phys.: Condens. Matter* **24** 284133.

[9] Das, S., Gompper, G. Winkler, R.G. Local stress and pressure in an inhomogeneous system of spherical active Brownian particles. *Sci Rep* **9**, 6608 (2019).

[10] Dufrêne, Y.F., Persat, A. Mechanomicrobiology: how bacteria sense and respond to forces. *Nat Rev Microbiol* **18**, 227–240 (2020)

[11] You Z, Pearce DJG, Sengupta A, Giomi L. Geometry and Mechanics of Microdomains in Growing Bacterial Colonies. Physical Review X. 2018;8(3):31065.

[12] Persat A., Nadell C. D., Kim M. K., Ingremeau F., Siryaporn A., Drescher K., Wingreen N. S., Bassler B. L., Gitai Z., Stone H. A., Cell 2015, 161, 988–997.

[13] DeCamp, S., Redner, G., Baskaran, A. et al. Orientational order of motile defects in active nematics. *Nature Mater* **14**, 1110–1115 (2015).

[14] M. Doi, *S*oft Matter Physics (OUP Oxford, 2013).

[15] D. Volfson, S. Cookson, J. Hasty, L. S. Tsimring, Biomechanical ordering of dense cell populations. *Proc Natl Acad Sci USA.* **105**, 15346–15351 (2008).

[16] Basaran M, Yaman YI, Yüce TC, Vetter R, Kocabas A. 2022 Large-scale orientational order in bacterial colonies during inward growth. *eLife* **11**, e72187.

[17] Balasubramaniam L, Mège R-M, Ladoux B. 2022 Active nematics across scales from cytoskeleton organization to tissue morphogenesis. *Curr. Opin. Genet. Dev.* **73**, 101897.

[18] P. M. Chaikin and T. C. Lubensky, *Principles of Condensed Matter Physics* (Cambridge University Press, Cambridge, England, 1995).

[19] M. J. Bowick, L. Giomi, H. Shin, and C. K. Thomas, *Bubble-Raft Model for a Paraboloidal Crystal*, Phys. Rev. E **77**, 021602 (2008).

[20] X. Li, R. Balagam, T. He, P.P. Lee, O.A. Igoshin, H. Levine, On the mechanism of long-range orientational order of fibroblasts, *Proc Natl Acad Sci USA.* **114** (34) 8974-8979,

[21] Dell'Arciprete, D., Blow, M.L., Brown, A.T. et al. A growing bacterial colony in two dimensions as an active nematic. *Nat Commun* **9**, 4190 (2018).

[22] Isensee Jonas, Hupe Lukas, Golestanian Ramin and Bittihn Philip. 2022 Stress anisotropy in confined populations of growing rods. *J. R. Soc. Interface.* **19**: 20220512.

[23] Farzan Beroz, Jing Yan, Yigal Meir, Benedikt Sabass, Howard A. Stone, Bonnie L. Bassler, and Ned S. Wingreen, "Verticalization of bacterial biofilms," Nat. Phys. **14**, 954–960 (2018).

[24] Matthew A. A. Grant, Bartlomiej Waclaw, Rosalind J. Allen, and Pietro Cicuta, "The role of mechanical forces in the planar-to-bulk transition in growing Escherichia coli microcolonies," J. R. Soc. Interface **11**, 20140400 (2014).

[25] Liu, Y., Li, B., Feng, X.Q., 2020. Buckling of growing bacterial chains. J. Mech. Phys. Solids **145**, 104146 (2020).

[26] L. Giomi, *The Geometry and Topology of Turbulence in Active Nematics*, Phys. Rev. X **5**, 031003 (2015).

[27] Y. Sumino, K. H. Nagai, Y. Shitaka, D. Tanaka, K. Yoshikawa, H. Chaté, and K. Oiwa, Large-Scale Vortex *Lattice Emerging from Collectively Moving Microtubules,* Nature (London) **483**, 448 (2012).

[28] T. Sanchez, D. N. Chen, S. J. DeCamp, M. Heymann, and Z. Dogic, *Spontaneous Motion in Hierarchically Assembled Active Matter*, Nature (London) **491**, 431 (2012).

[29] S. J. DeCamp, G. S. Redner, A. Baskaran, M. F. Hagan, and Z. Dogic, *Orientational Order of Motile Defects in Active Nematics*, Nat. Mater. **14**, 1110 (2015).

[30] P. Guillamat, J. Ignés-Mullol, and F. Sagués, *Control of Active Liquid Crystals with a Magnetic Field*, *Proc Natl Acad Sci USA.* **113**, 5498 (2016).

[31] Denis Boyer *et al* 2011 *Phys. Biol.* **8** 026008.

[32] Langeslay, B. and Juarez, G. Microdomains and stress distributions in bacterial monolayers on curved interfaces. *Soft Matter* **19**, 3605–3613 (2023).

[33] Sengupta A (2020) Microbial Active Matter: A Topological Framework. Front. Phys. 8:184.

[34] Doostmohammadi, A., Ignés-Mullol, J., Yeomans, J.M. *et al.* Active nematics. *Nat Commun* **9**, 3246 (2018).

[35] R. J. Allen, B. Waclaw, Bacterial growth: A statistical physicist's guide. *Rep. Prog. Phys.* **82** 016601 (2019).

[36] Murray J D 2002 *Mathematical Biology* (Berlin: Springer).

[37] Monod J 1949 The growth of bacterial cultures *Annu. Rev. Microbiol.* **3** 371–94.

[38] Blanchard, A.E., Lu, T. Bacterial social interactions drive the emergence of differential spatial colony structures. *BMC Syst Biol* **9**, 59 (2015).

[39] Bhattacharjee, T., Datta, S.S. Bacterial hopping and trapping in porous media. *Nat Commun* **10**, 2075 (2019).

[40] Jenna A Moore-OttSelena ChiuDaniel B AmchinTapomoy BhattacharjeeSujit S Datta (2022) A biophysical threshold for biofilm formation, *eLife* **11**:e76380.

[41] Pradeep S, Arratia PE. To biofilm or not to biofilm. *elife.* (2022); **11**:e80891.

[42] Arciola, C.R., Campoccia, D. Montanaro, L. Implant infections: adhesion, biofilm formation and immune evasion. *Nat Rev Microbiol* **16**, 397–409 (2018).

[43] Q. Zhang, J. Li, J. Nijjer, H. Lu, M. Kothari, R. Alert, T. Cohen, J. Yan, Morphogenesis and cell ordering in confined bacterial biofilms, *Proc Natl Acad Sci USA.* **118** (31) e2107107118.

[44] P. Ghosh, J. Mondal, E. Ben-Jacob, H. Levine, Mechanically-driven phase separation in a growing bacterial colony, *Proc Natl Acad Sci USA.* **112** (17) E2166-E2173.

[45] G. Sharma, S. Sharma, P. Sharma, D. Chandola, S. Dang, S. Gupta, R. Gabrani, Escherichia coli biofilm: development and therapeutic strategies, *Journal of Applied Microbiology*, **121**, 309–319 (2016).

[46] Sauer, K., Stoodley, P., Goeres, D.M. et al. The biofilm life cycle: expanding the conceptual model of biofilm formation. *Nat Rev Microbio*l **20**, 608–620 (2022).

[47] Sauer, K., Camper, A. K., Ehrlich, G. D., Costerton, J. W., Davies, D. G. Pseudomonas aeruginosa displays multiple phenotypes during development as a biofilm. *J. Bacteriol.* **184**, 1140–1154 (2002).

[48] Petrova, O. E., Sauer, K. A novel signaling network essential for regulating *Pseudomonas aeruginosa* biofilm development. *PLoS Pathog.* **5**, e1000668 (2009).

[49] Gupta, K., Marques, C. N. H., Petrova, O. E., Sauer, K. Antimicrobial tolerance of *Pseudomonas aeruginosa* biofilms is activated during an early developmental stage and requires the two-component hybrid SagS. *J. Bacteriol.* **195**, 4975–4987 (2013).

[50] Hall-Stoodley, L., Costerton, J. Stoodley, P. Bacterial biofilms: from the Natural environment to infectious diseases. *Nat Rev Microbiol* **2**, 95–108 (2004).

[51] Nadell CD, Xavier JB, Levin SA, Foster KR (2008) The Evolution of Quorum Sensing in Bacterial Biofilms. *PLoS Biol* **6** (1): e14.

[52] You Z, Pearce DJG, Giomi L. Confinement-induced self-organization in growing bacterial colonies. *Sci. Adv.* **7**, eabc8685(2021).

[53] Su PT, Liao CT, Roan JR, Wang SH, Chiou A, et al. (2012) Bacterial Colony from Two-Dimensional Division to Three-Dimensional Development. PLOS ONE **7** (11): e48098.

[54] Sheats Julian, Sclavi Bianca, Cosentino Lagomarsino Marco, Cicuta Pietro and Dorfman Kevin D. 2017 Role of growth rate on the orientational alignment of *Escherichia coli* in a slit *R. Soc. Open Sci.* **4**: 170463.

[55] Grant Matthew A. A., Wacław Bartłomiej, Allen Rosalind J. and Cicuta Pietro 2014The role of mechanical forces in the planar-to-bulk transition in growing *Escherichia coli* microcolonies *J. R. Soc. Interface.* **11**: 20140400

[56] Wang, L., Fan, D., Chen, W. et al. Bacterial growth, detachment and cell size control on polyethylene terephthalate surfaces. *Sci Rep* **5**, 15159 (2015).

[57] G. Lan, C.W. Wolgemuth, S.X. Sun, Z-ring force and cell shape during division in rod-like bacteria, *Proc Natl Acad Sci USA.* 104 (41) 16110-16115.

[58] Adams, D., Errington, J. Bacterial cell division: assembly, maintenance and disassembly of the Z ring. *Nat Rev Microbiol* **7**, 642–653 (2009).

[59] Gordon VD, Wang L. Bacterial mechanosensing: the force will be with you, always. J Cell Sci. 2019 Apr 3;132(7):jcs227694.

[60] Cho, H. et al. Self-organization in high-density bacterial colonies: efficient crowd control. *PLoS Biol.* **5**, e302 (2007).

[61] Lega, J. and Passot, T. Hydrodynamics of bacterial colonies. *Nonlinearity* **20**, C1 (2007).

[62] Farrell, F. D. C., Hallatschek, O., Marenduzzo, D. Waclaw, B. Mechanically driven growth of quasi-two-dimensional microbial colonies. *Phys. Rev. Lett.* **111**, 168101 (2013).

[63] Grant, M. A. A., Wacław, B., Allen, R. J. and Cicuta, P. The role of mechanical forces in the planar-to-bulk transition in growing *Escherichia coli* microcolonies. *J. R. S. Interface* **11**, 20140400 (2014).

[64] Farrell, F. D. C., Gralka, M., Hallatschek, O. and Waclaw, B. Mechanical interactions in bacterial colonies and the surfing probability of beneficial mutations. *J. R. Soc. Interface* **14**, 20170073 (2017).

[65] Silhavy TJ. Classic Spotlight: Gram-Negative Bacteria Have Two Membranes. J Bacteriol. 2015 ;198(2):201.

[66] Silhavy TJ, Kahne D, Walker S. The bacterial cell envelope. Cold Spring Harb Perspect Biol. 2010 ;2(5):a000414.

[67] Mai-Prochnow, A., Clauson, M., Hong, J. *et al.* Gram positive and Gram negative bacteria differ in their sensitivity to cold plasma. *Sci Rep* **6**, 38610 (2016).

[68] Mai-Prochnow, A., Murphy, A. B., McLean, K. M., Kong, M. G. and Ostrikov, K. Atmospheric pressure plasmas: Infection control and bacterial responses. International journal of antimicrobial agents **43**, 508–517 (2014).

[69] Yusupov, M. et al. Plasma-Induced Destruction of Bacterial Cell Wall Components: A Reactive Molecular Dynamics Simulation. The Journal of Physical Chemistry C **117**, 5993–5998 (2013).

[70] Christine E. Harper, Christopher J. Hernandez; Cell biomechanics and mechanobiology in bacteria: Challenges and opportunities. *APL Bioeng.* 1 June 2020; 4 (2): 021501.

[71] Dufrêne, Y.F., Persat, A. Mechanomicrobiology: how bacteria sense and respond to forces. Nat Rev Microbiol 18, 227–240 (2020).

[72] Tuson, H.H., Auer, G.K., Renner, L.D., Hasebe, M., Tropini, C., Salick, M., Crone, W.C., Gopinathan, A., Huang, K.C. and Weibel, D.B. (2012), Measuring the stiffness of bacterial cells from growth rates in hydrogels of tunable elasticity. Molecular Microbiology, 84: 874-891.

[73] M. Campos, I.V. Surovtsev, S. Kato, A. Paintdakhi, B. Beltran, S. E. Ebmeier, and C. Jacobs-Wagner, Cell **159**, 1433 (2014).

[74] Prathitha KarSriram Tiruvadi-KrishnanJaana MännikJaan MännikAriel Amir (2021) Distinguishing different modes of growth using single-cell data *eLife* **10**:e72565.

[75] Godin, M., Delgado, F., Son, S. et al. Using buoyant mass to measure the growth of single cells. *Nat Methods* **7**, 387–390 (2010).

[76] O. Hallatschek, P. Hersen, S. Ramanathan, D.R. Nelson, Genetic drift at expanding frontiers promotes gene segregation, *Proc Natl Acad Sci USA.* **104** (50) 19926-19930.

[77] Hannah H. Tuson, George K. Auer, Lars D. Renner, Mariko Hasebe, Carolina Tropini, Max Salick, Wendy C. Crone, Ajay Gopinathan, Kerwyn Casey Huang, and Douglas B. Weibel, "Measuring the stiffness of bacterial cells from growth rates in hydrogels of tunable elasticity," Mol. Microbiol. 84, 874–891 (2012).

[78] Furchtgott, L., Wingreen, N.S., and Huang, K.C. (2011) Mechanisms for maintaining cell shape in rod-shaped Gram-negative bacteria. *Mol Microbiol* **81**: 340–353.

[79] Huang, K.C., Mukhopadhyay, R., Wen, B., Gitai, Z., and Wingreen, N.S. (2008) Cell shape and cell-wall organiza-tion in Gram-negative bacteria. *Proc Natl Acad Sci USA.* **105**: 19282–19287.

[80] Wang, S., Arellano-Santoyo, H., Combs, P.A., and Shaevitz, J.W. (2010) Actin-like cytoskeleton filaments contribute to cell mechanics in bacteria. *Proc Natl Acad Sci USA.* **107**: 9182–9185.

[81] Si, F., Li, B., Margolin, W. et al. Bacterial growth and form under mechanical compression. *Sci Rep* **5**, 11367 (2015).

[82] P. Kumar, A. Libchar, *Pressure and temperature dependence of growth and morphology of Escherichia coli: Experiments and stochastic model,* Biophys J. **105**, 783 (2013).

[83] Wittmann, R., Nguyen, G.H.P., Löwen, H. et al. Collective mechano-response dynamically tunes cell-size distributions in growing bacterial colonies. Commun Phys 6, 331 (2023).

[84] B. I. Shraiman, *Mechanical Feedback as a Possible Regu- lator of Tissue Growth*, *Proc Natl Acad Sci USA.* **102**, 3318 (2005).

[85] F. Montel, M. Delarue, J. Elgeti, L. Malaquin, M. Basan, T. Risler, B. Cabane, D. Vignjevic, J. Prost, G. Cappello, and J.F. Joanny, *Stress Clamp Experiments on Multi- cellular Tumor Spheroids*, Phys. Rev. Lett. **107**, 188102 (2011).

[86] Rahbar S, Mohammad-Rafiee F, Santen L, Shaebani R, Growth of Nonmotile Stress-Responsive Bacteria in Three-Dimensional Colonies under Confining Pressure, *Biophysical Journal* (2025).

[87] Hans C. Anderson, *J. Chem. Phys.* **72**, 2384–2393 (1980).

[88] M. R. Shaebani, T. Unger, and J. Kertész, *International Journal of Modern Physics C* **20**, 847 (2009).

[89] M. Reza Shaebani, TamásUnger, and János Kertész, "Unjamming of granular packings due to local perturbations: Stability and decay of displacements," Phys. Rev. E **76**, 030301 (2007).

[90] Amchin, D. B., Ott, J. A., Bhattacharjee, T. and Datta, S. S. Influence of confinement on the spreading of bacterial populations. *PLoS Comput. Biol.* **18**, e1010063 (2022).

[91] Du H, Xu W, Zhang Z, Han X. Bacterial Behavior in Confined Spaces. Front Cell Dev Biol. 2021; 9:629820.

[92] Pradeep Kumar and Albert Libchaber, “Pressure and temperature dependence of growth and morphology of es- cherichia coli: Experiments and stochastic model,” Bio phys. J. **105**, 783–793 (2013).

[93] Sudip Nepal and Pradeep Kumar, “Dynamics of pheno- typic switching of bacterial cells with temporal fluctua- tions in pressure,” Phys. Rev. E **97**, 052411 (2018).

[94] Navita Sinha, Sudip Nepal, Timothy Kral, and Pradeep Kumar, “Survivability and growth kinetics of methanogenic archaea at various phs and pressures: Im- plications for deep subsurface life on mars,” Planet. Space Sci. **136**, 15–24 (2017).

[95] P. Rashtchi and M. Tempelaars and E. van der Linden and T. Abee and M. Habibi, “Lactobacillus plantarum strains show diversity in biofilm formation under flow conditions,” Heliyon **8**, e12602 (2022).

[96] Zahra Shojaaee, M. Reza Shaebani, Lothar Brendel, János Török, and Dietrich E. Wolf, “An adaptive hierar- chical domain decomposition method for parallel contact dynamics simulations of granular materials,” J. Comput. Phys. 231, 612–628 (2012).

[97] Luis M. A. Bettencourt and Jose Lobo and Dirk Heilbing and Christian Kühnert and Geoffrey B. West, "Growth innovation scaling, and the pace of life in cities," *Proc Natl Acad Sci USA*. **104**, 7301-7306 (2007).

[98] Alejandro Martinez-Calvo, Tapomoy Bhattacharjee, R. Konane Bay, Hao Nghi Luu, Anna M, Hancock, Ned S. Wingreen, and Sujit S. Datta, "Morphological instability and roughening of growing 3d bacterial colonies, " *Proc Natl Acad Sci USA*. **119**, e2208019199 (2022).

[99] Xinxian Shao, Andrew Mugler, Justin Kim, Ha Jun Jeong, Bruce R. Levin. and Ilya Nemenman, "Growth of bacteria in 3-d colonies," PLoS Comput. Biol **13**, e1005679 (2017).

[100] Brandon W. Peterson, Yan He, Yijin Ren, Aidan Zer- doum, Matthew R. Libera, Prashant K. Sharma, Arie- Jan van Winkelhoff, Danielle Neut, Paul Stoodley, Henny C. van der Mei, and Henk J. Busscher, “Vis- coelasticity of biofilms and their recalcitrance to mechan- ical and chemical challenges,” FEMS Microbiol. Rev. 39, 234–245 (2015).

[101] Fangwei Si, Bo Li, William Margolin, and Sean X. Sun, “Bacterial growth and form under mechanical compres- sion,” Sci. Rep. **5**, 11367 (2015).

[102] Flemming, Hans-Curt and Wingender, Jost, “The biofilm matrix,” Nat. Rev. Microbiol. **8**, 623–633 (2010).

[103] Dommerich, Steffen and Frickmann, Hagen and Ostwald, Jürgen and Lindner, Tobias and Zautner, Andreas Erich and Arndt, Kathleen and Pau, Hans Wilhelm and Pod- bielski, Andreas, “Effects of High Hydrostatic Pressure on Bacterial Growth on Human Ossicles Explanted from Cholesteatoma Patients,” PLOS ONE **7**, e30150 (2012).

[104] Giordano, Nicholas J. Computational Physics. Upper Saddle River, NJ :Pearson-/Prentice Hall, 2006.

[105] Humphrey, W., Dalke, A. and Schulten, K., "VMD - Visual Molecular Dynamics" *J. Molec. Graphics* **1996**, 14.1, 33-38.

Acknowledgment

At the end of my thesis, I would like to express my deepest gratitude to my supervisor, Professor Ludger Santen, for his outstanding guidance, insightful discussions, and constant support throughout my PhD journey. His expertise and encouragement have given me valuable opportunities to expand my knowledge and grow as a researcher.

I am also grateful to Dr. Reza Shaebani for his valuable assistance and the stimulating discussions that have significantly contributed to the progress of my research. Likewise, I extend my sincere appreciation to Dr. Farshid Mohammad-Rafiee for the productive collaboration and enlightening discussions that have helped shape the direction of my work.

Furthermore, I would like to acknowledge the German Research Foundation (DFG) for its financial support within the Collaborative Research Center SFB 1027, which provided funding and opportunities for PhD students to attend prestigious schools, seminars, and conferences. A special thanks to my supervisor, Professor Ludger Santen, and Professor Heiko Rieger for their generous support of my sabbatical program at the University of Pennsylvania, an experience that enriched my academic journey and broadened my expertise.

I also appreciate the Integrated Research Training Group (IRTG) for organizing informative seminars, training sessions, and summer camps that contributed to my professional development.

I am thankful to my colleagues for their support, and the insightful discussions we shared throughout this journey.

Finally, my heartfelt gratitude goes to my family, whose constant support, encouragement, and belief in me have been my greatest source of strength. Their love and faith in my dreams have played a crucial role in helping me reach this milestone.